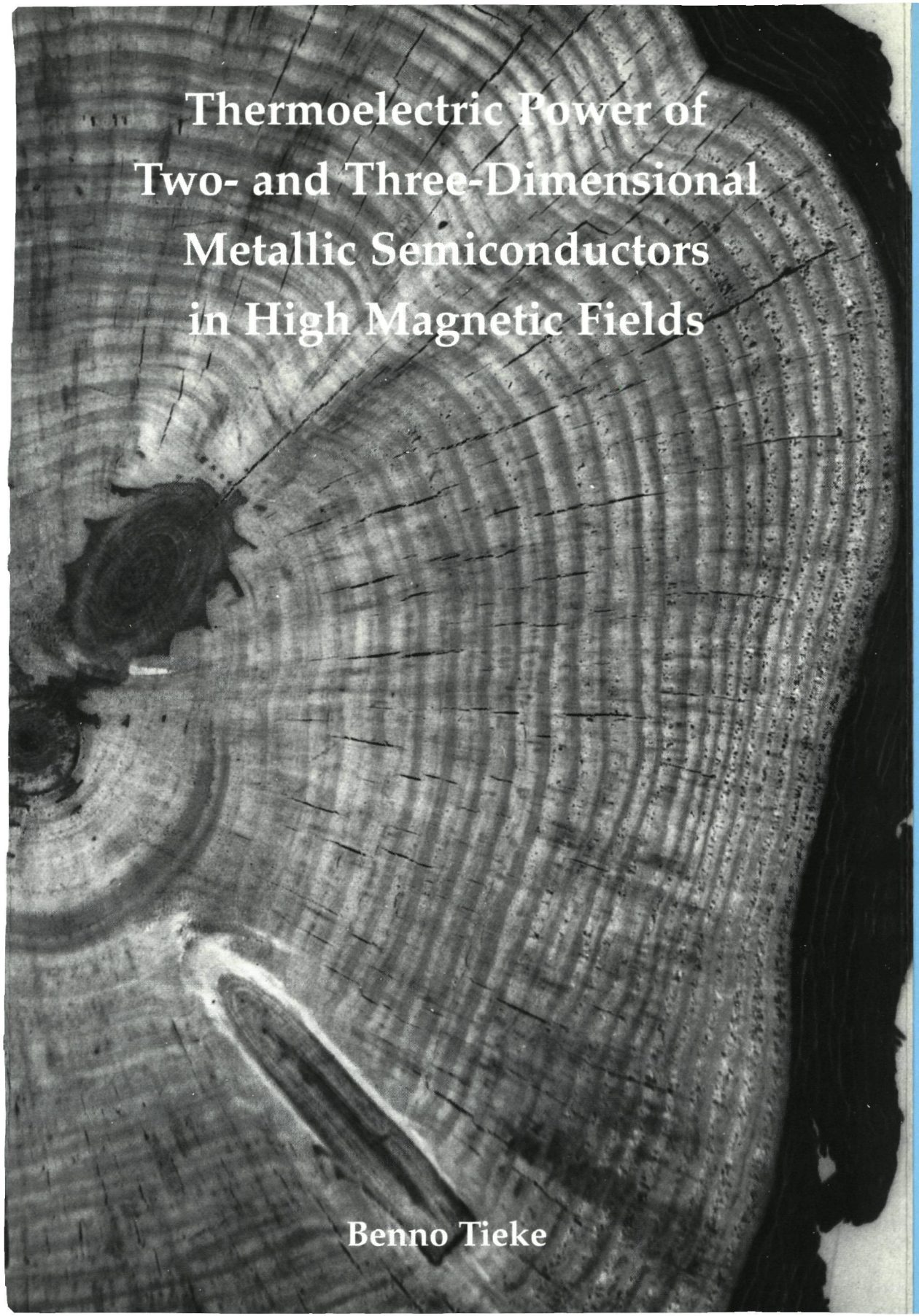

Thermoelectric Power of Two- and Three-Dimensional Metallic Semiconductors in High Magnetic Fields

Benno Tieke

Cover:
Trunk of a pine-tree from the garden of the author's parental home. The tree was planted on the author's birth and cut when this thesis was being finished.

Photograph:
Katholieke Universiteit Nijmegen

Thermoelectric Power of Two- and Three-Dimensional Metallic Semiconductors in High Magnetic Fields

Benno Tieke

ISBN 90-9010561-1

Thermoelectric Power of Two- and Three-Dimensional Metallic Semiconductors in High Magnetic Fields

een wetenschappelijke proeve op het gebied
van de Natuurwetenschappen

Proefschrift

ter verkrijging van de graad van doctor
aan de Katholieke Universiteit Nijmegen,
volgens besluit van het College van Decanen
in het openbaar te verdedigen op
maandag 12 mei 1997
des namiddags om 3.30 uur precies

door

Benno Tieke

geboren op 18 mei 1967
te Münster (Duitsland)

Promotor: Prof. Dr. ir. J. C. Maan

Manuscriptcommissie: Prof. Dr. R. Fletcher
(Queen's University, Kingston, Ontario, Canada)

Dr. P. M. Koenraad
(Technische Universiteit Eindhoven)

Preface

This book simply would not exist in its present form without the input of many people other than the author, and I am glad to have the opportunity to thank some of them by mentioning them here

The high magnetic field experiments reported in this thesis were done at the Nijmegen High Field Magnet Laboratory in measurement periods during endless nights or in the weekends The most important support which I want to acknowledge, and the most demanding for the helping colleagues, is the need for assistance during these measurement nights Voor deze echte hulp wil ik me graag bedanken bij Sjoerd, Stef, Uli, Robin, Ate, Fausto, Alex, Andrea, Marc, Andrey en zeker nog bij veel meer mensen In deze reeks horen ook Klaas, Hung en Jos thuis, die tijdens een memorable Hybrid-run het onmogelijke mogelijk hebben gemaakt met als resultaat dat in deze thesis een paar echte 30 Tesla-sweeps opgenomen konden worden

Prof Robin Fletcher has continuously participated in this research during the past four years with a lot of hard work (the E-mail counter says 414 mails!) and I have profited a lot from his experience It always was a pleasure to do experiments together, during his three visits to the Magnetlab and, in particular, my visit to Queen's University During this pleasant research stay in Canada the data reported in chapter 6 were taken

Die tatkraftige Unterstutzung von Dr Uli Zeitler in allen Bereichen hat sicherlich zum guten Gelingen beigetragen Besonders wichtig war es, einen kritischen (und begeisterungsfahigen) Diskussionspartner zu haben Auch einige seiner Demonstrationen in *effizientem Experimentieren* haben sicherlich einen positiven Effekt gehabt

Het feit dat een mengkoeler niet meer een onbegrijpelijk mysterie voor me is, is te danken aan Dr Stef Wiegers Hij heeft vooral gedurende de cruciale opstartfase van het experiment voor een groot deel ertoe bijgedragen dat het meten van thermospanningen in hoge magneetvelden bij millikelvin-temperaturen gerealiseerd werd Maar misschien even belangrijk om hier te vermelden, is het feit dat de lange meetnachten werkelijk nooit saai waren

Somewhere halfway the four years of this thesis I had intensive discussions with Dr Andrey Geim on the ideal sample design for termopower measurements in a two-dimensional electron gas The resulting samples were indeed the basis for the experimental results on two-dimensional systems presented in this thesis

Zonder de uitstekende technische ondersteuning op de universiteit en het magnetenlab zouden de hier beschreven experimenten niet mogelijk zijn geweest In het bijzonder gaat mijn dank uit naar Henk Neijenhuisen voor alle speciale electronica (bv *de Rolls-Royce onder de heater-schakelingen*) en naar Jos Rook voor alles rond de mengkoeler (ik weet de altijd lekdichte doorvoeren te waarderen) Verder wil ik iedereen op het magnetenlab, met name Martha Geurts en Elma Burg, bedanken voor alle hulp en ondersteuning Ik heb er

met veel plezier gewerkt.

Graag wil ik ook mijn mede-AiO's op het Magnetenlab bedanken voor de gezellige tijd samen. Een paar van hen wil ik speciaal noemen. Vanaf de eerste pilsjes op het Koningsplein zijn Ate van Steenbergen en ik een goed team geweest. Dit kwam ook goed van pas bij de opbouw (samen met Stef) vanaf nul van 'B/T', ons lage-temperaturen-lab dat nodig was voor het preciese voorbereidingswerk voor de metingen. Living and working in the Netherlands as a foreigner was not so bad at all. However, I must admit that sometimes it was very pleasant to share with Fausto Piazza our foreigners' point-of-views on some Dutch peculiarities. Moreover, his relaxed attitude often reminded me not to take physics too seriously (a very valuable influence). Sjoerd Lok heeft me met zijn onovertroffen hulpvaardigheid vele malen uitstekend geholpen. Het maakte absoluut niet uit of het om kleine klusjes ging of om het begeleiden van gasten gedurende meerdere weken. Marc Boonman organiseerde alles perfect, niet alleen de cabaret-bezoeken maar ook een bedrijfsbezoek aan ... mijn huidige werkgever. En Urs Wyder (en de velen anderen mensa-bezoekers) wil ik bedanken voor de altijd interessante gesprekken in de mensa.

Natuurlijk wil ik me ook bedanken bij de (min of meer) fanatieke vrijdagmiddagvoetballers die voor een altijd zeer stimulerende afsluiting van een zware werkweek zorgden. Ook al stonden op het veld vaak niet voldoende voetballers voor een kompleet elftal, het is verbazingwekkend hoe groot het totale aantal voetballers is, die ooit eens hebben meegedaan, zodat ik hier helaas niet iedereen met naam kan vermelden.

Schliesslich darf die andauernde Unterstützung meiner Eltern und Familie während des Studiums und der Promotion nicht unerwähnt bleiben, und möchte ich mich bei meinem Onkel Theodor Büldt bedanken, der durch seinen grosszügigen Beitrag ganz wesentlich zum Drucken dieses Buches beigetragen hat.

Ganz zum Schluss bedanke ich mich bei Armelle für all die Geduld, die sie in den letzten Jahren für diese Doktorarbeit aufgebracht hat.

Nijmegen, maart 1997 Benno Tieke

Contents

Introduction

The subject of this thesis is the study of magneto-quantum oscillations in the thermoelectric power of two-dimensional and three-dimensional metallic semiconductors. In a magnetic field the electronic density-of-states is altered into a set of energy levels, called Landau levels, separated by the cyclotron energy. This new energy level structure is reflected in magneto-oscillations in the resistivity (Shubnikov-de Haas effect) and in the magnetization (de Haas-van Alphen effect), effects which are extensively studied. Here we discuss magneto-oscillations in the thermoelectric power from which new information not yet exploited in the same detail as the more common de Haas-van Alphen and Shubnikov-de Haas effects can be obtained.

The thermoelectric power S is defined as the voltage difference ΔV between two contacts having different temperatures, i.e. $S = \Delta V/\Delta T$, where ΔT is the temperature difference. In magnetic fields, S is a tensor quantity with, just like the resistivity, two independent components, called thermopower S_{xx} and Nernst-Ettingshausen coefficient S_{yx}. In semiconductors there are two contributions to thermoelectric power (TEP), namely diffusion and phonon drag. Diffusion TEP is due to diffusive motion of electrons from the hot to the cold reservoir and can be easily understood from the difference in kinetic energy of hot and cold carriers.

The other mechanism is phonon drag TEP, denoted S^g, and is dominant in our range of experimental parameters. Here the most important effect of an applied temperature gradient ∇T is that it leads to a preferential flow of phonons from hot to cold. Through electron-phonon scattering this phonon flow causes direct momentum transfer to the electrons resulting in a drag current j_g. This momentum transfer is roughly analogous to the effect of an electric field E. Thus, the influence of the temperature gradient in phonon drag can be thought of as being equivalent to a fictitious electric field parallel to ∇T. Since there is no external current, there is a charge build-up and the drag current is compensated by a current j_e due to an electric field E. Thus, the ratio of electric field and temperature gradient is just the phonon drag TEP. In a magnetic field, which does affect the electronic system but hardly influences the phonons, there is a (Hall) angle between j_g and ∇T in exactly the same way as there is between j_e and E which gives $E \| \nabla T$ just like in zero magnetic field. Thus, to a first approximation only S_{xx} is expected to have a phonon drag part and $S^g_{yx} = 0$.

It is clear that this experiment provides information on the electron-phonon coupling which in a magnetic field, due to the quantized density-of-states, differs from that at zero field. To obtain a clearer image of the specific nature of this work, it is important to note that the nature of the electron-phonon interaction in metallic semiconductors is quite different from that of bulk metals. In metals, every atom contributes one or two electrons to the conduction band and this large number of electrons forms part of the "glue" that keeps

the lattice together. Propagating lattice vibrations, i.e. phonons, therefore are intimately coupled to the electronic system. In metallic semiconductors the carriers come from doping with a density many orders of magnitude below the number of elementary cells per unit volume and adjustable by controlling the doping level. Therefore, the free carriers play no significant role in the phonon properties of the material and the electronic and phononic properties are to a large extent decoupled. On the other hand, a metallic semiconductor has a metal-like electrical conductivity, i.e. finite conductivity at $T = 0$, and can therefore be described as a Fermi gas of electrons with a fixed electron concentration just like normal metals.

The present thesis deals with a three-dimensional (3D) and a two-dimensional (2D) model system. In three dimensions, the semiconductor HgSe is used which is degenerately doped with Fe to create an electron gas in the conduction band. This material has a high electron mobility and is known to show strong magneto-oscillations in the de Haas-van Alphen and Shubnikov-de Haas effect. For the 2D-system electrons in a triangular potential well formed at the interface of a heterostructure of two semiconductors having a different band gap are used. By doping in the semiconductor with the higher band gap, this potential well can be filled with electrons giving a (quasi-)2D electron gas (2DEG). These materials can nowadays be produced by growth techniques with mono-layer resolution, e.g. molecular beam epitaxy and metal organic vapour deposition. The material in which the highest electron mobilities and richest oscillatory structure are realized are GaAs-$Ga_{1-x}Al_xAs$ heterostructures. We have chosen this material as the model 2D electron system.

An interesting aspect of phonon drag TEP in 2DEGs and HgSe:Fe is the relative importance of the different scattering processes for electrons and phonons. The thermal conductivity is dominated by phonons and contrary to normal metals the electronic contribution is negligible. For phonons, scattering with electrons is negligible just because there are so few of them. The process limiting the phonon mean free path Λ at low temperatures is scattering at the sample boundaries giving a constant Λ. For electrons, the dominant scattering process at low temperatures is impurity scattering. However, because of the compensation origin of TEP the impurity relaxation time τ_{imp}, on which both j_g and j_e depend, cancels in the final result and the thermopower only depends on electron-phonon scattering. Thus, we have the remarkable situation that in 2DEGs and, to a lesser extent, in 3D degenerate semiconductors the phonons are not affected by the electrons and that the electrons are not affected by the phonons, but that in the presence of a temperature gradient the phonon drag TEP measures the electron-phonon interaction because all other scattering processes cancel out. This property makes TEP a subtle and unique probe of the electron-phonon interaction in metallic semiconductors.

The electronic structure of 2DEGs has brought up many surprising results, with the quantum Hall effect, for which K. von Klitzing was awarded the 1985 Nobel prize for physics, as the primary example. In this so-called *integer* quantum Hall effect, the Hall resistance of a 2DEG in high magnetic fields is found to show precisely quantized plateaus in units of h/ie^2, with i an integer, h Planck's constant, and e the electron charge, when the Fermi energy is in-between Landau levels. In this case, there are only localized states which do not contribute to transport. Consequently, the longitudinal resistivity vanishes at the same time. The remarkable accuracy of this quantization (of the order of 10^{-9} relative error) exceeding the precision of standard resistors has led to a new recommended

value for the Ohm based on the quantum Hall effect.

The *fractional* quantum Hall effect is of an entirely different origin although is experimentally observed as a very much similar behaviour which in the quantum-limit occurs at a fractional filling of the lowest Landau level. This effect cannot be understood in a single particle picture like the integer quantum Hall effect since the electronic density-of-states has no structure in the quantum limit. Instead, electron-electron interactions within a Landau level are important in this case. The most pronounced fraction, i.e. $\frac{1}{3}$, has theoretically been well understood in terms of a many-body trial-wavefunction. Ground states at other fractions (e.g. $\frac{2}{5}$, $\frac{3}{7}$, $\frac{4}{9}$ etc.), the so-called *daughter* states, can be constructed from this *parent* state, a method known as the hierarchical model. The quantitative agreement with experimental observations is good for the $\frac{1}{3}$-state but diminishes for the higher order states where the calculations also become more complex. The major shortcoming of this model was the lack of a simple picture for the underlying physics. Such an intuitive and entirely new picture of the fractional quantum Hall effect has recently been provided by the composite fermion model which postulates new quasi-particles, the composite fermions, consisting of an electron and an even number of magnetic flux quanta. This theory has initiated intensive research on the effects of these quasi-particles in the past few years.

The behaviour of the TEP in the integer quantum Hall effect has been established experimentally in the past but is still not completely understood. The component S_{xx} was reasonably well theoretically explained but the existence of a dominant phonon drag contribution to S_{yx} remains a mystery. In the fractional quantum Hall effect there have been first experimental observations of the TEP showing characteristic features such as two plateaus around a half and a quarter filling of the last Landau level and a strong enhancement in absolute value in this range. These features remained unexplained in the hierarchical model but nowadays they can be associated with composite fermions. The aim of the research project (concerning 2DEGs) described in this thesis was to study in detail the behaviour of TEP in the fractional quantum Hall effect experimentally and answer the two major open questions which in today's terminology can be formulated like this: 1) 'How does the phonon drag TEP of the new composite fermion quasi-particles behave?', and 2) 'Why does a phonon drag contribution to S_{yx} exist?'. This thesis presents a detailed experimental study of the phonon drag TEP in the fractional quantum Hall effect and answers both questions convincingly.

As compared to 2DEGs, surprisingly few experimental studies were reported on the magneto-thermopower of 3D metallic semiconductors. This is all the more astonishing since the theoretical description available for 2D can almost directly be applied to the 3D case. An interesting topic is the different electron-phonon coupling in 3D. Here phonons and free electrons exist everywhere in the sample contrary to 2D where the phonons propagate through the entire sample as well but the electrons are only present in a thin sheet. Therefore, the electronic system also influences the phonons in 3D. Like in 2D, the interplay between diffusion and phonon drag TEP is a key subject in 3D as well. In particular, the comparison of the Nernst-Ettingshausen coefficient S_{yx} in 2D and 3D provides deep insight into the similarities and differences of these two systems.

The thesis is structured as follows. Chapter 1 gives an introduction of composite fermions in connection with the fractional quantum Hall effect. Furthermore, the basic concepts of thermoelectric power in 2D and 3D are introduced. A Boltzmann theory for the case of zero magnetic field is described in detail which is adapted for experimental

thermopower data of composite fermions presented in chapters 3 and 5. Chapter 2 describes the experimental techniques to measure thermoelectric power at low temperatures.

Chapter 3 shows that the thermopower in the fractional quantum Hall effect can be interpreted as the thermopower of composite fermions. We find that different composite fermions with the same number of magnetic flux quanta bound in the composite fermion have the same value of the thermopower. The theoretical concept of an *effective* magnetic field which vanishes for certain filling fractions of a Landau level is confirmed by the very notable similarities with thermopower in *real* zero magnetic field.

In chapter 4, the Nernst-Ettingshausen coefficient in quantum Hall systems is shown to be given by the relation $S_{yx} = \alpha B(dS_{xx}/dB)$ which is similar to the relation between the resistivity components, $\rho_{xx} = \alpha B(d\rho_{xy}/dB)$. Moreover, the scaling factor α is the same for both rather different phenomena.

Chapter 5 describes the phonon drag thermoelectric power in the fractional quantum Hall regime in greater detail. In addition to the main findings which are highlighted in chapters 3 and 4 in concise form, chapter 5 shows the dependence of the thermopower on the crystallographic orientation of the temperature gradient which is due to phonon focusing.

Chapter 6 contains the complete picture of thermoelectric power in a 3D metallic semiconductor. The striking separation of phonon drag and diffusion into S_{xx} and S_{yx}, the effects of electron-phonon scattering not only on thermopower but also on the thermal conductivity, and the agreement with theory make HgSe:Fe a model system for thermoelectric power.

Chapter 1

Theory

1.1 Composite Fermion Description of the Fractional Quantum Hall Effect

In a magnetic field B, the density-of-states of a two-dimensional electron gas (2DEG) is given by discrete Landau levels. The number of occupied Landau levels is the filling factor $\nu = n_e h/eB$, where n_e is the electron density. At low temperatures and high magnetic fields, plateaus are observed in the Hall resistivity ρ_{xy} when ν is close to an integer value. At the same time, the longitudinal resistivity ρ_{xx} tends to zero (see Fig. 1.1). This is the integer quantum Hall effect discovered by K. von Klitzing in 1980 [1]. The value of the Hall resistance inside a plateau is given by fundamental constants, $\rho_{xy} = (h/e^2)/i = 1/i \times 25812.8\,\Omega$, where i is an integer corresponding to ν. This value is temperature and sample independent and constant in time. Therefore, the quantum Hall effect is used nowadays as the fundamental resistance standard [2].

The *fractional* quantum Hall effect, discovered by D. C. Tsui, H. L. Störmer, and A. C. Gossard [3], exhibits similar minima and plateaus at special fractional filling factors (see Fig. 1.1). The strongest features are observed at $\nu = \frac{1}{3}$ but also $\nu = \frac{2}{3}, \frac{1}{5}, \frac{2}{5}$ etc. show the same behaviour characteristic for the quantum Hall effect. This behaviour cannot be described within a single-particle picture like the integer quantum Hall effect. Obviously, electron-electron interactions are important in this case. The description of the fractional quantum Hall effect was a major challenge in theoretical solid state physics. The many particle ground state for $\nu = \frac{1}{3}$ constructed by R. B. Laughlin [4] was successful to describe this particular state. Other so called 'daughter' states can be derived from this 'parent' state. This concept evolved into the hierarchical model for the fractional quantum Hall effect giving all the fractions observed experimentally. Two reviews of the quantum Hall effect give many details of this theory [5, 6].

The hierarchical model treats the fractional quantum Hall effect starting at $\nu = \frac{1}{3}$ where the strongest minimum in ρ_{xx} appears. However, there is another characteristic filling factor in the experimental observations, namely $\nu = \frac{1}{2}$. At this filling factor apparently nothing happens, ρ_{xy} is linear here and ρ_{xx} is approximately constant, especially no activated minimum is observed. The state at $\nu = \frac{1}{2}$ is the starting point for the theory of composite fermions which was recently developed by J. K. Jain [7, 8] to describe the fractional quantum Hall effect. The theoretical treatment by B. I. Halperin, P. A. Lee, and N. Read [9] who predicted the existence of a Fermi surface for composite fermions was another important

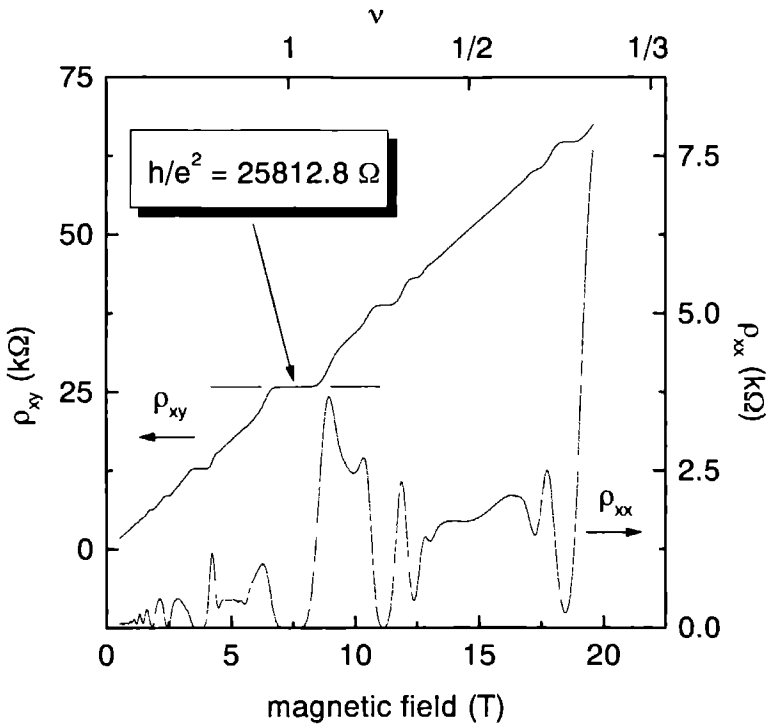

Figure 1.1: Example of the quantum Hall effect: ρ_{xy} has plateaus quantized in units of $h/e^2 = 25812.8\Omega$; ρ_{xx} has minima at integer and fractional filling factors. Data are at $T = 272$ mK for sample 1A (sample numbering as in chapter 5).

step in the understanding of the physics at $\nu = \frac{1}{2}$ and other even denominator filling factors.

A composite fermion is a quasi-particle consisting of an electron to which an even number Φ of magnetic flux quanta ϕ_0 is attached (see Fig. 1.2). $\phi_0 = \frac{h}{e}$ for a charge e. This picture is the equivalent to a gauge transformation using a Chern-Simons gauge field. The consequence of such a gauge transformation is that the magnetic field is rescaled to an effective magnetic field B_{eff},

$$B_{\text{eff}} = B - B_{1/2}, \tag{1.1}$$

where $B_{1/2}$ is the external magnetic field at $\nu = \frac{1}{2}$. Thus, $B_{\text{eff}} = 0$ for composite fermions at $\nu = \frac{1}{2}$. The transformation can be intuitively understood by comparing the number of electrons and flux quanta in the system. For $\nu = \frac{1}{2}$, the density of flux quanta is $B_{1/2}/\phi_0 = 2n_e$. Thus, per electron there are two flux quanta in the system. Combining each electron with two flux quanta to form a composite fermion effectively cancels the external field for the quasi-particles.

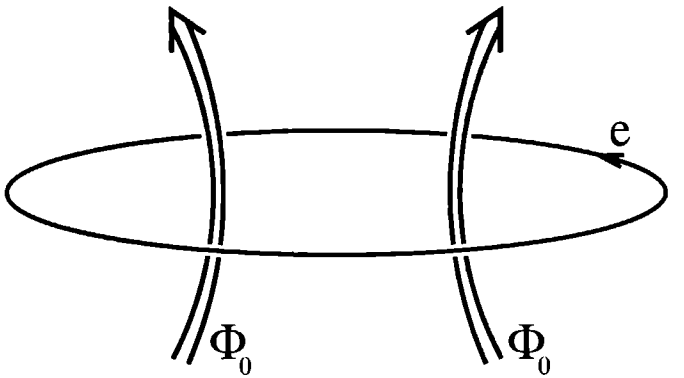

Figure 1.2: A composite fermion at $\nu = \frac{1}{2}$. Two flux quanta $\phi_0 = \frac{h}{e}$ are attached to an electron e.

After the above the term *composite* is clear. It remains to show that these quasi-particles are indeed fermions. The statistics of particles is characterized by how their wave functions behave under particle conjugation. Interchanging two quasi-particles yields a phase factor $\exp(i\theta)$ with $\theta = \pi(\Phi + 1)$ [9]. Of course, an electron without any flux quantum attached is a fermion ($\Phi = 0$), but also all quasi-particles with $\Phi = 2, 4, \ldots$ are fermions as well and therefore are denoted *composite fermions*.

The concept of a transformation of B to B_{eff} has its equivalent for the filling factor as well, and it is in fact this definition of effective composite fermion parameters which is one of the reasons why the composite fermion picture is so intuitive as a description of the fractional quantum Hall effect. The total filling factor ν can be expressed in terms of the effective filling factor $\nu_{\text{eff}} = n_e h/eB_{\text{eff}}$ for composite fermions as [8]

$$\nu = \frac{\nu_{\text{eff}}}{\Phi\nu_{\text{eff}} \pm 1}. \tag{1.2}$$

The + and − sign corresponds to positive and negative B_{eff}, respectively. ν_{eff} can be interpreted as the Landau level number of composite fermions. In the integer quantum Hall effect, $\Phi = 0$, hence ν and ν_{eff} are identical. For $\Phi \neq 0$, Eq. (1.2) gives all ν observed in the fractional quantum Hall effect just by going along the intuitive series $\nu_{\text{eff}} = 1, 2, 3, \ldots$. Table 1.1 and Fig. 1.3 apply this scheme in detail for a typical example of the measured thermopower S_{xx}. Note that the fractions with the lowest quantum numbers ν_{eff} and Φ are most pronounced whereas fractions with the highest quantum numbers are not observed (see Fig. 1.3). Therefore, the fractional quantum Hall effect can consistently be regarded as the integer quantum Hall effect of new quasi-particles formed in high magnetic fields, the composite fermions.

Properties characteristic for 'usual' fermions can be assigned to composite fermions as well. The composite fermion-state at $\nu = \frac{1}{2}$ has a well defined Fermi surface with Fermi wave vector k_F^Q and an effective mass m_Q^* can be attributed to the quasi-particles [9]. We denote all parameters referring to the quasi-particles (composite fermions) by an index 'Q'. However, k_F^Q and m_Q^* differ in some details from the known electron quantities. Since the

	$\Phi = 2$		$\Phi = 4$
ν_{eff}	ν^-	ν^+	ν^-
1	1	$\frac{1}{3}$	$\frac{1}{3}$
2	$\frac{2}{3}$	$\frac{2}{5}$	$\frac{2}{7}$
3	$\frac{3}{5}$	$\frac{3}{7}$	
4	$\frac{4}{7}$		
$\vdots$			
∞	$\frac{1}{2}$	$\frac{1}{2}$	$\frac{1}{4}$

Table 1.1: Scheme in the composite fermion model for fractional filling factors ν observed as minima in S_{xx} of sample 2 for fields up to $B = 30$ T. The first column is the effective filling factor ν_{eff} which indicates Landau levels of composite fermions in the fractional quantum Hall effect. Other columns give the corresponding total filling factor ν which are exactly the fractions observed in the experiment (see Fig. 1.3). Columns are for different composite fermion families with $\Phi = 2$ and 4 flux quanta, indices + and − give the sign used in Eq. (1.2).

electrons in the lowest spin-split Landau level are spin polarized, the composite fermions at $\nu = \frac{1}{2}$ are spin polarized, too, giving $k_f^Q = \sqrt{4\pi n_Q}$ which is a factor $\sqrt{2}$ bigger than for electrons in zero field, $k_f = \sqrt{2\pi n_e}$. n_Q and n_e are the density of quasi-particles and electrons, respectively.

The effective mass m_Q^* is strongly enhanced compared to the effective band mass m^* in GaAs, $m^* = 0.067 m_e$, where m_e is the free electron mass, typically by more than an order of magnitude as observed in resistivity measurements [10, 11]. Because m_Q^* originates from electron-electron interactions with energy scale $e^2/(4\pi\epsilon_0\epsilon l_0)$, where $l_0 = \sqrt{\nu/2\pi n_e}$ is the magnetic length, it is density dependent as $m_Q^* \propto \sqrt{n_Q} \propto \sqrt{B_{1/2}}$ [9]. m_Q^* for $\nu \to \frac{1}{2}$ is predicted to be weakly diverging [9]. There are indications for this behaviour in some transport experiments [12, 13], while in other similar measurements no such behaviour is seen [11].

This introduction to the composite fermion model mainly concentrated on the situation of $\nu = \frac{1}{2}$ and the corresponding composite fermion with $\Phi = 2$. However, the theory is more general. The application to a composite fermion with $\Phi = 4$ is straightforward. Higher values of Φ probably are not realistic because of the competition with the insulating phase which appears for $\nu \lesssim \frac{1}{5}$ [8]. Furthermore, other states can be described as composite fermions because of a) the symmetry between particles and holes in the last Landau level ($\frac{3}{4} \leftrightarrow \frac{1}{4}$), and b) a filled Landau level can always be added to an existing state ($\frac{3}{2} \leftrightarrow \frac{1}{2}$) [8, 9].

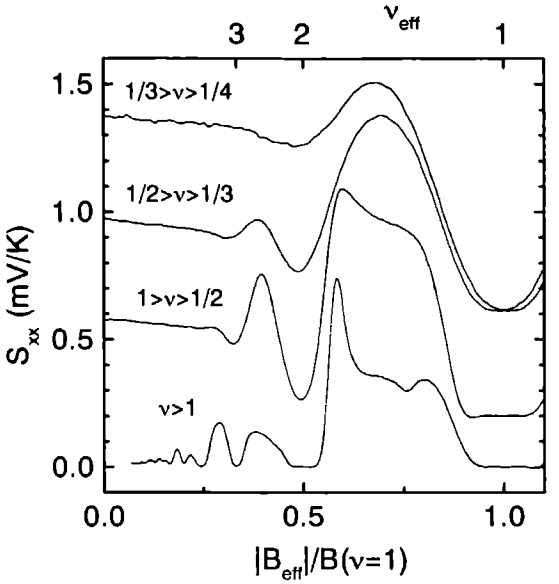

Figure 1.3: Example of the composite fermion description of the FQHE. Filling factors $\nu = \frac{1}{2}$ and $\nu = \frac{1}{4}$ are transformed to $B_{\text{eff}} = 0$. Minima with the same numerator, i.e. effective Landau level filling factor ν_{eff}, all align at the same position in B_{eff}. Data are from sample 2 at $T = 504$ mK for B up to 30 T. Curves $\frac{1}{3} > \nu > \frac{1}{4}$ and $\frac{1}{2} > \nu > \frac{1}{3}$ are offset by 0.6 mV/K and $1 > \nu > \frac{1}{2}$ by 0.2 mV/K, respectively.

1.2 Thermoelectric Power in Two and Three Dimensions

1.2.1 Basic Concepts of Thermoelectric Power

A temperature gradient ∇T applied to a conductor gives rise to an electric field $\boldsymbol{E}$,

$$\boldsymbol{E} = S\nabla T, \tag{1.3}$$

which is known as the Seebeck effect. The proportionality factor S is the thermoelectric power (TEP). Thermoelectric transport in general is given by the equations for the electrical and thermal current density, $\boldsymbol{J}$ and $\boldsymbol{U}$, respectively, under the influence of $\boldsymbol{E}$ and ∇T [14],

$$\boldsymbol{J} = \sigma\boldsymbol{E} - \epsilon\nabla T, \tag{1.4}$$

$$\boldsymbol{U} = T\epsilon\boldsymbol{E} - \lambda\nabla T, \tag{1.5}$$

where σ is the electrical conductivity, ϵ the thermoelectric tensor, and λ the thermal conductivity. Since TEP is measured without an external current, i.e. $\boldsymbol{J} = 0$, we have $\boldsymbol{E} = \rho\epsilon\nabla T$, thus the TEP is given by $S = \rho\epsilon$.

Without magnetic field in an isotropic crystal, the tensor S is a scalar. In a magnetic field perpendicular to the temperature gradient, there are two independent components, the thermopower S_{xx} and the Nernst-Ettingshausen coefficient S_{yx}. Expressed in components of ρ and ϵ these are

$$S_{xx} = \rho_{xy}\epsilon_{yx} + \rho_{xx}\epsilon_{xx}, \tag{1.6}$$

$$S_{yx} = \rho_{xx}\epsilon_{yx} + \rho_{yx}\epsilon_{xx}, \tag{1.7}$$

$S_{yy} = S_{xx}$, and $S_{xy} = -S_{yx}$.

In the limit of weak electron-phonon interaction there are two distinct processes, diffusion TEP S^d which is a result of the diffusive motion of electrons in a temperature gradient, and phonon drag TEP S^g which arises from momentum transfer from the phonons to the electrons, giving two independent contributions to the total TEP [15], i.e. $S = S^d + S^g$. Theoretical models for both mechanisms are rather similar for 2D and 3D. Diffusion thermopower is given by the Mott formula [15]

$$S^d = -\frac{\pi^2 k_B}{3|e|}\frac{k_B T}{\sigma}\left.\frac{d\sigma}{dE}\right|_{E_f}, \tag{1.8}$$

where E_F is the Fermi energy. In zero magnetic field for the 3D case one obtains [15]

$$S^d = -\frac{\pi^2 k_B}{3|e|}\frac{k_B T}{E_F}\left(\frac{3}{2} + p\right), \tag{1.9}$$

and for a 2DEG

$$S^d = -\frac{\pi^2 k_B}{3|e|}\frac{k_B T}{E_F}(1 + p), \tag{1.10}$$

where $p = (E_F/\tau)(\partial\tau/\partial E)|_{E_f}$ is the energy dependence of the electron scattering at E_f.

The dominant mechanism for the thermopower in 2DEGs and for 3D metallic semiconductors at low temperatures is phonon drag. The net phonon flow in a temperature gradient drags electrons with it due to electron-phonon scattering. Since there is no net current this drag current J^g is compensated via a current J^e due to an electric field. It is important to note that, for both phonons and electrons, electron-phonon scattering is by far a minor scattering event. The phonon mean free path Λ is limited by boundary scattering at low temperatures, the electron transport lifetime τ_t is dominated by τ_{imp}, the impurity scattering time. Because both drag and compensation current depend on τ_{imp}, and there is no net current, the thermopower is independent of τ_{imp}. Instead, the usually negligible electron-phonon scattering is observable in phonon drag TEP because there is a preferential scattering direction defined by the net phonon flow in ∇T.

The idea of a compensation of the drag current is used in two phenomenological approaches to describe phonon drag thermopower. The 'Peltier' approach goes back to the original model of phonon drag thermopower in three-dimensional semiconductors by C. Herring [16] and was applied to 2DEGs by R. J. Nicholas [17]. An electrical current $\boldsymbol{J}$ has an associated heat flow $\boldsymbol{U}$, $\boldsymbol{U} = \pi'\boldsymbol{J}$, where π' is the Peltier coefficient. Via the fundamental thermodynamic relation between π' and the thermopower, i.e. $S = \pi'/T$, S is calculated as [15, 17]

$$S = \frac{\Lambda v}{\mu_{\text{ph}} T}, \tag{1.11}$$

where μ_{ph} is the phonon limited electron mobility. Eq. (1.11) is valid for 2D and 3D in the limit of elastic scattering as was shown by comparison with Boltzmann equation results [18].

In another approach, the thermopower is calculated from the balance of the forces phonons and electric field exert on the electrons [15, 18]. In the 3D case,

$$S = \frac{\lambda}{n_{3D} e v^2} \tau_{pe}^{-1}, \tag{1.12}$$

and in the 2D case,

$$S = \frac{\lambda d}{n_{2D} e v^2} \tau_{pe}^{-1}, \tag{1.13}$$

with n_{3D} and n_{2D} the 3D and 2D electron density, respectively, d the thickness of the substrate, v the sound velocity, and τ_{pe}^{-1} the phonon relaxation rate due to scattering with electrons.

The results for both models, Eqs. (1.11-1.13), illustrate the characteristics of TEP discussed above, namely that at low temperatures, where electron-phonon interaction is negligible in the mobility, it is still observable in thermopower which can therefore provide unique information. Eq. (1.11) gives $S \propto \mu_{ph}^{-1}$. In resistance measurements, the contribution of μ_{ph}^{-1} becomes unmeasurably small. Eqs. (1.12) and (1.13) give $S \propto \tau_{pe}^{-1}$, i.e. S measures the relaxation time of the phonon system if the only process was scattering with electrons. However, the practical use of Eqs. (1.11-1.13) to interpret the experimental thermopower is limited since dependences on experimental parameters like n_e and T are hidden in the quantities μ_{ph} and τ_{pe}.

The basic principle of phonon drag remains the same in the presence of a magnetic field. Of course, there is the Hall angle between J^e and E and, in exactly the same way, between J^s and ∇T which gives $E \| \nabla T$ just like in zero magnetic field. Thus, neglecting quantum oscillations we expect S_{xx}^s to be constant and that $S_{yx}^s = 0$ in 3D and 2D. For 2DEGs, also detailed semi-classical calculations show that the magnetic field dependence is negligible at low temperatures [19]. According to theoretical considerations [15], S_{xx}^s reflects in high magnetic fields oscillations in the density-of-states and $S_{yx}^s = 0$. Thus, the Nernst-Ettingshausen coefficient is expected to be purely due to diffusion. In 3D, this is indeed found to be the case (see chapter 6). In 2D, however, S_{yx} is found to be dominated by phonon drag as well. The origin of S_{yx}^s is discussed in chapters 4 and 5.

1.2.2 Boltzmann Model for the Thermopower of a 2DEG in Zero Magnetic Field

For two-dimensional electron gases, a detailed theory of the phonon drag thermopower in zero magnetic field going beyond the simple models of section 1.2.1 has been formulated by B. G. Cantrell and P. N. Butcher who solve the coupled Boltzmann equations for the 2-dimensional electrons and the 3-dimensional phonons to obtain the phonon drag thermopower [20, 21]. We review this model in some detail here because we will apply it to composite fermions in section 1.2.3. For electrons, collisions with phonons and static scatterers are included, the latter being by far the dominating process. However, the phonon

scattering part is, of course, not negligible since it is responsible for the phonon drag thermopower. The phonons considered are bulk phonons in the acoustic branch, interface and surface phonons are neglected. Boundary scattering is assumed to be the dominant process determining the phonon mean free path Λ.

The electron-phonon interaction assumed in the original model is an unscreened deformation potential scattering. However, piezoelectric scattering plays an important role in GaAs-$Ga_{1-x}Al_xAs$ heterostructures at low temperatures as well. Its influence has been calculated by S. K. Lyo in an extension to the model of Cantrell and Butcher with the result that screened piezoelectric scattering gives the same temperature dependence as the calculations for unscreened deformation potential [22]. A combination of the two scattering processes yields good agreement [22] with experimental data of R. Fletcher *et al* [23].

In our treatment, we will write V_{eff} as an effective scattering potential. In quantitative calculations, V_{eff} has to be substituted by the expression for the considered scattering mechanism, i.e. for deformation potential scattering $V_{\text{eff}} = E_1$, where $E_1 = -11$ eV is the acoustic-phonon deformation potential, and for piezoelectric scattering $V_{\text{eff}}^2 = (eh_{14})^2 A/(q^2 + q_z^2)$, where $h_{14} = 1.2 \times 10^7$ V/cm is the piezoelectric constant, and the anisotropy factor $A = 9q^4q_z^2/2(q^2 + q_z^2)^3$ for longitudinal acoustic phonons and $A = (8q^2q_z^4 + q^6)/4(q^2 + q_z^2)^3$ for transverse acoustic phonons, respectively [19, 22], where q and q_z are the in-plane and out-of-plane phonon wave vector, respectively. The simplified notation puts forward all qualitative dependencies and facilitates the understanding of the underlying physics.

Solution of the Boltzmann equations results in the thermoelectric current due to phonon drag, J_x^g. Since a thermopower measurement is current-less ($J_x^g + J_x^e = 0$) there is a compensating electrical current J_x^e given by

$$J_x^e = \sigma_{xx} E_x = -\sigma_{xx} S_{xx}^g \nabla T. \tag{1.14}$$

Both J^g and J^e are proportional to τ_{imp} which therefore drops out of the final result for S_{xx}^g. Thus, the thermopower can be obtained from $S_{xx}^g \nabla T = \rho_{xx} J_x^g$. Both J^g and J^e are proportional to the transport lifetime τ_t which therefore drops out of the final result for S_{xx}^g given by [21]

$$S_{xx}^g = -A \iint \left| \int \phi^2(z) e^{iq_z z} dz \right|^2 \frac{q^3 (q^2 + q_z^2)\, V_{\text{eff}}^2}{\sqrt{(\hbar^2 k_l q/m^*)^2 - \left[\hbar\omega - (\hbar^2 q^2/2m^*)\right]^2}} \times \frac{e^\gamma}{(e^\gamma - 1)^2}\, dq\, dq_z, \tag{1.15}$$

with

$$A = \frac{\hbar m^* v \Lambda}{8\pi^3 k_B T^2 n_e e \rho'}. \tag{1.16}$$

where m^* is the effective electron mass, n_e the electron density, ρ' the mass density of GaAs, $\hbar\omega$ the phonon energy, and $\gamma = \hbar\omega/k_B T$. The double integral has to be calculated in the range where the argument of the square root is positive, i.e.

$$(\hbar^2 k_l q/m^*)^2 \geq (\hbar\omega - \hbar^2 q^2/2m^*)^2. \tag{1.17}$$

Eq. (1.17) represents in fact the energy and momentum conservation in the electron-phonon scattering event.

This expression can be simplified because [21]

$$\left| \int \phi^2(z) e^{iq_z z} dz \right|^2 = 1 \tag{1.18}$$

for the z-component of the scattering matrix element. This simplification is in fact a consequence of Heisenberg's uncertainty principle. The 2DEG is localized in z-direction within a distance δ resulting in an uncertainty of the momentum. Therefore, all scattering events with $q_z < q_z^c$, where q_z^c is a cut-off value for the wave vector, have matrix element unity. The cut-off value for the layer thickness δ_c for typical phonon wave vectors is [21]

$$\delta_c \simeq 3\pi/q_z = 3\pi\hbar v/k_B T. \tag{1.19}$$

At $T = 1$ K this corresponds to $\delta_c = 370$ nm, compared to typical potential widths in heterostructures of $\delta \sim 10$ nm. Thus, momentum conservation in the scattering event only has to be satisfied for the in-plane wave vector q and not for the z-component q_z. Consequently, the electron-phonon scattering between a 2DEG and acoustic phonons is very effective which is one of the reasons why phonon drag plays such a dominant role in these systems.

Equation (1.15) with simplification Eq. (1.18) is the final result of Cantrell and Butcher for GaAs heterostructures [21]. We now rewrite Eq. (1.15) in a further simplified form which is convenient in the interpretation. Defining dimensionless in-plane and out-of-plane phonon wave vectors $\xi = (\hbar v/k_B T)q$ and $\xi_z = (\hbar v/k_B T)q_z$, respectively, substituting these in Eq. (1.15) and using $\hbar\omega = \hbar v\sqrt{q^2 + q_z^2}$, we obtain

$$S_{xx}^g = -\frac{k_B^5}{8\pi^3\hbar^6} T^4 \frac{\Lambda}{v^6\rho'} \frac{m^*}{en_e} \iint \frac{\xi^3(\xi^2 + \xi_z^2)\, V_{\text{eff}}^2}{\sqrt{(\hbar k_F/m^* v)^2 \xi^2 - \left[\sqrt{\xi^2 + \xi_z^2} - (k_B T/2m^* v^2)\,\xi^2\right]^2}} \times \frac{e^{\sqrt{\xi^2+\xi_z^2}}}{\left(e^{\sqrt{\xi^2+\xi_z^2}} - 1\right)^2} d\xi\, d\xi_z. \tag{1.20}$$

In Eq. (1.20) we have split up the prefactor into numerical constants, the explicit temperature dependence, phonon parameters, and electron parameters coming from the conductivity of the 2DEG.

An interesting detail in Eq. (1.20) are the two factors scaling ξ in the denominator of the integral. The first one, $\hbar k_F/m^* v$, is the ratio of the momentum of an electron at the Fermi surface to the momentum of an electron moving with v, the second, $k_B T/2m^* v^2$, is the ratio of thermal energy to kinetic energy of an electron moving with v. Thus, the sound velocity v appears as a velocity for electrons here. This at first sight astonishing fact becomes clear in another approach which was used to calculate phonon drag currents in surface acoustic wave experiments. V. I. Fal'ko *et al* consider the system in the moving frame of the phonons in which the complete electron gas moves with velocity v with respect to the lattice [24].

1.2.3 Zero-Field Boltzmann Model for the Thermopower of Composite Fermions

The composite fermion theory describes the state at $\nu = \frac{1}{2}$ as a Fermi liquid in (effective) zero magnetic field (see section 1.1), thus it seems straightforward to apply the Boltzmann theory for zero field phonon drag thermopower to composite fermions. The Fermi wave vector k_F and the effective mass m^* are replaced by k_F^Q and m_Q^*, respectively. The transport lifetime changes as well but since both ρ_{xx} and J^g depend on τ_t it cancels in the final result for the thermopower. Furthermore, the scattering potential with phonons may differ for composite fermions compared to electrons. In lack of a microscopic theory for composite fermion-phonon scattering at the moment[1], we use the same scattering potential as for electrons. A different scattering potential can have an influence on the absolute value and the temperature dependence of the thermopower, the general behaviour is independent of that. Since our model should encompass apart from $\nu = \frac{1}{2}$ also other even denominator filling factors which can be described as composite fermions the quasi-particle density n_Q has to be modified as well. For $\nu = \frac{1}{2}$, we simply have $n_Q = n_e$. However, for $\nu = \frac{3}{2}$ only one third of all electrons form composite fermions, the other two thirds are regarded as electrons in a filled Landau level [9]. Table 1.2 gives n_Q for the filling factors of interest.

ν	$\frac{1}{2}$	$\frac{1}{4}$	$\frac{3}{2}$	$\frac{3}{4}$
n_Q	n_e	n_e	$\frac{1}{3}n_e$	$\frac{1}{3}n_e$

Table 1.2: Quasi-particle density n_Q for the even denominator filling factors which are described as composite fermions.

As described in section 1.2.2, S_{xx}^g is obtained from ρ_{xx} and J^g. In the composite fermion model the resistivity of the total system is given by [9]

$$\rho_{xx} = \frac{m^*}{n_e e^2 \tau_t} \times \frac{n_Q}{n_e}. \tag{1.21}$$

This expression for the resistivity does not seem to be in very good agreement with experimental observations on ρ_{xx} as discussed in Ref. [9]. The difficulty lies in the theoretical description of the impurity scattering dominated transport lifetime τ_t. However, since τ_t cancels out in the final result this problem does not concern the thermopower. The important characteristic of Eq. (1.21), which is essential for the further derivation, is the scaling with a factor n_Q/n_e [9] which certainly remains valid as has been observed in conductivity measurements in Corbino devices [26].

Also the current density has to be rescaled by such a factor. The fraction of the current

[1] Note added in proof: Very recently, scattering of composite fermions with acoustic phonons has been calculated [25].

carried by the quasi-particles is[2] [9]

$$J_Q = \frac{n_Q}{n_e} J_{\text{tot}}. \tag{1.22}$$

To proceed, k_F, m^*, and n_e are substituted by k_F^Q, m_Q^*, and n_Q, respectively, in the expression for J^g of Ref. [20]. Note that this is only the thermoelectric drag current of the quasi-particles. With Eq. (1.22) the *total* drag current is given by

$$J_{\text{tot}}^g = \frac{n_e}{n_Q} J_Q^g. \tag{1.23}$$

For the thermopower it follows that

$$S_{xx}^g = -\rho_{xx} J_{\text{tot}}^g = \left(\frac{m^*}{n_e e^2 \tau_t} \frac{n_Q}{n_e}\right) \left(\frac{n_e}{n_Q} J_Q^g\right) = \frac{m^*}{n_e e^2 \tau_t} J_Q^g. \tag{1.24}$$

Thus, analogously to Eq. (1.20) the thermopower of composite fermions at even denominator filling factors with $B_{\text{eff}} = 0$ is given by

$$S_{xx}^{g,Q} = -\frac{k_B^5}{8\pi^3\hbar^6} T^4 \frac{\Lambda}{v^6 \rho'} \frac{m^*}{e n_e} \iint \frac{\xi^3 (\xi^2 + \xi_z^2)\, V_{\text{eff}}^2}{\sqrt{(\hbar k_I^Q / m_Q^* v)^2 \xi^2 - \left[\sqrt{\xi^2 + \xi_z^2} - (k_B T / 2 m_Q^* v^2)\, \xi^2\right]^2}} \times \frac{e^{\sqrt{\xi^2+\xi_z^2}}}{\left(e^{\sqrt{\xi^2+\xi_z^2}} - 1\right)^2} d\xi\, d\xi_z. \tag{1.25}$$

Note that inside the scattering integral the parameters are related to composite fermions whereas the prefactor contains the quantities n_e and m^* related to the total electron system.

The advantage of writing S_{xx}^g as a function of ξ and ξ_z in the form of Eq. (1.25) becomes obvious when studying the integral for typical experimental parameters. We denote the function inside the integral (without V_{eff}^2) as $f(\xi, \xi_z)$ and plot it for different cases in Fig. 1.4 and 1.5. The parameters are $m^* = 0.067 m_e$ and $m_Q^* = m_e \simeq 15 m^*$, where m_e is the free electron mass, $n_e = 1.75 \times 10^{15}$ m^{-2}, and $T = 0.5$ K, except where indicated otherwise. The plots mainly give examples for the composite fermion case. However, the situation for electrons is very similar.

The first observation is that $f(\xi, \xi_z)$ is nearly temperature independent, especially in its effect on S_{xx} because the important quantity is $\int f(\xi, \xi_z)\, d\xi\, d\xi_z$. The function $f(\xi, \xi_z)$ has two weak divergences, one at approximately[3] $q \simeq 2k_I$ and the other at small ξ for finite values of ξ_z. Cantrell and Butcher have shown that the divergences can be treated using lifetime broadening and, since the divergences are weak, $\int f(\xi, \xi_z)\, d\xi\, d\xi_z$ remains finite [21]. The divergence at $q = 2k_I$ is associated with the Kohn anomaly and gives a maximum in S_{xx}/T^3 when the dominant phonon wave vector q_d, the maximum of $f(\xi, \xi_z)$, coincides

[2] Equation (1.22) is quite a subtle relation. It implies that for $n_Q \neq n_e$ a certain quasi-particle current is necessarily accompanied by an electron current in a filled Landau level. The application of this relation is crucial for obtaining the final result for S_{xx} in agreement with experimental observations as will be clear from the remainder of this chapter.

[3] The exact position of the divergence is $(k_B T/\hbar v)\xi = q = 2k_I(1 + m^* v/\hbar k_I)$ for $\xi_z = 0$.

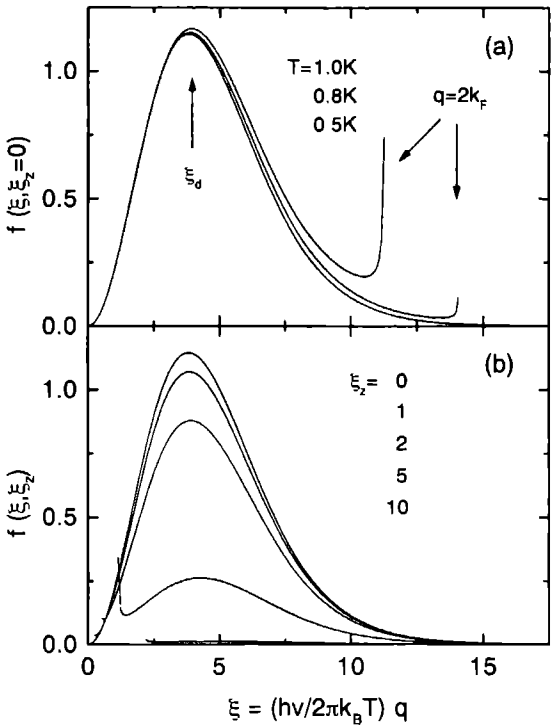

Figure 1.4: $f(\xi, \xi_z)$ giving the electron-phonon interaction as a function of in-plane phonon wave vector ξ for composite fermions at $\nu = \frac{1}{2}$. a) $f(\xi, \xi_z)$ for three different temperatures for $\xi_z = 0$. The divergence at $q = 2k_F^Q$ which is visible at higher T has only negligible effect on $\int f d\xi$ below $T \approx 1$ K. b) Influence of finite out-of-plane wave vector ξ_z on $f(\xi, \xi_z)$. Phonons with small ξ_z contribute most. The second divergence at low ξ again has only minor effect on $\int f d\xi$.

with $2k_I$ [21]. Such maxima have been observed experimentally in Si-MOSFETs [15] and in GaAs-heterostructures typically around $T \sim 2$ K [15, 27, 28].

The reason for $f(\xi, \xi_z)$ being nearly temperature independent is that the dominating term in the denominator of $f(\xi, \xi_z)$ is $(\hbar k_F/m^* v)^2 \xi^2$. Therefore, we can make the approximation of leaving out the other terms in the denominator and simplify Eq. (1.25) further to

$$S_{xx}^{g,Q} = -A' T^4 \frac{m^*}{n_e} \iint \frac{m_Q^* v}{\hbar k_F^Q} \xi^2 (\xi^2 + \xi_z^2)\, V_{\text{eff}}^2 \frac{e^{\sqrt{\xi^2+\xi_z^2}}}{\left(e^{\sqrt{\xi^2+\xi_z^2}} - 1\right)^2} d\xi\, d\xi_z, \tag{1.26}$$

with $A' = (k_B^5 \Lambda / 8\pi^3 \hbar^6 v^6 \rho' e)$. Eq. (1.26) is indeed a good approximation as can be seen in Fig. 1.5 (a) where we plot the full [Eq. (1.25)] and approximate [Eq. (1.26)] expression for

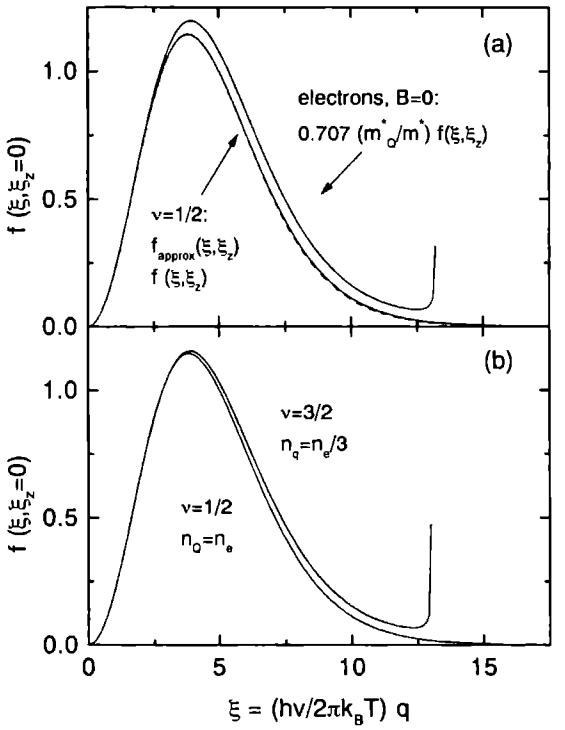

Figure 1.5: a) The complete $f(\xi, \xi_z)$ (full curve) and approximated $f_{\text{approx}}(\xi, \xi_z)$ (dashed curve) are indistinguishable for composite fermions. For electrons, the complete $f(\xi, \xi_z)$ multiplied with the scaling factor $m_Q^*/m^*\sqrt{2}$ of approximation Eq. (1.26) is close to $f(\xi, \xi_z)$ for $\nu = \frac{1}{2}$. b) $f(\xi, \xi_z)$ is nearly identical for $\nu = \frac{1}{2}$ and $\nu = \frac{3}{2}$.

$\nu = \frac{1}{2}$ which agree to high accuracy. Moreover, $f(\xi, \xi_z)$ for electrons from Eq. (1.20) multiplied by $m_Q^*/m^*\sqrt{2}$, which should be the appropriate scaling factor according to Eq. (1.26), is equal to $f(\xi, \xi_z)$ for $\nu = \frac{1}{2}$. Fig. 1.4 (b) shows that $f(\xi, \xi_z)$ is the same for $\nu = \frac{1}{2}$ and $\nu = \frac{3}{2}$ which is in fact equivalent to changing n_Q by a factor of three. The reason is that both k_f^Q and m_Q^* scale as $\sqrt{n_Q}$.

With Eq. (1.25) and its approximation Eq. (1.26) we have obtained expressions ideal for comparison with experimental results. All dependencies on experimental parameters have become explicit. The electron-phonon interaction is expressed by an universal integral $\int f(\xi, \xi_z)\, d\xi\, d\xi_z$ which is approximately independent of experimental parameters[4].

[4]There still is a hidden dependence of $\int f(\xi, \xi_z)\, d\xi\, d\xi_z$ on temperature. The upper integration limit ξ^u is defined by Eq. (1.17), i.e. $\xi^u \propto q/T = 2k_f/T$. However, because of the Bose factor of the phonon density-of-states $f(\xi, \xi_z) \to 0$ for high values of ξ. Thus, the contribution for $\xi > \xi^u$ to $\int f(\xi, \xi_z)\, d\xi\, d\xi_z$ is negligible if $q_d \ll 2k_F$ and there is indeed no temperature dependence.

1.3 References

[1] K. von Klitzing, G. Dorda, and M. Pepper, Phys. Rev. Lett. **45**, 494 (1980).

[2] *Landolt-Börnstein, Numerical Data and Functional Relationships in Science and Technology*, Vol. Units and Fundamental Constants in Physics and Chemistry of *New Series*, edited by O. Madelung (Springer-Verlag, Berlin, 1993), pp. 107–116.

[3] D. C. Tsui, H. L. Stormer, and A. C. Gossard, Phys. Rev. Lett. **48**, 1559 (1982).

[4] R. B. Laughlin, Phys. Rev. Lett. **50**, 1395 (1983).

[5] *The Quantum Hall Effect*, edited by R. E. Prange and S. M. Girvin (Springer-Verlag, New York, 1987).

[6] *The Fractional Quantum Hall Effect*, edited by T. Chakraborty and P. Pietiläinen (Springer-Verlag, Berlin, 1988).

[7] J. K. Jain, Phys. Rev. Lett. **63**, 199 (1989).

[8] J. K. Jain, Adv. in Phys. **41**, 105 (1992).

[9] B. I. Halperin, P. A. Lee, and N. Read, Phys. Rev. B **47**, 7312 (1993).

[10] R. R. Du, H. L. Stormer, D. C. Tsui, L. N. Pfeiffer, and K. W. West, Phys. Rev. Lett. **70**, 2944 (1993).

[11] D. R. Leadley, R. J. Nicholas, C. T. Foxon, and J. J. Harris, Phys. Rev. Lett. **72**, 1906 (1994).

[12] R. R. Du, H. L. Stormer, D. C. Tsui, A. S. Yeh, L. N. Pfeiffer, and K. W. West, Phys. Rev. Lett. **73**, 3274 (1994).

[13] P. T. Coleridge, Z. W. Wasilewski, P. Zawadzki, A. S. Sachrajda, and H. A. Carmona, Phys. Rev. B **52**, 11603 (1995).

[14] N. W. Ashcroft and N. D. Mermin, *Solid State Physics* (Saunders College, Philadelphia, 1976).

[15] B. L. Gallagher and P. N. Butcher, in *Handbook on Semiconductors*, edited by P. T. Landsberg (Elsevier, Amsterdam, 1992), Vol. 1, pp. 721–816.

[16] C. Herring, Phys. Rev. **96**, 1163 (1954).

[17] R. J. Nicholas, J. Phys. C: Solid State Phys. **18**, L695 (1985).

[18] M. J. Smith and P. N. Butcher, J. Phys.: Condens. Matter **2**, 2375 (1992).

[19] X. Zianni, P. N. Butcher, and M. J. Kearney, Phys. Rev. B **49**, 7520 (1994).

[20] D. G. Cantrell and P. N. Butcher, J. Phys. C: Solid State Phys. **20**, 1985 (1987).

[21] D. G. Cantrell and P. N. Butcher, J. Phys. C: Solid State Phys. **20**, 1993 (1987).

[22] S. K. Lyo, Phys. Rev. B **38**, 6345 (1988).

[23] R. Fletcher, J. C. Maan, and G. Weimann, Phys. Rev. B **32**, 8477 (1985).

[24] V. I. Fal'ko and S. V. Iordanskii, J. Phys.: Condens. Matter **4**, 9201 (1992).

[25] D. V. Khveshchenko and M. Y. Reizer (unpublished).

[26] L. P. Rokhinson, B. Su, and V. J. Goldman, Phys. Rev. B **52**, 11588 (1995).

[27] U. Zeitler, J. C. Maan, P. Wyder, R. Fletcher, C. T. Foxon, and J. J. Harris, Phys. Rev. B **47**, 16008 (1993).

[28] U. Zeitler, *Electronic transport in three-dimensional and two-dimensional metallic semiconductors under extreme quantum conditions*, Vol. 441 of *Konstanzer Dissertationen* (Hartung-Gorre Verlag, Konstanz, 1994), Ph.D. thesis, Universität Konstanz.

Chapter 2

Experimental Technique

The basic principle of a measurement of the thermoelectric power is to apply a temperature gradient to a device and measure the resulting voltage. For a thermopower measurement at low temperatures, a good thermal joint is needed to a cold sink on one end and to a heater on the other end of the sample, and the sample has to be in vacuum to maintain a uniform temperature gradient. The required techniques have been described by Fletcher *et al* in the ^{4}He temperatures range [1] and by Zeitler *et al* in the ^{3}He temperatures range [2, 3]. The measurements on 3D metallic semiconductors described in chapter 6 were done in a ^{4}He-cryostat following these principles. To reach even lower temperatures in the experiments on 2DEGs, we have set up the experiment in a ^{3}He/^{4}He-dilution refrigerator which is described in detail in this chapter along with general considerations valid also at higher temperatures.

The setup is designed for use in very high magnetic fields available at the High Field Magnet Laboratory in Nijmegen, in particular a 20 T, 32 mm room temperature bore Bitter magnet and a 30 T hybrid magnet, i.e. a Bitter magnet placed in a huge superconducting magnet supplying a background field. Therefore, special care has to be taken to avoid eddy current heating. Eddy currents are due to a variation of the magnetic field in time and to vibrations of conducting parts in the magnetic field, conditions which are more severe in water-cooled Bitter magnets than in superconducting magnets commonly used in research laboratories. The particular demands are met by the plastic dilution refrigerator built at the High Field Magnet Laboratory [4, 5]. The mixing chamber and the heat exchangers near the field center are made from HYSOL epoxy [6] and kapton polyimide films.

2.1 Sample Holder for Thermopower Measurements

Since the sample has to be in vacuum to ensure a uniform temperature gradient, a HYSOL sample holder is designed which places the sample in the inner vacuum space underneath the mixing chamber (see Fig. 2.1 for a schematic drawing and Figs. 2.2 and 2.3 for photographs of the sample holder). The inner diameter of the vacuum can is 19 mm. Allowing for a 2 mm clearance around[1] leaves a an effective space for the experiment of 15 mm

[1]This rather large clearance is chosen because a touch with the vacuum can, which is at $T = 4.2$ K, would disturb the temperature gradient and could even lead to the sample breaking off.

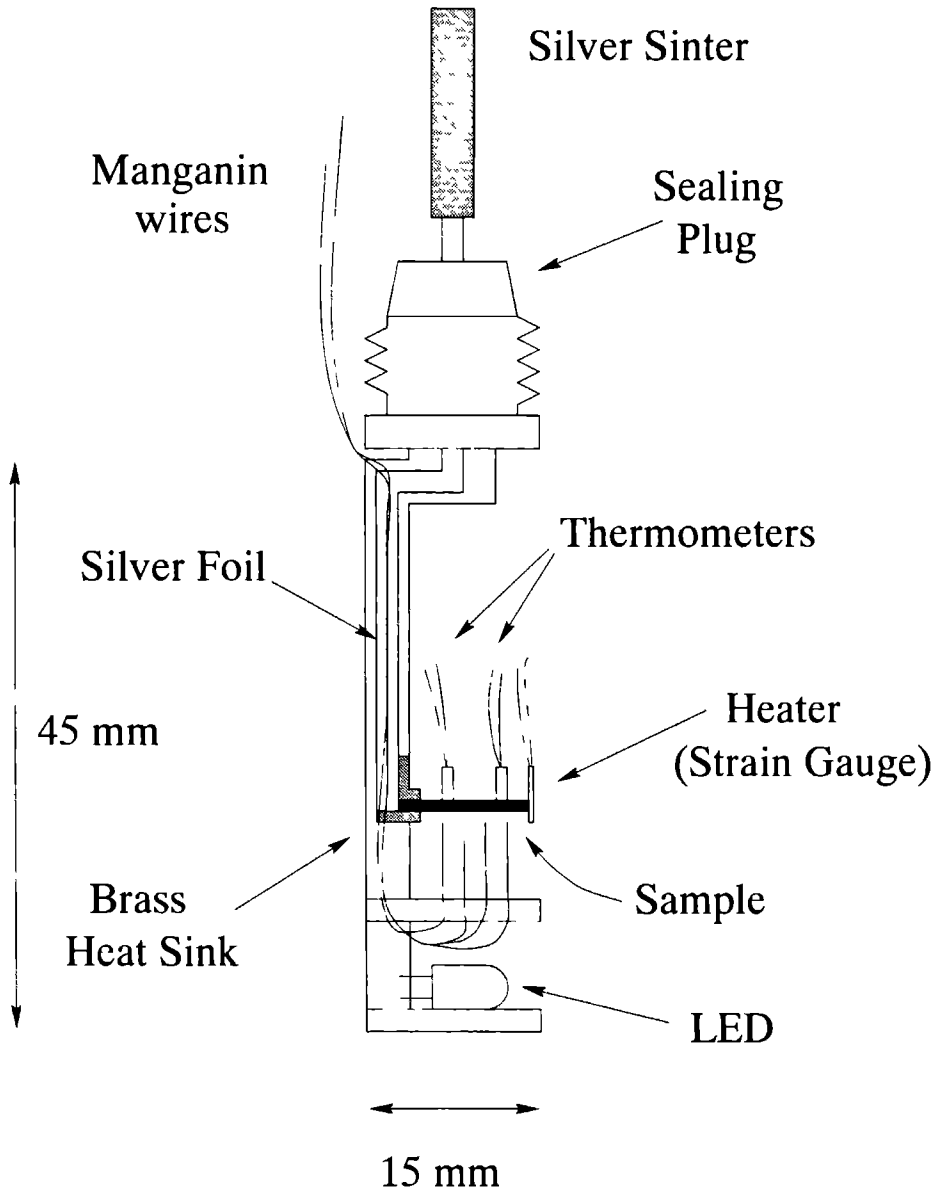

Figure 2.1: Sketch of sample holder for thermopower measurements. Side view as in photograph of Fig. 2.2. Note that the backside of the sample with the thermometers glued to it is pointing upwards and the front side with the 2DEG downwards.

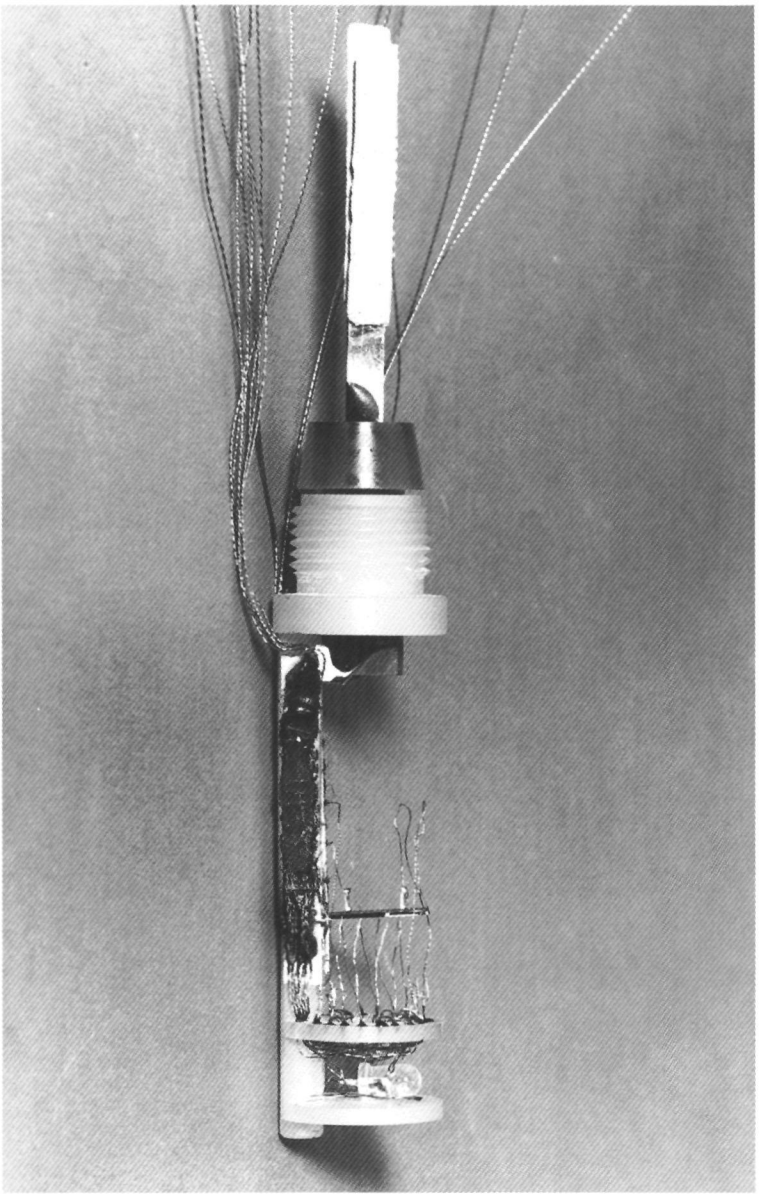

Figure 2.2: Side view of sample holder with mounted sample. Elements are as in drawing Fig. 2.1.

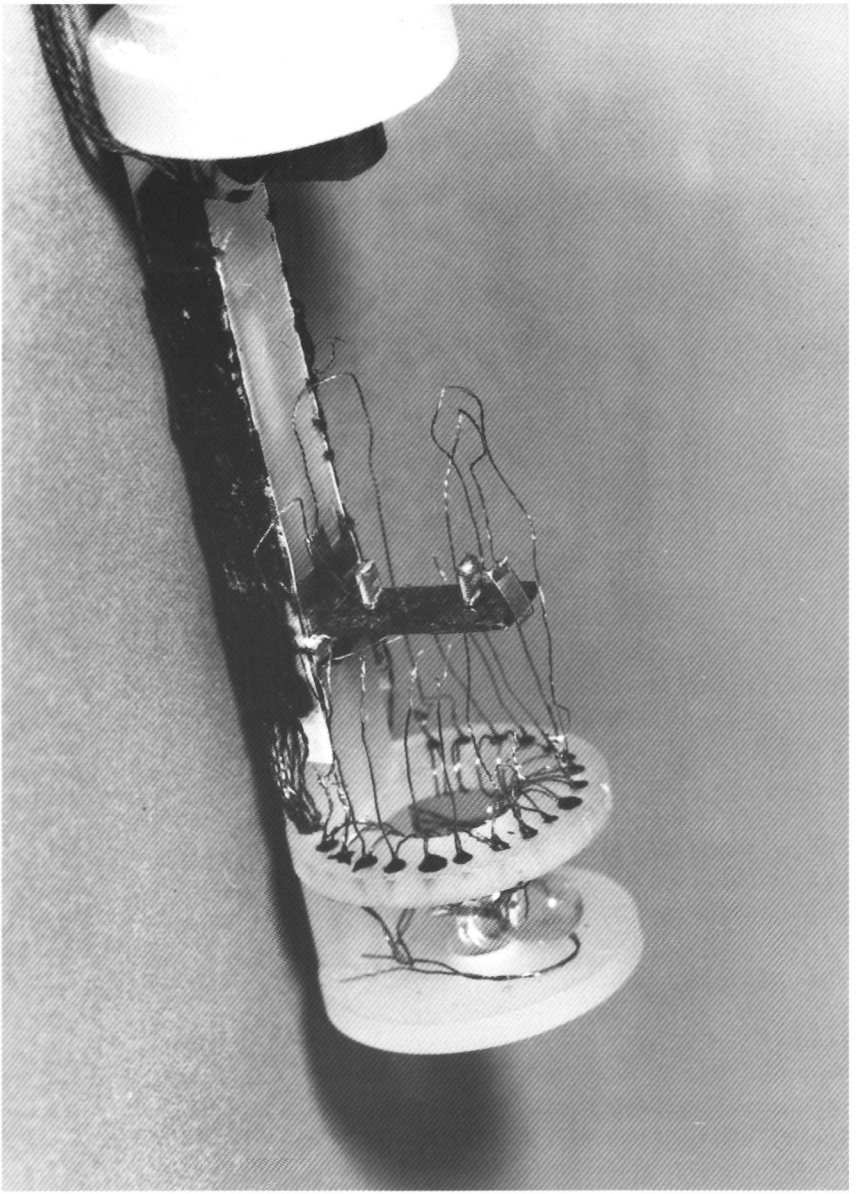

Figure 2.3: Angled view of sample holder with mounted sample.

diameter which is also the outer diameter of the mixing chamber.

The GaAs sample is soldered with indium to a brass support piece in the sample holder. The indium provides a reasonably good thermal contact and takes part of the strain due to the difference in thermal expansion, thus preventing the sample from breaking off during cooldown. Strips of annealed silver foil (thickness 125 μm, residual resistance ratio $\sim$ 800 after annealing) [7] are soldered with non-superconducting solder to the brass piece. The silver strips go into the mixing chamber via a feedthrough. On the mixing chamber side, the silver foils are surrounded by sinters of pressed silver powder [8] which were fabricated following a standard procedure [9]. In this way, the sample is on one end thermally anchored to the mixing chamber.

A heater is glued with STYCAST epoxy [10] directly to the other end of the sample. As heater resistors we used strain gauges. Although strain gauges are developed for a completely different reason, they are ideal for our purpose. The gauges used are small grids of constantan on a thin polyimide supporting film [11]. Their resistance is nearly temperature independent with only small magnetoresistance (5% at 20 T). The heater and thermometers are connected to the contact board by 50 micron manganin wires to ensure that the applied heat is conducted to the cold sink only through the sample.

The wiring is done using twisted pairs of 100 micron manganin wires, the wiring for thermometers and heaters consists of double twisted pairs enabling 4-point measurements. The thermoelectric power of manganin, which has to be considered due to the temperature differences of the contacts, is negligible compared to the thermopower of the 2DEG. The wires are thermally anchored first to the 1K-plate, which is about 70 cm above the sample holder, and then to the mixing chamber by gluing them to the silver foils with STYCAST. In this way, the external heat load to the sample was minimized. The manganin wires were distributed onto a connector board. Electrical connections to the sample were done with 2.5 micron gold bond wire which was chosen because it is more flexible than the stiff manganin and therefore reduces the possibility for the sample breaking. The bond wires were connected to the contact pads of the heterostructure with EPO-TEK [12], a silver filled epoxy which provides low resistance contacts with high mechanical strength. Furthermore, the sample holder contains an infrared LED operating at low temperatures to change the electron density of the 2DEG.

2.2 Temperature Calibration

To obtain reliable absolute values for the thermopower, an accurate knowledge of temperature and temperature gradient is essential. For this purpose, two resistance thermometers were glued with STYCAST directly to the backside of the substrate. Thermometers used were matched pairs of RuO_2 chip resistors of either Dale Electronics (1kΩ room temperature value) [13] or Philips (2.21 kΩ) [14] depending on the experimental run. Both resistor types were suitable, with the Philips resistors having the advantage of more sensitivity at higher temperatures around $T = 1$ K and negligible magnetoresistance. The magnetoresistance of the Dale resistors, which was determined in a separate calibration, is positive and typically 10% at 20 T. It was corrected for in the temperature calibration.

The thermometers were at zero magnetic field calibrated to a Speer resistor situated in the mixing chamber which in turn had been calibrated before down to $T = 50$ mK

with a Lakeshore germanium temperature sensor [15]. This calibration of the RuO_2 thermometers[2] was done, of course, without applying any power to the sample heater assuming that the sample is in thermal equilibrium with the mixing chamber. This assumption is valid down to about $T = 100$ mK which was checked by monitoring a RuO_2 resistor of the same batch in the mixing chamber. The calibration consists of two parts, one for R_{cold} against T, where R_{cold} is the resistor close to the thermal anchoring, and another one for ΔR against R_{cold}, where ΔR is difference between the two thermometers on the sample. For a thermopower measurement, the 'zero-heat offset' in ΔR is subtracted from ΔR with applied heater power.

The resistance values were measured in a bridge setup by matching an external calibration resistor to R_{cold} and ΔR, respectively. A Lock-In at a frequency of 33 Hz was used as a Null-detector. The advantage of this method is that the difference between the two thermometers, which is necessary to obtain the temperature difference ΔT, is measured directly. Two independent measurements of R_{cold} and R_{hot}, where R_{hot} is the resistor close to the heater, would result in a too big experimental error for ΔT. This advantage is more important than the little disadvantage, which in the experiment proves not to be severe, that this method is a 2-point measurement including the lead resistance of the wires. The calibrated Speer resistor is measured 4-point. Typical accuracies are better than 10^{-3} for R_{cold} and better than 10^{-2} for ΔR with somewhat higher errors at the low and high temperature ends of the calibration.

The thermometry was checked by determining for every calibration point[3] (T, ΔT) needed for a thermopower measurement the thermal conductivity λ as well using the measured heater power. λ was always found to have a T^3-dependence characteristic for phononic thermal conductivity in the boundary scattering limit. Calibration points in high magnetic fields were consistent with the calibration in zero field. The calibration for magnetic field sweeps was done at a small finite field of typically 0.2 T due to the particular regulation of the power supply of the Bitter magnets. The finite field also ensures that the indium solder used for the thermal contact of the sample to the cold finger is in the normal state and not superconducting as in zero field, thus giving the same thermal contact as for the entire field range. The low field calibration was completed with additional calibrations at high fields.

2.3 Heater Excitation and Signal Detection

The thermoelectric power was measured both DC and AC. DC-measurements, which was mainly useful in zero magnetic field, were done with an analogue EM-Electronics nanovoltmeter [16]. Data acquisition was automated taking averages over many 'on/off' switches of the heater. An accuracy for the thermoelectric voltage of about 1 nV standard deviation was achieved. This small error enabled us to measure the zero field thermopower down to below 250 mK where typical signals are as low as a few nanovolts.

Because in magnetic fields the noise level of DC-measurements increases, thermopower was measured with a low-frequency AC Lock-In technique for the field sweeps.

[2] In some experimental runs, RuO_2 thermometers directly calibrated to the Lakeshore thermometer were used. This method gave no different results from the standard procedure described here.

[3] The temperature T given for thermopower and thermal conductivity in this thesis is the mean temperature of R_{hot} and R_{cold}.

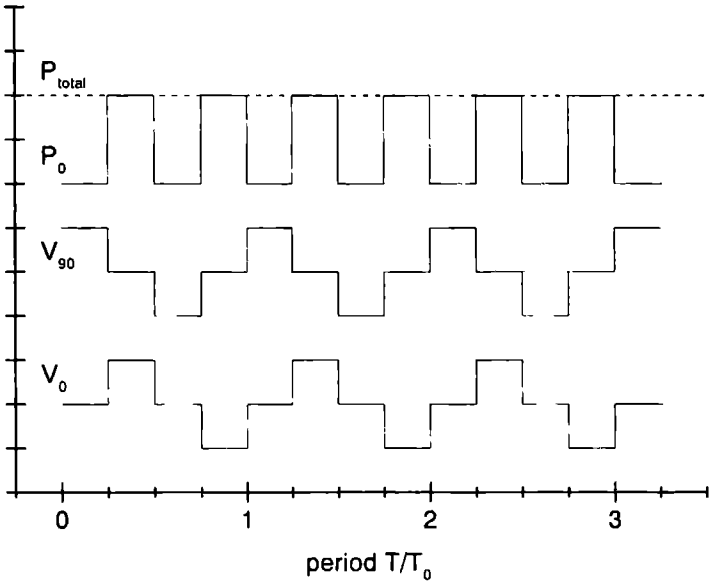

Figure 2.4: Wave form of the heater voltage and resulting power. V_0 and V_{90} are the voltages of the sample heater and the 90° phase shifted heater on the cold finger, respectively. P_0 and P_{total} are the power on the sample and the total power dissipated, respectively.

At low temperatures, such an AC-technique is possible because the thermal response times of the system are fast enough to establish a temperature gradient. We used a block wave with alternating signs with typical frequencies in the range of 5 ... 10 Hz (see Fig. 2.4). A block wave was chosen because it approaches a quasi-steady state during the time the heater is 'on' or 'off'. Thus, the AC-measurement is thermally equivalent to a DC thermopower measurement and the temperature calibration obtained DC can be applied to the AC thermopower measurement. The alternating sign ensures that the fundamental frequency of the dissipated power is twice the fundamental frequency of the heater voltage which excludes effects of voltage pick-up in the thermopower detection. In addition, we placed a second heater on the cold finger near the thermal anchoring of the sample. The excitation voltage of the second heater was the same as for the 'real' heater on the sample but with a 90° phase shift. Thus, the second heater dissipates the same amount of power on the cold finger in the period where there is no dissipated power in the sample heater. This extra heat prevents the sample from cooling too much in average temperature during that period and keeps the total dissipated power constant in time. The second heater was found to have only minor effect on the measured thermopower.

To obtain absolute thermopower values from AC-measurements, one needs to scale the raw voltage by a conversion factor. Because measurements are done using a band pass filter, the Lock-In detects only the first Fourier component of the block-wave excitation which has the prefactor $2/\pi$ in the Fourier series. Furthermore, the Lock-In gives

rms-values which adds a factor of $1/\sqrt{2}$. Thus the ideal AC-to-DC conversion factor is $\pi/\sqrt{2} = 2.221$. In the experimental situation there is an additional signal reduction, e.g. because the excitation frequency is too high for the temperature gradient to follow completely. The experimental factor is determined by measuring the temperature dependence of the thermopower at zero (or any fixed) magnetic field both DC and AC. For a typical measurement frequency of about 7 Hz the experimental AC-to-DC factor is ~ 2.7; a slight temperature and excitation dependence is accounted for in the analysis.

The heater excitation circuit was designed to give a constant heater power. If a resistance R_p of the same value as the load resistance $R = R_0$ is put in series with R, then the power dissipated in R, i.e. the sample heater, is to first order constant even if the load resistance changes, $R = R_0 + \delta R$. The dissipated power P is given by

$$P = \frac{V_0^2}{R_0} \times \frac{1+x}{(2+x)^2}, \tag{2.1}$$

where V_0 is the voltage of the (ideal) voltage source and $x = \delta R/R_0$ is the relative change in resistance. E.g. a relative change of the heater resistance by $x = 10\%$ changes the dissipated power only by less than 0.3%.

2.4 Sample Design

The 2DEG-samples for chapters 3 to 5 of this thesis are GaAs-$Ga_{1-x}Al_xAs$ heterostructures MBE-grown at the University of Nottingham. All samples with slightly differing geometry were taken from the same wafer. Electron density n_e and mobility μ could be varied in the range $n_e = 1.0 \ldots 1.9 \times 10^{15}$ m^{-2} and $\mu = 60 \ldots 100$ m^2/Vs, respectively, by illumination with an infrared light emitting diode using the persistent photoconductivity effect.

The sample masks defining the Hall bar for the 2DEG were designed for the particular demands of thermopower measurements. The amplitude of the measured voltages depends of course on the applied temperature gradients. In contrast to resistivity measurements, where the applied current can be varied over wide ranges, the applied gradients are much more restricted because a strong increase in heater power heats up the sample considerably. Therefore, signals at low temperatures are typically in the order of microvolts or less and any tool to maximize the measured signals has to be used.

In order to obtain the maximum temperature difference between contacts, the Hall bar has to be as long as possible; in our case the length of the mesa is $l_m = 4$ mm. A typical sample mask is shown in Fig. 2.5. Note that the measured voltage does not depend on the width of the mesa in contrast to a resistivity measurement where the important geometry factor is l_m/w_m. The thermopower S_{xx} is best measured on what would be called 'current contacts' in a resistivity measurement. Note that in a thermopower measurement there are no current contacts since the driving force for the potential difference is the temperature gradient. In the experiment, thermopower voltages measured on 'current contacts' are indeed consistent with voltages on 'voltage contacts' when scaled with the distance ratio. Also for the Nernst-Ettingshausen coefficient S_{yx} the measured voltage scales with the distance between the contacts (see chapter 5 for the experimental demonstration).

Because the distance between contacts is so crucial for the size of the voltages measured, it is important to minimize the physical extension of the contacts to obtain a well

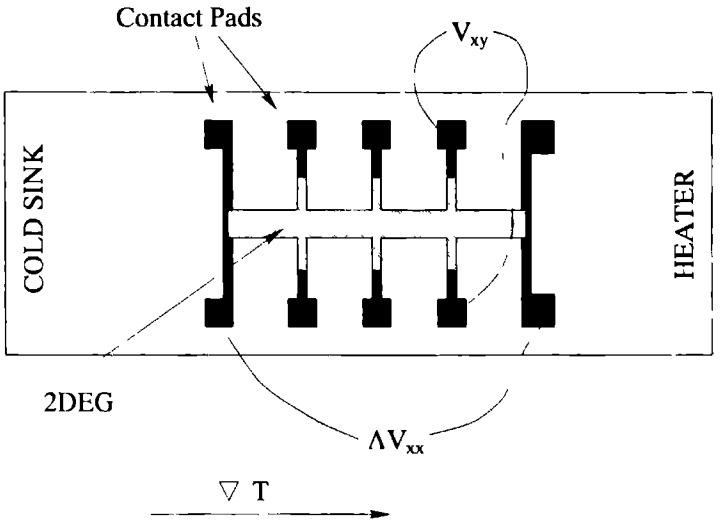

Figure 2.5: Sample mask optimized for thermopower measurements. The length and width of the the conducting channel are $l_m = 4$ mm and $w_m = 300$ μm, respectively.

defined distance. Therefore, the overlap between 2DEG and the metallic AuNiGe contact pads is 50 μm times the width of the bar giving a relative error for the absolute value of S_{xx} (S_{yx}) of 2.5% (10%) due to the geometry.

Another advantage of small contact areas is that possible disturbances of the homogeneous temperature gradient by the metallic pads is minimized. Also for this reason, the 'current contacts' are symmetric to both sides of the Hall bar and the large pads for the contacts to the bond wires using silver epoxy are placed as far away from the 2DEG as possible.

2.5 Overall Performance and Limitations

At zero magnetic field, a base temperature on the sample of $T \approx 60$ mK can be reached for a mixing chamber temperature of about 25 mK. For magnetic field sweeps the lowest sample temperature in resistivity measurements is $T \approx 100$ mK. When power is dissipated in the sample heater to produce a temperature gradient, the average sample temperature rises. For thermal conductivity measurements, the lowest temperature therefore is about 100 mK. For thermoelectric power, the noise level at low temperatures increases inevitably since the thermopower is strongly temperature dependent ($S \propto T^{3-4}$). Therefore, the thermopower field sweeps give significant information down to $T \approx 150$ mK.

The bottleneck to reach lower temperatures is mainly the thermal contact to the mixing chamber. Especially the soldered joints at the brass piece seem to be important. In a set-up for a thermopower measurement in a superconducting magnet, where there is less

eddy-current heating, the cold finger could be optimized for a better thermal link to the mixing chamber. Furthermore, the mechanical vibrations due to the water-cooling of a Bitter magnet are another obstacle to reach lower temperatures. However, these drawbacks are largely compensated by the possibility to reach higher magnetic fields, i.e. $B = 30$ T in hybrid Nijmegen II. At very low temperatures, a radiation shield for the sample holder could improve the performance because the surrounding inner vacuum can is at $T = 4.2$ K. Such a radiation shield was not implemented in the present set-up because of the restricted space of 15 mm in diameter.

At the high temperature side, thermopower and thermal conductivity measurements are reasonable up to a sample temperature of $T = 1.2$ K. Above that temperature on the sample, the temperature in the mixing chamber is unstable. Moreover, the temperature calibration becomes inaccurate because the thermometers have not much sensitivity in this range, in particular for ΔR which gives the temperature gradient. Note that changing the thermometers is not easily done because they have to be glued to the sample.

For a typical thermopower measurement at $T = 500$ mK, the temperature difference between the contacts is $\Delta T \simeq 40$ mK. The experimental error in determining ΔT is about 2 mK giving a relative statistical error of 5%. The accuracy of the absolute temperature is estimated to 1%, which gives an error of 4% in the absolute value of the thermopower since $S \propto T^{3-4}$. Typical voltages are of the order of a few μV with a noise level of about 10 nV in the AC-measurements. Furthermore, there are systematic errors introduced by the finite contact and thermometer size to determine the temperature difference between contacts, the AC-to-DC conversion factor. Thus, the error for the absolute value of the thermopower can be estimated to about 20% including systematic errors. However, the error for thermopower data within the same sample, e.g. comparison of S_{yx} and S_{xx} or of different filling factors in the same sweep, are far smaller. As discussed above, the experimental errors at the low and high temperature ends increase compared to the typical values in the intermediate range.

2.6 References

[1] R. Fletcher, J. C. Maan, K. Ploog, and G. Weimann, Phys. Rev. B **33**, 7122 (1986).

[2] U. Zeitler, J. C. Maan, P. Wyder, R. Fletcher, C. T. Foxon, and J. J. Harris, Phys. Rev. B **47**, 16008 (1993).

[3] U. Zeitler, *Electronic transport in three-dimensional and two-dimensional metallic semiconductors under extreme quantum conditions*, Vol. 441 of *Konstanzer Dissertationen* (Hartung-Gorre Verlag, Konstanz, 1994), Ph.D. thesis, Universität Konstanz.

[4] P. A. A. Teunissen, *Quantum Oscillations in High Magnetic Fields*, Ph.D. thesis, University of Nijmegen, 1993.

[5] J. A. A. J. Perenboom, K. van Hulst, S. A. J. Wiegers, and J. C. Maan, Physica B **201**, 507 (1994).

[6] HYSOL epoxy CP4-4285, The Dexter Corporation, Olean, New York, U.S.A.

[7] Ag-foil, purity 99.99+%, Goodfellow, Cambridge, England.

[8] Ag-powder, purity 99.97+%, max. particle size 2 micron, Goodfellow, Cambridge, England.

[9] F. Pobell, *Matter and Methods at Low Temperatures* (Springer-Verlag, Berlin, 1992).

[10] STYCAST 2850 FT, Grace N.V., Westerlo, Belgium.

[11] Strain gauge PA06-060-EAA 350, SEEA, Chartres, France.

[12] EPO-TEK H20E, Gentec, Brussels, Belgium.

[13] 1.001 kΩ resistor CRCW-0805, Dale Electronics, Columbus, Nebraska, U.S.A.

[14] 2.21 kΩ resistor RC12H2K21 (1%), 100ppm, Philips, Eindhoven, The Netherlands.

[15] Germanium temperature sensor GR-200A-30, Lakeshore, Westerville, Ohio, U.S.A.

[16] DC nanovoltmeter N11, EM Electronics, Brockenhurst, England.

Chapter 3

Even Denominator Filling Factors in the Thermoelectric Power of a Two-Dimensional Electron Gas

Abstract

We have investigated the interaction of phonons with a two-dimensional electron gas in the fractional quantum Hall regime with phonon drag thermoelectric power (TEP). The TEPs at filling factors with the same even denominator are found to be identical; at other even denominator filling factors they differ only by a constant factor. Treating these states as Composite Fermions, the findings are explained by a zero magnetic field theory for phonon drag. A maximum observed in the TEP at $\nu = \frac{1}{2}$ is modeled by a weakly diverging effective mass of the Composite Fermions at this filling factor.

3.1 Introduction

New ground states appear in the energy spectrum of a two-dimensional electron gas (2DEG) at high magnetic fields and low temperatures when an odd fraction of Landau levels is occupied, an effect known as the fractional quantum Hall effect (FQHE). In a recently developed model [1, 2], the FQHE is attributed to quantum oscillations of new quasi-particles, called Composite Fermions (CFs), consisting of electrons to which an even number $2m$ of flux quanta is attached. A profound consequence is that, at exactly even denominator filling factors $\nu = \frac{1}{2m}$, these new quasi-particles behave as fermions in a magnetic field which is effectively zero. This interpretation has proved to be highly successful in describing experimental results, including transport [3, 4], geometrical resonances in samples with antidots [5], and in surface acoustic wave experiments [6].

In this chapter we report thermoelectric experiments which probe the interaction of these quasi-particles with phonons. For a broad range of temperatures and electron densities, the experimental results convincingly demonstrate that states observed at half filled

This work has been published in:
B. Tieke, U. Zeitler, R. Fletcher, S. A. J. Wiegers, J. C. Maan, and M. Henini, Physical Review Letters **76**, 3630–3633 (1996).

Landau levels have the same value of the thermoelectric power (TEP), and that states at quarter filling are also related in a similar way. These results find an elegant explanation in terms of a zero-field Boltzmann theory for the phonon drag TEP with the appropriate CF parameters.

TEP can be used to study the interaction of phonons with 2DEGs at temperatures below 4 K where the dominant mechanism is phonon drag and where also the FQHE can be observed. Therefore, this technique provides information on the CF-phonon interaction [7]. At the very lowest temperatures the phonons are frozen out and diffusion TEP, which has been observed in 2D hole gases [8], dominates but this is not relevant in the present case. Phonon drag TEP is due to the flow of phonons in an applied temperature gradient which produces an electron current caused by electron-phonon interaction. Since no net current is drawn from the sample during measurements, an electric field appears which provides a compensating electric current, and the ratio of this electric field to the temperature gradient is the TEP. It is important to note that both the drag and compensation current are proportional to the same impurity relaxation time τ_i, so that TEP becomes independent of this quantity. Thus phonon drag TEP is fundamentally different from the resistivity ρ_{xx} which is almost completely determined by τ_i at low temperatures.

3.2 Experimental Setup

The TEP of a high mobility GaAs-$Ga_{1-x}Al_xAs$ heterostructure was measured at temperatures down to 150 mK in magnetic fields up to 20 T. The density and mobility of the 2DEG were varied in the range $n_e = 1.0 - 1.9 \times 10^{15}$ m^{-2} and $\mu = 60 - 100$ m^2/Vs, respectively, using illumination from an infrared diode. For TEP measurements, a calibrated temperature gradient was applied to the sample and the thermally created electric field measured. For this purpose a heater and two thermometers were glued to the substrate which was mounted on a cold finger in the vacuum space of a dilution refrigerator. The known thermal conductivity of the substrate was used as a check of the thermometry both in zero and high magnetic fields [7]. We will concentrate on S_{xx}, the component of the TEP along the direction of the temperature gradient.

3.3 Experimental Results

Fig. 3.1 shows the experimental magnetic field dependence of S_{xx} at two different temperatures. As commonly observed for ρ_{xx}, we see that also for S_{xx} the minima in the FQH regime are deepened as the temperature is lowered. However, Fig. 3.1 also shows the extraordinary result that the relative magnitude of the TEPs at even denominator filling factors $\nu = \frac{1}{2}$, $\frac{3}{2}$ and $\frac{3}{4}$ is independent of temperature, with the first pair actually being identical within experimental error.

This striking experimental result can be seen more clearly in Fig. 3.2 where the ratios of $S_{xx}(\frac{3}{2})$ and $S_{xx}(\frac{3}{4})$ to $S_{xx}(\frac{1}{2})$ are shown as a function of the inverse temperature. Both ratios increase as temperature decreases, but below a characteristic temperature T_c they remain constant corresponding to $S_{xx}(\frac{3}{2})/S_{xx}(\frac{1}{2}) = 0.99 \pm 0.03$ and $S_{xx}(\frac{3}{4})/S_{xx}(\frac{1}{2}) = 2.15 \pm 0.05$. At an electron density $n_e = 1.76 \times 10^{15}$ m^{-2}, $T_c = 480$ mK for both $\nu = \frac{3}{2}$ and $\frac{3}{4}$, which coincides

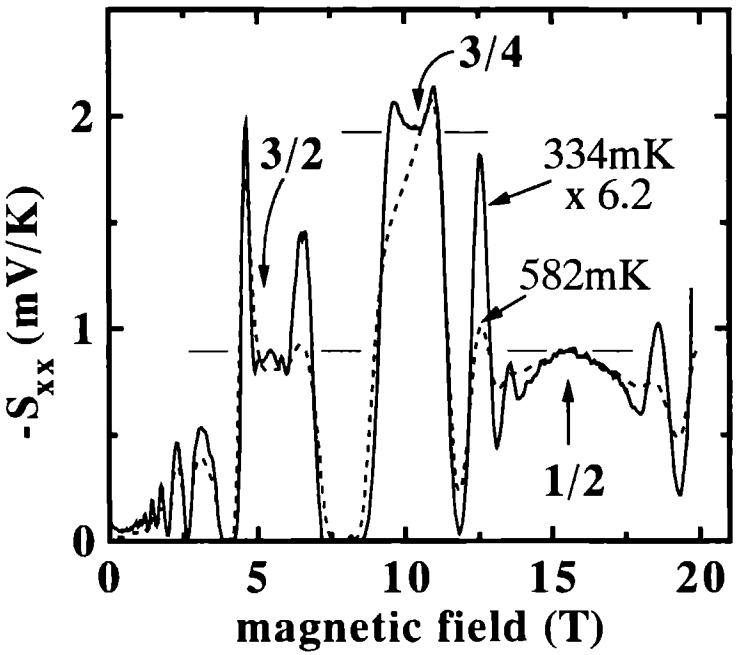

Figure 3.1: Examples of the magnetic field dependence of the longitudinal component S_{xx} of the TEP. The horizontal lines mark the constant relative value for the even denominator filling factors $\nu = \frac{3}{2}$ and $\nu = \frac{3}{4}$. Note the scaling factor for the lower temperature curve.

with the temperature at which features of the FQHE around $\nu = \frac{3}{2}$ become visible (e.g. minima at $\nu = 5/3$ and $4/3$).

We note that the constant relative TEP below T_c is unique to the even denominator filling factors $\nu = \frac{3}{2}$ and $\frac{3}{4}$. The TEPs at other filling factors in the FQH regime clearly have different temperature dependences; an example is given in Fig. 3.2. A similar correspondence between even denominator filling factors is not observed in ρ_{xx}, e.g. in our sample we find $\rho_{xx}(\frac{3}{2})/\rho_{xx}(\frac{1}{2}) \approx 0.2$.

This behavior of the TEP is found for all electron densities n_e studied, the only variation being that T_c increases with density. At lower electron densities the $\nu = \frac{1}{4}$ state becomes visible below 20 T. S_{xx} shows an almost field independent plateau around $\nu = \frac{1}{4}$ as observed in other samples before [7] and is not affected by the proximity of an insulating phase in our temperature range. We find $S_{xx}(\frac{1}{4})/S_{xx}(\frac{1}{2}) \simeq 2.4$, which is close enough to $S_{xx}(\frac{3}{4})/S_{xx}(\frac{1}{2})$ to suggest that $S_{xx}(\frac{3}{4})/S_{xx}(\frac{1}{4})$ is also unity as for the $\frac{1}{2}$-states.

The absolute magnitude of the observed TEP varies strongly with temperature as can be seen in Fig. 3.3, which makes the constant relative magnitude of the TEP at even denominator filling factors all the more remarkable. This figure also shows the strong similarity between $S_{xx}(\frac{1}{2})$ and the zero field TEP S_0 with the ratio $S_{xx}(\frac{1}{2})/S_0$ being approximately constant. The power law behavior $S \propto T^k$ which is approached at low temperatures is

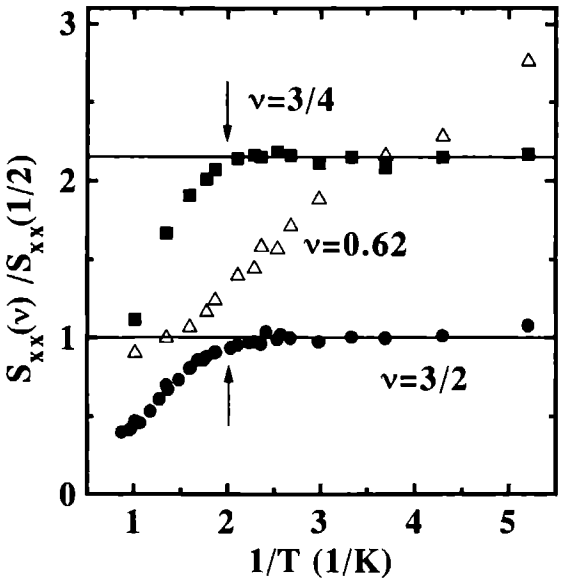

Figure 3.2: The relative TEP $S_{xx}(\nu)/S_{xx}(\frac{1}{2})$ at filling factors $\nu = \frac{3}{2}$ and $\frac{3}{4}$ as a function of inverse temperature. Arrows indicate T_c below which these ratios remain constant. Data for an arbitrary filling factor ($\nu = 0.62$, a maximum in the TEP) are shown for comparison.

very similar for $B = 0$ ($k = 4.0 \pm 0.5$) and $\nu = \frac{1}{2}$ ($k = 3.5 \pm 0.5$) confirming that the TEP for both zero magnetic field and for even denominator filling factors is caused by phonon drag. Furthermore, as seen in the inset of Fig. 3.3, the explicit density dependence of the absolute magnitude of the TEP at half filling at a fixed temperature is found to be $1/n_e$.

3.4 Two-Dimensional Electrons and Composite Fermions in Zero Magnetic Field

A 2DEG at even-denominator filling factor can be regarded as a metallic state of CFs in zero effective magnetic field. This concept together with the experimental results at even denominator filling factors strongly suggests that the coupling to the phonons is very similar for CFs and electrons. Therefore we use a model for the phonon drag TEP based on the solution of the Boltzmann equation for a 2DEG in zero magnetic field [9] to analyze our results. This calculation consists of two steps: the evaluation of (i) the thermally created drag current of quasi-particles and (ii) the electric field required to produce the compensating current. When $\nu = \frac{3}{2}$ and $\frac{3}{4}$ are considered, one must also account for the role of the filled Landau level to which the CF-state is added. In this case, only a fraction n_Q/n_e (where n_Q is the CF density) of the total current $j_{\rm tot}$ is carried by the quasi-particles [2]. In the derivation of Eq. 3.1 below, we have used the above relation between $j_{\rm tot}$ and the CF

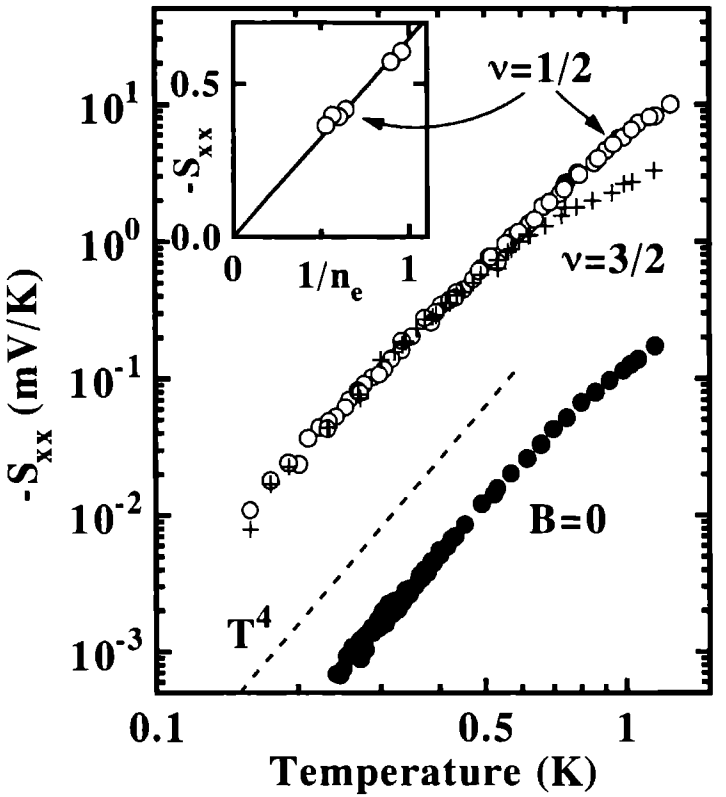

Figure 3.3: The temperature dependence of the absolute value of the TEP for even denominator filling factors and zero magnetic field. The dashed curve indicates a T^4 dependence. The inset shows $S_{xx}(\frac{1}{2})$ at $T =$ 440 mK (in mV/K) versus the inverse density $1/n_e$ (in units of 10^{-15} m^2).

current density j_Q, and have also made the assumption that the thermally created quasi-particle current must be compensated by a current of quasi-particles only. This gives the result that the total electron density n_e appears in the prefactor; a behavior similar to the Hall resistivity which is also based on an effect of a compensation current.

For the range of temperatures and densities studied, typical phonon wave vectors ($q \sim 4kT/\hbar v$, where v is the velocity of sound in GaAs) are small compared to the diameter of the Fermi circle for both electrons and CFs, and with this condition we obtain for the phonon drag TEP of CF-states in zero effective magnetic field [9]

$$S_{xx}^{g,Q} = -AV^2T^4\frac{m_e^*}{n_e}\int\int\frac{m_Q^* v}{\hbar k_f^Q}f(\xi,\xi_z)\mathrm{d}\xi\mathrm{d}\xi_z. \tag{3.1}$$

In this equation $f(\xi,\xi_z)$ is a function containing the thermal distribution of the phonons and takes into account all possible scattering events with the quasi-particles consistent

with energy and momentum conservation, with $\xi = q\hbar v/kT$ and $\xi_z = q_z\hbar v/kT$ being dimensionless phonon wave vectors in the plane of the 2DEG and perpendicular to it, respectively. The effective mass and Fermi wave vector of the CFs are denoted by m_Q^* and $k_F^Q = \sqrt{4\pi n_Q}$, and m_e^* is the effective (band) mass of electrons in GaAs. The prefactor A contains only fundamental constants and fixed parameters of the phonon system, and V is an effective scattering potential for the CF-phonon coupling which in our case may taken to be constant [10]. The double integral is to be evaluated in the range $\sqrt{q^2+q_z^2} \leq 2k_F$, and in its dimensionless form is almost independent of T in our range of parameters.

In the CF-model, the fundamental difference between $\nu = \frac{1}{2}$ and $\nu = \frac{3}{2}$ is that the quasiparticle density n_Q differs by a factor of 3 for constant total electron density n_e [2]. Since the integral contains only the ratio m_Q^*/k_F^Q, and both m_Q^* and k_F^Q are proportional to $\sqrt{n_Q}$ [2], S^g becomes independent of n_Q and we obtain $S^g(\frac{3}{2}) = S^g(\frac{1}{2})$ and $S^g(\frac{3}{4}) = S^g(\frac{1}{4})$ as observed experimentally. This result is independent of whether the $\nu = \frac{3}{2}$ state is totally polarized or only partially as recently observed [11] as long as m_Q^* and k_F^Q depend in the same way on the spin polarization leaving the ratio m_Q^*/k_F^Q unaltered. Furthermore, for the states with four flux quanta, it is plausible that the ratio $S_{xx}(\frac{3}{4})/S_{xx}(\frac{1}{2}) \simeq 2.2$ arises from an increased effective mass m_Q^* in Eq. 3.1 as observed in calculations [12] and other experiments [3] for $m^*(\frac{1}{4})$. In any case, the TEP results clearly indicate that CF-states with different numbers of flux quanta are indeed very similar.

Eq. 3.1 not only describes the remarkable experimental fact that S^g is independent of n_Q for different even fractions with the same denominator, but also that $S^g \propto 1/n_e$ at $\nu = \frac{1}{2}$ as seen in the inset of Fig. 3.3, whereas the experimental zero field TEP S_0 is found to vary between $n_e^{-1.5}$ and n_e^{-2}. This observation can be explained by the fact that the electron mass m_e^* does not depend on n_e, in contrast to m_Q^* for CFs, so that Eq. 3.1 does indeed predict a stronger density dependence for electrons, $S_0 \propto n_e^{-1}k_f^{-1} \propto {n_e}^{1.5}$.

Focusing on the temperature dependence of electrons at zero magnetic field and CFs, they agree within experimental accuracy, $S_0 \propto T^{4.0\pm0.5}$ and $S_{xx}(\frac{1}{2}) \propto T^{3.5\pm0.5}$. Eq. 3.1 predicts a T^4 behavior for both particles in excellent agreement with this. In a recent paper, an evaluation of a related quantity, the phonon contribution μ_{ph} to the electron (CF) mobility, has been inferred from ρ_{xx} data, and a significant difference in T-dependence ($\mu_{\rm ph}^{CF} \propto T^{-3}$ and $\mu_{\rm ph}^{e} \propto T^{-5}$) has been found [13]. However, S_{xx}^g, which depends to first order on electron (CF)-phonon scattering and, contrary to ρ_{xx}, is independent of impurity scattering, does not show this difference but, at most, an only marginally weaker T-dependence for CFs than for electrons.

Extending the comparison of the zero field TEP with the CF-states further, we find $S_{xx}(\frac{1}{2})/S_0 = 50$ which would result in $m_Q^*(\frac{1}{2}) \approx 5\, m_0$ (where m_0 is the free electron mass) if the magnitude of the change is attributed solely to mass enhancement. This is a very high value compared to those from Shubnikov-de Haas analyses which yield $m_Q^*(\frac{1}{2}) \approx m_0$ [3]. On the other hand, masses in the range $m_Q^*(\frac{1}{2}) = 2-6\, m_0$ have also been reported from the mobility analysis mentioned above [13]. A possible explanation could be that the scattering potential V in Eq. 3.1 differs not so much in T-dependence but in absolute value for CFs and electrons, but a more elaborate theory would be needed to confirm this statement.

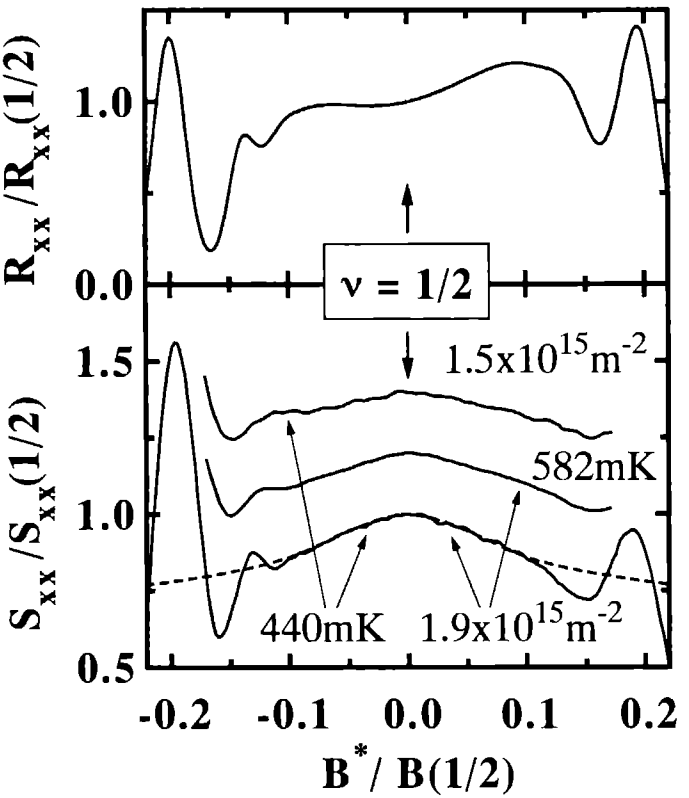

Figure 3.4: The vicinity of $\nu = \frac{1}{2}$: In the lower panel, S_{xx} with the characteristic symmetric maximum at $\nu = \frac{1}{2}$ is shown for different temperatures and densities, respectively. The dashed line is a fit to the background of the lowest curve assuming a logarithmically diverging mass at $\nu = \frac{1}{2}$. For comparison, the resistivity, which exhibits no similar symmetry around $\nu = \frac{1}{2}$, is shown in the upper panel.

3.5 The Vicinity of $\nu = \frac{1}{2}$ – Composite Fermions in Low Magnetic Field

Finally we draw attention to the important feature that the TEP has a maximum at exactly half filling with an amplitude which increases with decreasing temperature and increasing density (see Fig. 3.4). This structure of the TEP is strikingly symmetric around $\nu = \frac{1}{2}$ showing that $S^s(B^*) = S^s(-B^*)$, where $B^* = B - B(\frac{1}{2})$ is the effective magnetic field, a result completely consistent with the theoretical conjecture that $B(\frac{1}{2})$ is an effectively zero magnetic field for CFs [2]. A similar symmetry is absent in the resistivity ρ_{xx} where only a minimum-like structure on a rising background is observed (see top panel of Fig. 3.4).

We attribute the lack of symmetry in the background of ρ_{xx} to the fact that it is governed by the field dependence of τ_i.

Using the result from Eq. 3.1 that $S \propto m_Q^*$, we can assign the symmetric peak in the TEP around $\nu = \frac{1}{2}$ to a property characteristic for the quasi-particle mass. In the CF-theory weak divergences of the form $m_Q^* \propto a' + b'/|B^*|^{0.5}$ or $m_Q^* \propto a + b \ln |B^*|$ for short range and Coulombic interactions, respectively, are expected as $\nu \to \frac{1}{2}$ [2, 4]. We have calculated the effect of a logarithmically diverging mass on the TEP using a simple distribution for the broadening of the effective field, $P(B) = (1 - |B - B_0|/\Delta B^*)/\Delta B^*$, and assuming that B^* affects only m_Q^*, thus, $S(B_0)/S(\frac{1}{2}) = \int P(B)\, m^*(B)\, dB\, /\, m^*(\frac{1}{2})$ for the normalized TEP. Using the fit parameters $b/a = 0.16$ and $\Delta B^* = 0.099$ [in units of $B(\frac{1}{2})$] this function perfectly reproduces the smooth background in the vicinity of $\nu = \frac{1}{2}$ (see Fig. 3.4) demonstrating the consistency of the peak with a weakly diverging m_Q^* as theoretically predicted. The value of ΔB^* is comparable to the width of the field region where no quantum oscillations are observed which coincides with the range of vanishing (or negative) gaps in activated transport measurements of ρ_{xx} [3]. In a detailed analysis of these Shubnikov-de Haas experiments, a mass enhancement was also found as $\nu \to \frac{1}{2}$ [4] although these are not able to probe the region very close to $\nu = \frac{1}{2}$.

3.6 Conclusions

In conclusion, our experiments have shown that the TEPs of 2DEGs are identical for even denominator filling factors with the same denominator and that the TEPs at different even denominators scale with a fixed constant. We have interpreted these findings by applying a zero field theory for the phonon drag TEP to CFs. This approach provides an understanding not only of these results, but also of the temperature and density dependence of the TEP for both electrons and CFs, perhaps leaving only the high value of the ratio $S_{xx}(\frac{1}{2})/S_0$ as an open question. Our results fully support the theoretical concept of CFs as Fermions in an effective zero magnetic field. Finally, the symmetric peak in the TEP at $\nu = \frac{1}{2}$ is found to be in agreement with a weakly diverging effective mass of CFs at this filling factor.

3.7 References

[1] J. K. Jain, Adv. Phys. **41**, 105 (1992).

[2] B. I. Halperin, P. A. Lee, and N. Read, Phys. Rev. **B47**, 7312 (1993).

[3] R. R. Du, H. L. Stormer, D. C. Tsui, L. N. Pfeiffer, and K. W. West, Phys. Rev. Lett. **70**, 2944 (1993); D. R. Leadley, R. J. Nicholas, C. T. Foxon, and J. J. Harris, Phys. Rev. Lett. **72**, 1906 (1994).

[4] R. R. Du, H. L. Stormer, D. C. Tsui, L. N. Pfeiffer, and K. W. West, Phys. Rev. Lett. **73**, 3274 (1994); P. T. Coleridge, Z. W. Wasilewski, P. Zawadzki, A. S. Sachrajda, and H. A. Carmona, Phys. Rev. B **52**, R11603 (1995).

[5] W. Kang, H. L. Stormer, L. N. Pfeiffer, W. Baldwin, and K. W. West, Phys. Rev. Lett. **71**, 3850 (1993).

[6] R. L. Willett, R. R. Ruel, K. W. West, and L. N. Pfeiffer, Phys. Rev. Lett. **71**, 1846 (1993).

[7] U. Zeitler, B. Tieke, S. A. J. Wiegers, J. C. Maan, R. Fletcher, V. I. Fal'ko, C. T. Foxon, and J. J. Harris, in: *High Magnetic Fields in the Physics of Semiconductors*, edited by D. Heiman (World Scientific, Singapore, 1995) p. 38;

[8] V. Bayot, E. Grivei, H. C. Manoharan, X. Ying, and M. Shayegan, Phys. Rev. B **52**, R8621 (1995).

[9] D. G. Cantrell and P. N. Butcher, J. Phys. C: Solid State Phys. **20**, 1985 (1987); **20**, 1993 (1987).

[10] It has been shown by Lyo [S. K. Lyo, Phys. Rev. B **38**, 6345 (1988)] that expressions like Eq. 3.1 with a T^4 dependence are obtained for both unscreened deformation potential and screened piezoelectric scattering in the case of a 2DEG in zero magnetic field. In the case of deformation potential scattering, $V = E_1$, the deformation potential coefficient, while for piezoelectric scattering V is an effective potential.

[11] R. R. Du, A. S. Yeh, H. L. Stormer, D. C. Tsui, L. N. Pfeiffer, and K. W. West, Phys. Rev. Lett. **75**, 3926 (1995).

[12] R. Morf and N. d'Ambrumenil, Phys. Rev. Lett. **74**, 5116 (1995).

[13] W. Kang, Song He, H. L. Stormer, L. N. Pfeiffer, W. Baldwin, and K. W. West, Phys. Rev. Lett. **75**, 4106 (1995).

Chapter 4

Fundamental Relation Between Electrical and Thermoelectric Transport Coefficients in the Quantum Hall Regime

Abstract

The two components S_{xx} and S_{yx} of the phonon drag thermoelectric power in two-dimensional electron gases in the integer and fractional quantum Hall regime are found to be related by $S_{yx} = \alpha B(dS_{xx}/dB)$, with α a dimensionless constant. A similar relation has already been established for the electrical resistivity components, $\rho_{xx} = \alpha B(d\rho_{xy}/dB)$, and we show that experimentally α is the same in both cases. These results also provide a phenomenological explanation for the behavior of S_{yx} which hitherto has not been understood.

4.1 Introduction

More than 15 years after the discovery of the quantum Hall effect (QHE) [1], our fundamental understanding is still challenged by the close relation observed experimentally by Chang and Tsui [2] between the two independent components of the resistivity tensor ρ at high magnetic fields B (where $\rho_{xy} \gg \rho_{xx}$), i.e.

$$\rho_{xx} = \alpha_r B \frac{d\rho_{xy}}{dB}, \tag{4.1}$$

where α_r is a scaling constant. The validity of Eq. (4.1) has been confirmed in a number of experimental studies [3–6] in both the integer and fractional QHE. Not only are the zeros in ρ_{xx} correctly given when ρ_{xy} is in a plateau, but practically all of the finer details are faithfully reproduced as well. The possible origin of the relation has been studied theoretically by Vagner and Pepper [7] using a scaling argument, and more recently by Simon

Parts of this work have been submitted for publication in:
B. Tieke, R. Fletcher, U. Zeitler, A. K. Geim, M. Henini, and J. C. Maan, Physical Review Letters.

and Halperin [8] who proposed an analysis based on inhomogeneities. In another development, a phenomenological analysis of the peak heights of Shubnikov-de Haas oscillations by Coleridge *et al.* [9] suggested that α_r is related to the ratio of quantum lifetime τ_q to transport lifetime τ_t, i.e. $\alpha_r = \tau_q/2\tau_t$.

The present paper will demonstrate that the two components of the thermoelectric power (TEP) tensor S, S_{xx} and S_{yx}, behave in a similar way. S is defined by $\boldsymbol{E} = S\nabla T$, where $\boldsymbol{E}$ is the electric field which appears in the sample as a result of an applied temperature gradient ∇T. The principal driving mechanisms for TEP are diffusion and phonon drag [10] but in the present work only phonon drag is considered since it dominates the experiments. The phonon drag component of S_{xx} is understood reasonably well, but that of S_{yx} is not. The latter is predicted to have no phonon drag [10, 11], but experimentally it is found to have a magnitude comparable to S_{xx} and there is direct evidence that it is caused by phonon drag [12–14]. It is instructive to compare this situation with that for three-dimensional degenerate semiconductors. Here too we expect no phonon drag in S_{yx} and this is exactly what is observed, even when S_{xx} is completely dominated by phonon drag [15]. Thus, the phonon drag contribution to S_{yx} is clearly related to the reduced dimensionality of a 2DEG.

In this chapter we will show that, for the 2DEG case, S_{yx} is related to S_{xx} by

$$S_{yx} = \alpha_s B \frac{dS_{xx}}{dB}. \tag{4.2}$$

Equation (4.2) is an important result because it expands the generality of Eq. (4.1) to another transport property, and at the same time sheds new light upon the origin of phonon drag in S_{yx} in 2DEGs. The relation is found to hold for many samples with widely different mobilities and densities, both in the integer as well as fractional QHE regime, and over a broad range of temperature. Moreover, within experimental error, the dimensionless scaling factor α_s is found to be identical with the factor α_r relating the resistivities in Eq. (4.1).

Equation (4.2) can be derived from the tensor relations between the electrical and thermal current densities $\boldsymbol{J}$ and $\boldsymbol{U}$ produced by an applied electric field $\boldsymbol{E}$ and a temperature gradient ∇T,

$$\boldsymbol{J} = \sigma \boldsymbol{E} - \epsilon \nabla T, \tag{4.3}$$

$$\boldsymbol{U} = T\epsilon \boldsymbol{E} - \lambda \nabla T, \tag{4.4}$$

with the electrical conductivity σ, the thermoelectric tensor ϵ, and the thermal conductivity λ. Because of the Onsager symmetry relations, ϵ appears in both Eqs. (4.3) and (4.4) and gives an electrical current due to ∇T in Eq. (4.3) and a heat current due to $\boldsymbol{E}$ in Eq. (4.4). $S = \rho\epsilon$ since in a TEP experiment $\boldsymbol{J} = 0$.

We note that ϵ and σ fulfill similar roles in Eqs. (4.3) and (4.4) because each relates a driving force ($\boldsymbol{E}$ or ∇T) to a current density ($\boldsymbol{J}$ or $\boldsymbol{U}$). Since Eq. (4.1) is equivalent to $\sigma_{xx} = \alpha_r B(d\sigma_{xy}/dB)$ at high magnetic fields [5], we make the assumption that the two independent components of ϵ, ϵ_{xx} and ϵ_{xy}, are related in a similar way in the quantum Hall regime, namely $\epsilon_{xx} = \alpha_s B(d\epsilon_{xy}/dB)$, where α_s is not necessarily identical to α_r. With the experimental condition $\nabla T_y = 0$, $S_{xx} = \rho_{xx}\epsilon_{xx} + \rho_{yx}\epsilon_{xy}$. Omitting the term $\rho_{xx}\epsilon_{xx}$ which is

sample no.	ref.	n (10^{15}m^{-2})	μ (m^2/Vs)	B (T) $\nu = 1$	B_{max} (T)	T (K)	*ill.*	fit parameters α_r	$\pm\sigma_r$	α_s	$\pm\sigma_s$	syst. err.
1A	[16]	1.77	95.9	7.31	20	0.4 – 0.7	×	0.030	0.005	0.018	0.005	14%
1A	[16]	1.12	60.9	4.60	20	0.3 – 0.9	–	0.033	0.012	0.024	0.003	14%
1B		1.75	106	7.22	20	0.3 – 1.1	×	0.015	0.003	0.023	0.005	14%
2		1.75	93.0	7.25	30	0.2 – 1.0	×	0.022	0.007	0.028	0.008	14%
G645	[14]	0.87	232	3.65	20	1.1	×	0.015	0.002	0.014	0.009	59%
G647	[14]	0.43	266	1.80	7.2	0.4 – 0.7	×	0.024	0.004	0.028	0.017	59%
G650	[14]	1.00	189	4.21	20	0.8 – 1.3	–	0.045	0.007	0.041	0.006	59%
A1	[13]	2.21	4.2	9.14	7.9	1.7 – 4.2	–	0.065	-	0.052	0.002	20%
A4	[13]	5.95	19.3	24.6	7.9	1.7 – 4.1	×	0.033	-	0.025	0.003	20%
2	[12]	4.80	37.7	19.8	20	1.8 – 5.6	–	0.047	0.009	0.041	0.005	55%
3	[12]	6.82	24.9	28.2	20	2.1 – 9.0	–	0.049	0.018	0.035	0.012	27%

Table 4.1: Overview of parameters for samples that were used to verify Eqs. (4.2) and (4.1).

experimentally found to be negligible, it follows that

$$\begin{aligned} \alpha_s B\frac{dS_{xx}}{dB} &= \alpha_s B\frac{d\epsilon_{xy}}{dB}\rho_{yx} + \alpha_s B\frac{d\rho_{yx}}{dB}\epsilon_{xy} \\ &= \rho_{yx}\epsilon_{xx} + \rho_{xx}\epsilon_{yx} + \frac{\Delta\alpha}{\alpha_r}\rho_{xx}\epsilon_{yx}, \end{aligned} \tag{4.5}$$

where $\Delta\alpha = \alpha_s - \alpha_r$. We will show that $\alpha_s \simeq \alpha_r$ so that the last term is negligible. However, even if $\Delta\alpha \neq 0$, $\rho_{xx}\epsilon_{yx}$ is at most only 10% of the first two terms in Eq. (4.5). Thus Eq. (4.2) follows immediately from Eq. (4.5) since $S_{yx} = \rho_{xx}\epsilon_{yx} + \rho_{yx}\epsilon_{xx}$. As might be expected, α_s relating the two components of S is the same factor as for the components of the thermoelectric tensor ϵ.

A notable difference between Eq. (4.2) and Eq. (4.1) is that the off-diagonal component of S is given by the derivative of the diagonal component, whereas for ρ it is the opposite. Another interesting observation is that the two primary coefficients, σ_{xy} and ϵ_{xy}, are both independent of impurity scattering at high field (at least in a semi-classical approximation), whereas the derived quantities, σ_{xx} and ϵ_{xx}, are not.

4.2 Analysis of Experimental Results

To investigate the validity of Eq. (4.2), we have analyzed many results on a variety of $GaAs/Ga_{1-x}Al_xAs$ heterostructures, including previously published data [12–14] as well as new results obtained specifically for this purpose. The analysis covers broad ranges of temperature ($T = 0.2 - 10$ K), density ($n = 0.4 - 6.7 \times 10^{15}$ m ^{2}), mobility ($\mu = 3.8 - 266$ m^2/Vs), and magnetic field ($B = 1 - 30$ T), and both the integer and fractional QHE regime.

In the following, curves obtained from ρ_{xy} and S_{xx} using Eqs. (4.1) and (4.2) will be denoted by $\rho_{xx}^{\rm calc}$ and $S_{yx}^{\rm calc}$, respectively. The derivatives $d\rho_{xy}/dB$ and dS_{xx}/dB were computed numerically. The scaling constant, either α_r or α_s, was used as the single free parameter in a least mean squares fit of either Eqs. (4.1) or (4.2) to the appropriate experimental ρ_{xx} or S_{yx} data. As an indication for the level of agreement we define a quality factor $\Delta = \int(S_{yx} - S_{yx}^{\rm calc})^2 dB / \int(S_{yx}^2 + (S_{yx}^{\rm calc})^2)dB$ which quantifies the relative deviation, with $\Delta = 0$ for perfect agreement and $\Delta = 1$ for no correlation. In all cases we find $\Delta \lesssim 0.1$ for both $S_{yx}^{\rm calc}$ and $\rho_{xx}^{\rm calc}$.

Figure 4.1 gives a typical example for the measured quantities, ρ_{xx} and S_{yx}, and calculated curves, $\rho_{xx}^{\rm calc}$ and $S_{yx}^{\rm calc}$, for an older high-density, low-mobility sample (A4 in Ref. [13]) in the integer QHE regime. $S_{yx}^{\rm calc}$ strikingly resembles S_{yx}, with a quality ($\Delta = 0.05$) similar to that for ρ ($\Delta = 0.08$). All extremal positions and sign changes of S_{yx} are well accounted for, as well as the absolute magnitude and the shape of the oscillations. We emphasize that this degree of agreement is obtained with α_s as the only adjustable parameter in the fit. A minor discrepancy between $S_{yx}^{\rm calc}$ and S_{yx} is that the derivative tends to accentuate structure which is weak in the experimental S_{yx} as can be seen for the developing spin splitting at $\nu = 5$ in Fig. 4.1. Such behavior is also found for $\rho_{xx}^{\rm calc}$ [6] and can be seen in Fig. 4.1.

Figure 4.2 presents new experimental data for S_{yx} and ρ_{xx}, together with $S_{yx}^{\rm calc}$ and $\rho_{xx}^{\rm calc}$, in the integer and fractional QHE regime for a low-density, high-mobility sample ($n = 1.75 \times 10^{15}$ m^{-1}, $\mu = 93.0$ m^2/Vs: for data on S_{xx} see Ref. [16]). Again the agreement

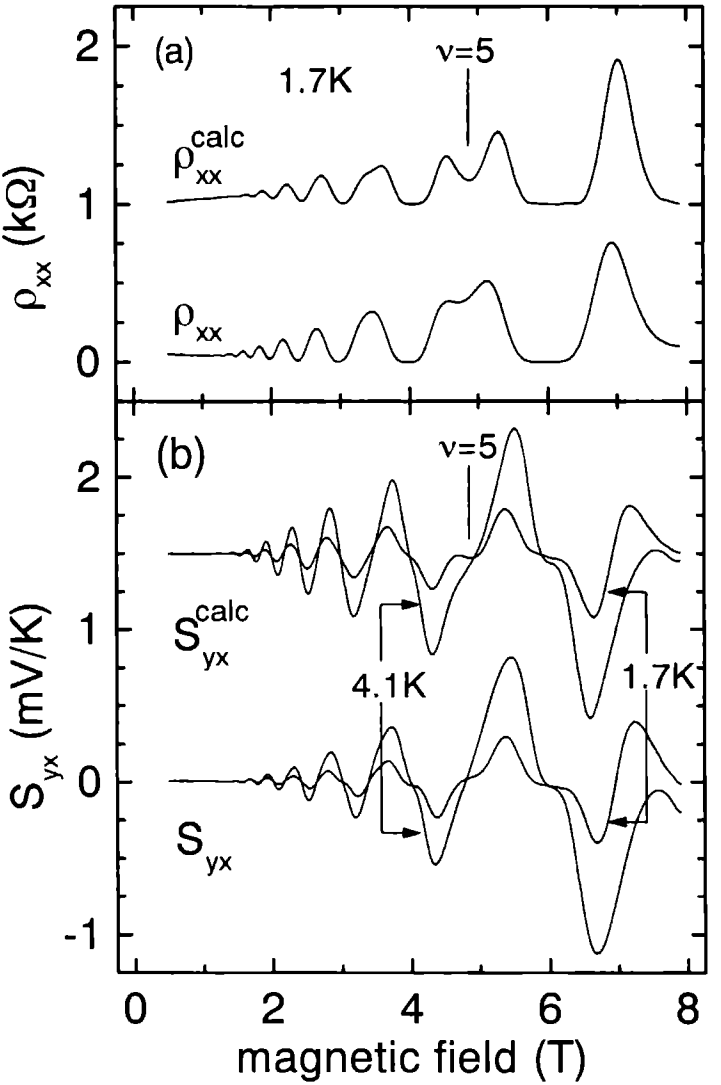

Figure 4.1: Example for the integer QHE regime. (a) Longitudinal resistivity ρ_{xx} and ρ_{xx}^{calc} calculated from the Hall resistance ρ_{xy} with Eq. (4.1), $\alpha_r = 0.033$. The curve for ρ_{xx}^{calc} is offset by 1 kΩ. (b) NE-coefficient S_{yx} and S_{yx}^{calc} calculated from S_{xx} with Eq. (4.2) for $T = 4.12$ K (1.74 K), with $\alpha_s = 0.027$ (0.022). The curves for S_{yx}^{calc} are offset by 1.5 mV/K. Original experimental data are taken from Ref. [13], sample A4.

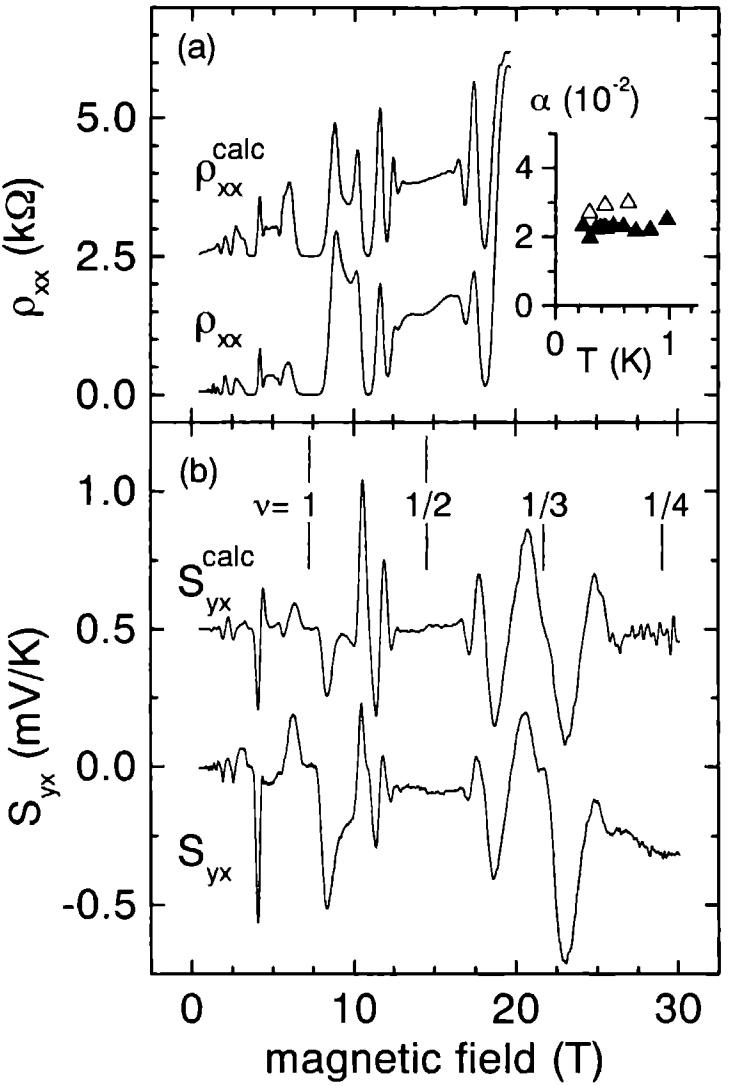

Figure 4.2: Example for the fractional QHE regime. (a) Longitudinal resistivity ρ_{xx} and ρ_{yx}^{calc} calculated with Eq. (4.1) at $T = 297$ mK, with $\alpha_r = 0.030$. The curve for ρ_{xx}^{calc} is offset by 2.5 kΩ. (b) NE-coefficient S_{yx} and S_{yx}^{calc} calculated from S_{xx} with Eq. (4.2) for $T = 504$ mK, $\alpha_s = 0.027$. The curve for S_{yx}^{calc} is offset by 0.5 mV/K. Special filling factors ν are indicated in the graph. The inset in the upper panel shows the temperature dependence for fit parameters α_r (△) and α_s(▲) obtained in the range $B = 1 - 20$ T. Both are constant and agree within experimental error.

between S_{yx} and S_{yx}^{calc} is remarkable ($\Delta = 0.09$). The positions and shapes of the oscillations, with the characteristic sign changes, as well as the relative magnitudes in the IQH and FQH regime are all well reproduced. In Fig. 4.2 a slight discrepancy can be observed around the even denominator filling factors $\nu = \frac{1}{2}, \frac{3}{2}, \frac{1}{4}$, and $\frac{3}{4}$ where S_{yx}^{calc} vanishes but the experimental S_{yx} is finite. However, this additional background in the fractional QHE does not significantly detract from the overall agreement between S_{yx}^{calc} and S_{yx}. In fact, the value of α_s we obtain is insensitive to whether this background is subtracted or not.

The inset to Fig. 4.2 shows that α_s and α_r are independent of temperature. This is consistent with previous observations that α_r is constant for $T \lesssim 40$ K [3, 17], but a constant α_s for TEP is more noteworthy since, in contrast to ρ_{yx}, the absolute magnitude of S_{xx} varies by several orders of magnitude in this temperature range due to phonon drag [16]. This fact stresses the common origin of S_{xx} and S_{yx}.

Another striking result is that the required values of α_s and α_r are always very similar as is obvious from the figures, especially the inset to Fig. 4.2. Figure 4.3 and Table 4.1 summarize the results for α_s and α_r for the different samples investigated. The values lie in the range $0.01 - 0.07$ for all samples and show no clear dependence on mobility μ or density n as can be seen in Fig. 4.3. It is possible that α decreases for higher mobilities, a trend which is most pronounced if μ is increased by persistent photoconductivity in a specific sample. In fitting, α_s and α_r are obtained with a standard deviation of $\sim 15\%$. Systematic uncertainties arise with the TEP (unlike the resistivity) from the dimensions of the contacts, and are reflected directly in α_s. These errors are sample-specific and are typically $\sim 20\%$. Taking all samples [18] into account, we see no significant difference between α_s and α_r and conclude that the two scaling parameters are identical within experimental error.

4.3 Interpretation

The similarity of α_s and α_r over the wide range of experimental parameters implies that the physical mechanism responsible for the effect must be common to both ρ and S. The available evidence indicates that the relationships of Eqs. (4.1) and (4.2) are specific to the case of 2DEGs and are not exhibited by 3D degenerate gases. As noted above, it has been suggested [9] that $\alpha_r = \tau_q/2\tau_t$ when both transport lifetimes, τ_t and τ_q, are dominated by impurity scattering which is independent of temperature. It is not immediately obvious how this result can be extended to phonon drag TEP which reflects the strongly temperature dependent, inelastic, electron-phonon scattering, though it is certainly true that ϵ_{xx} scales as τ_t (as does σ_{xx}) and that τ_q still controls the Landau level width.

Simon and Halperin [8] suggested Eq. (4.1) results from inhomogeneity effects. Although a simple expression for α_r is not given they remark that a typical value of $\alpha_r = 0.03$ would correspond to large scale density fluctuations of $\sim 6\%$ which they believe to be unreasonably large. Nevertheless, since inhomogeneities are essentially geometrical in nature and thus temperature independent, such a mechanism is general enough to encompass both resistivity and TEP. The decrease of α for illuminated samples is consistent with this treatment since illumination is believed to make the 2DEG more homogeneous.

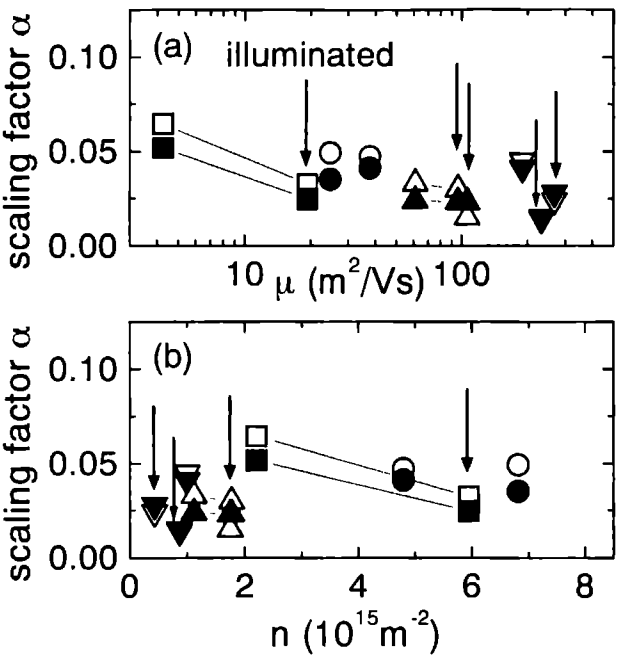

Figure 4.3: Scaling parameters α_r (open symbols) and α_s (closed symbols) as a function of (a) mobility and (b) density for a variety of samples. Data points are connected for the same sample illuminated (marked by arrows) and non-illuminated. Original data are taken from Ref. [12], samples 2 and 3 (•), Ref. [13], samples A1 and A4 (■), Ref. [14], samples 1, 2, and 3 (▼), and samples from the same wafer as the sample in Fig. 4.2 (▲).

4.4 Conclusions

In summary, we have shown that, just as there exists a relation Eq. (4.1) between the tensor components for electrical transport in quantum Hall systems, there is an equivalent relation Eq. (4.2) valid for thermoelectric transport. Moreover, the dimensionless scaling factors are identical in the two cases emphasizing the fact that the significance of such relations is more fundamental than was previously assumed. In addition, our analysis also provides a consistent description for the experimental results on the Nernst-Ettingshausen coefficient S_{yx} which were not previously understood. It might be speculated that relations similar to Eqs. (4.1) and (4.2) may also exist for other properties of a 2DEG, e.g. diffusion TEP, surface acoustic wave scattering and electronic thermal conductivity.

This work has been supported by the European Commission under contract CHGE-CT93-0051 (Large Installation Plan) and, in part, by NSERC, Canada.

4.5 References

[1] K. von Klitzing, G. Dorda, and M. Pepper, Phys. Rev. Lett. **45**, 494 (1980).

[2] A. M. Chang and D. C. Tsui, Sol. State Comm. **56**, 153 (1985).

[3] T. Rötger, G. J. C. L. Bruls, J. C. Maan, P. Wyder, K. Ploog, and G. Weimann, Phys. Rev. Lett. **62**, 90 (1989).

[4] N. G. Morawicz, K. W. J. Barnham, C. Zammit, J. J. Harris, C. T. Foxon, and P. Kujawinski, Phys. Rev. B **41**, 12687 (1990).

[5] H. L. Stormer, K. W. Baldwin, L. N. Pfeiffer, and K. W. West, Sol. State Comm. **84**, 95 (1992).

[6] A. A. Allerman, W. Xu, N. Hauser, and C. Jagadish, J. Appl. Phys. **77**, 2052 (1995).

[7] I. D. Vagner and M. Pepper, Phys. Rev. B **37**, 7147 (1988).

[8] S. B. Simon and B. I. Halperin, Phys. Rev. Lett. **73**, 3278 (1994).

[9] P. T. Coleridge, P. Zawadzki, and A. S. Sachrajda, Phys. Rev. B **49**, 10798 (1994).

[10] B. L. Gallagher and P. N. Butcher, in *Handbook on Semiconductors*, edited by P. T. Landsberg (Elsevier, Amsterdam, 1992), Vol. 1, pp. 721–816.

[11] T. M. Fromhold, P. N. Butcher, G. Qin, B. G. Mulimani, J. P. Oxley, and B. L. Gallagher, Phys. Rev. B **48**, 5326 (1993).

[12] R. Fletcher, J. C. Maan, K. Ploog, and G. Weimann, Phys. Rev. B **33**, 7122 (1986).

[13] R. Fletcher, M. D'Iorio, W. T. Moore, and R. Stoner, J. Phys. C: Solid State Phys. **21**, 2681 (1988).

[14] U. Zeitler, J. C. Maan, P. Wyder, R. Fletcher, C. T. Foxon, and J. J. Harris, Phys. Rev. B **47**, 16008 (1993).

[15] B. Tieke, R. Fletcher, J. C. Maan, W. Dobrowolski, A. Mycielski, and A. Wittlin, Phys. Rev. B **54**, 10565 (1996).

[16] B. Tieke, U. Zeitler, R. Fletcher, S. A. J. Wiegers, A. K. Geim, J. C. Maan, and M. Henini, Phys. Rev. Lett. **76**, 3630 (1996).

[17] D. R. Leadley, R. J. Nicholas, W. Xu, F. M. Peeters, J. T. Devreese, J. Singleton, J. A. A. J. Perenboom, L. van Bockstal, F. Herlach, C. T. Foxon, and J. J. Harris, Phys. Rev. B **48**, 5457 (1993).

[18] For one low-density, low-mobility sample (no. 4 from Ref. [12]) we find an enhanced α_r of about $2 \times \alpha_s$. We attribute this to the sample being close to a Hall-insulator state. We do not expect Eq. (1) to be a good description for such states as is obvious from the strongly temperature dependent ρ_{xx} in the insulating phase for filling factors close to $\nu = \frac{1}{5}$ which is observed in high mobility 2DEGs.

Chapter 5

Magneto-thermoelectric Properties of Two-Dimensional Electron Gases in the Fractional Quantum-Hall Regime

Measurements of the two coefficients of the phonon drag thermoelectric power (TEP), the thermopower S_{xx} and the Nernst-Ettingshausen coefficient S_{yx}, in two-dimensional electron gases (2DEGs) are presented for the temperature range $T = 0.15 \ldots 1.2$ K in magnetic fields up to $B = 30$ T. Our main interest is focussed on the regime of the fractional quantum Hall effect. We demonstrate the phonon drag origin of the thermopower by its dependence on the crystallographic orientation of the temperature gradient in zero magnetic field as at half filling of the lowest Landau level.

The phonon drag TEP in the fractional quantum Hall regime is described consistently within the recent model of composite fermions. The magnetic field dependent quantum oscillations in S_{xx} are well understood in this model. The thermopower at $\nu = \frac{1}{2}$, $S_{xx}(\frac{1}{2})$, is experimentally shown to have many similarities with the thermopower in zero magnetic field, S_0, in line with the theoretical concept of vanishing effective magnetic field for composite fermions. For the temperature dependence we find $S_{xx}(\frac{1}{2}) \propto T^{3.5}$ and $S_0 \propto T^4$, respectively. Furthermore, the thermopowers for different composite fermions are found to be related as $S_{xx}(\frac{3}{2}) = S_{xx}(\frac{1}{2})$ and $S_{xx}(\frac{3}{4}) = S_{xx}(\frac{1}{4})$, respectively, thus determined by the number of flux quanta bound in the composite fermion. The dependence of the TEP on electron density is studied as well. The experimental results can be understood by applying an existing theory for phonon drag TEP in zero magnetic field based on a solution of the Boltzmann equations to composite fermions. The low effective magnetic field behaviour with a characteristic maximum in S_{xx} at $\nu = \frac{1}{2}$, is discussed as well.

In contrast to the rather intuitive S_{xx}, the very existence of S_{yx}, the other component of phonon drag TEP was in the entire quantum Hall regime not understood so far. We show that S_{yx} is given by the relation $S_{yx} = \alpha B(dS_{xx}/dB)$. A similar relation holds for the resistivity, $\rho_{xx} = \alpha B(d\rho_{xy}/dB)$. Moreover, the scaling constants α are experimentally found to be identical. The equivalence of the two equations is made clear in two independent approaches. S_{yx} has another

contribution which is only observable in the fractional quantum Hall regime and given by a constant offset at filling factors $\nu = \frac{1}{2}$, $\frac{1}{4}$, $\frac{3}{2}$, and $\frac{3}{2}$. These offsets are related to the thermopower of composite fermions although their exact origin is not yet fully understood.

5.1 Introduction

The recent theory of composite fermions [1–3] was very successful in describing the fractional quantum Hall effect which until then was best described in the hierarchical model [4, 5]. The composite fermion picture has renewed the interest of both experimentalists and theoreticians in the fractional quantum Hall effect because of the fascinating properties of the predicted quasi-particles. Composite Fermions are quasi-particles consisting of an electron to which an even number of magnetic flux quanta are bound. The external magnetic field B is transformed to an effective magnetic field, e.g. $B_{\text{eff}} = B - B_{1/2}$ for composite fermions containing two flux quanta. $B_{1/2}$ is the magnetic field at $\nu = \frac{1}{2}$, where $\nu = n_e h/eB$ is the Landau level filling factor for the electron density n_e. Thus, certain even denominator filling factors can be regarded as composite fermion states with $B_{\text{eff}} = 0$ which have a well-defined Fermi surface [3]. In this model, the fractional quantum Hall effect is interpreted as the integer quantum Hall effect of composite fermions.

Besides resistivity [6–11] and conductivity [12] measurements, experiments involving the semi-classical trajectories of composite fermions, e.g. geometric resonances in antidot arrays [13] and magnetic focusing [14, 15], convincingly demonstrated that the new quasi-particles are 'real'. In addition to these electrical transport studies, experiments studying the interaction of composite fermions with acoustic phonons played a prominent role in their investigation, e.g. surface acoustic waves [16], phonon limited mobility [17], and phonon drag thermoelectric power (TEP) [18–23].

Phonon drag thermopower is due to the interaction between acoustic bulk phonons and the 2DEG. The net phonon flow in a temperature gradient drags electrons with it due to electron-phonon scattering. Since there is no net current this drag current is compensated via a current due to an electric field. It is important to note that, for both phonons and electrons, electron-phonon scattering is by far a minor scattering event. The phonon mean free path Λ is limited by boundary scattering at low temperatures, the electron scattering is dominated by τ_{imp}, the impurity scattering time. Because both drag and compensation current depend on τ_{imp}, and there is no net current, the thermopower is independent of τ_{imp}. Instead, the usually negligible electron-phonon scattering is observable in phonon drag TEP because there is a preferential scattering direction defined by the net phonon flow in ∇T. This property makes phonon drag TEP an interesting experiment to investigate 2DEGs in the quantum Hall regime.

There are two components for TEP, the thermopower S_{xx} and the Nernst-Ettingshausen coefficient S_{yx}. TEP in the integer quantum Hall effect has been a subject of research for many years; the major results have been summarized in a recent review [24]. Apart from phonon drag, there is another contribution due to diffusion which usually, and also in this study, is negligible except for very high or very low temperatures. In the integer quantum Hall effect S_{xx} is theoretically understood, however, the experimental observation of S_{yx} being phonon drag dominated could not be explained since theory predicts

$S_{yx} = 0$ [24, 25]. In the fractional quantum Hall regime, phonon drag TEP had been measured in low density samples in the ^{3}He-temperature range [26–28]. The characteristic plateau structure in S_{xx} around $\nu = \frac{1}{2}$ and $\nu = \frac{1}{4}$ and the behaviour of S_{yx} could not be explained in the hierarchical model. Observations of the phonon drag [18, 21–23] and diffusion [19, 29] dominated component S_{xx} have been related to composite fermions in later studies. In a recent paper [20], we have shown that the composite fermion picture indeed provides an intuitive description for the experimental observations when combined with a zero-field Boltzmann approach for phonon drag TEP.

In this work, we present detailed experimental studies of both components of the phonon drag TEP, S_{xx} and S_{yx}, of high mobility 2DEGs in the fractional quantum Hall regime for magnetic fields up to $B = 30$ T in the temperature range $T = 0.15 \ldots 1.2$ K. The phonon drag origin of the thermopower is demonstrated by its dependence on the crystallographic orientation of the temperature gradient. The study of the thermopower of composite fermions includes the temperature and density dependence, the relation between different composite fermion states, the field dependence in low *effective* magnetic field and implications for the phonon limited mobility of electrons and composite fermions. The experimental findings find a natural explanation in the theoretical description using a Boltzmann approach in zero magnetic field [30, 31], which we adapt for use with composite fermions. Furthermore, the oscillatory structure of S_{yx} in the integer and fractional quantum Hall regime is shown to be described by the simple relation $S_{yx} = \alpha(dS_{xx}/dB)$ in an analogue way to a known relation between the resistivity coefficients. Composite fermion related features in S_{yx} are discussed as well.

This chapter is organized as follows. Section 5.2 gives the basic theoretical concepts for thermoelectric power in 2D systems. Section 5.3 describes the investigated samples section 5.4 proves experimentally that it is indeed phonon drag which is measured, and section 5.5 presents an overview of the magnetic field dependence of both components of TEP, the thermopower S_{xx} and Nernst-Ettingshausen coefficient S_{yx}. Section 5.6 deals with the manifestations of composite fermions in S_{xx} and shows that it can be understood completely in this model. Finally, S_{yx} is analyzed in detail in section 5.7.

5.2 Basic Theory

Thermoelectric transport in general is described by the equations for the electrical and thermal current density, $\boldsymbol{J}$ and $\boldsymbol{U}$, respectively, under the influence of $\boldsymbol{E}$ and ∇T [32],

$$\boldsymbol{J} = \sigma \boldsymbol{E} - \epsilon \nabla T, \tag{5.1}$$

$$\boldsymbol{U} = T\epsilon \boldsymbol{E} - \lambda \nabla T, \tag{5.2}$$

where σ is the electrical conductivity, ϵ the thermoelectric tensor, and λ the thermal conductivity. Since the thermoelectric power S, which is defined as $\boldsymbol{E} = S\nabla T$, is measured without external current, i.e. $\boldsymbol{J} = 0$, we have $\boldsymbol{E} = \rho\epsilon\nabla T$, thus $S = \rho\epsilon$. In a magnetic field perpendicular to the temperature gradient, there are two independent components, the thermopower S_{xx} and the Nernst-Ettingshausen coefficient S_{yx}, which expressed in components of ρ and ϵ these are

$$S_{xx} = \rho_{xy}\epsilon_{yx} + \rho_{xx}\epsilon_{xx}, \tag{5.3}$$

$$S_{yx} = \rho_{xx}\epsilon_{yx} + \rho_{yx}\epsilon_{xx}. \tag{5.4}$$

There are two distinct processes, diffusion TEP S^d which is a result of the diffusive motion of electrons in a temperature gradient, and phonon drag TEP S^g which arises from momentum transfer from the phonons to the electrons. In the limit of weak electron-phonon interaction [24], the two contributions to the total TEP are independent, i.e. $S = S^d + S^g$.

The diffusion thermopower of a 2DEG can be obtained from the Mott formula [24]

$$S^d = -\frac{\pi^2 k_B}{3|e|}\frac{k_B T}{\sigma}\left.\frac{d\sigma}{dE}\right|_{E_F}, \tag{5.5}$$

where E_F is the Fermi energy. In terms of electronic relaxation time τ, S^d in zero magnetic field is therefore given by [24]

$$S^d = -\frac{\pi^2 k_B}{3|e|}\frac{k_B T}{E_F}(1+p), \tag{5.6}$$

where E_F is the Fermi energy and $p = (E_F/\tau)(\partial\tau/\partial E)|_{E_F}$ is the energy dependence of the electron scattering at E_F. However, diffusion thermopower is negligible for our experimental parameters; the dominant mechanism is phonon drag.

To describe phonon drag thermopower, the idea of a compensation of the drag current is used in two phenomenological approaches. The 'Peltier' approach goes back to the original model of phonon drag thermopower in three-dimensional semiconductors by C. Herring [33] and was applied to 2DEGs by R. J. Nicholas [34]. An electric current $\boldsymbol{J}$ has an associated heat flow $\boldsymbol{U}$, $\boldsymbol{U} = \pi'\boldsymbol{J}$, where π' is the Peltier coefficient. Via the fundamental thermodynamic relation between π' and the thermopower, i.e. $S = \pi'/T$, S is calculated as [24, 34]

$$S = \frac{\Lambda v}{\mu_{\rm ph} T}, \tag{5.7}$$

where $\mu_{\rm ph}$ is the phonon limited electron mobility. Eq. (5.7) is valid for 2D and 3D in the limit of elastic scattering as was shown by comparison with Boltzmann equation results [35].

In another approach, the thermopower is calculated from the balance of the forces phonons and electric field exert on the electrons [24, 35]. In the 2D case,

$$S = \frac{\lambda d}{n_e e v^2}\tau_{pe}^{-1}, \tag{5.8}$$

with n_e the electron density, d the thickness of the substrate, v the sound velocity, and τ_{pe}^{-1} the phonon relaxation rate due to scattering with electrons.

The results for both models, Eqs. (5.7) and (5.8), illustrate the characteristics of TEP discussed above, namely that at low temperatures where electron-phonon interaction is negligible it is still observable in thermopower which can therefore provide unique information. Eq. (5.7) gives $S \propto \mu_{\rm ph}^{-1}$. In resistance measurements, the contribution of $\mu_{\rm ph}^{-1}$ becomes unmeasurably small. In the force balance approach Eq. (5.8) gives $S \propto \tau_{pe}^{-1}$, i.e. S measures the relaxation time of the phonon system if the only process was scattering with electrons. However, the practical use of Eqs. (5.7) and (5.8) to interpret the experimental thermopower is limited since dependences on experimental parameters like n_e and T are hidden in the quantities $\mu_{\rm ph}$ and τ_{pe}.

For two-dimensional electron gases, a detailed theory of the phonon drag thermopower in zero magnetic field going beyond the phenomenological models described above has been formulated by B. G. Cantrell and P. N. Butcher who solve the coupled Boltzmann equations for the 2-dimensional electrons and the 3-dimensional phonons to obtain the phonon drag thermopower [30, 31]. In this model, the phonon drag thermopower S_{xx}^g, written in terms of the dimensionless in-plane and out-of-plane phonon wave vectors $\xi = (\hbar v/k_B T)q$ and $\xi_z = (\hbar v/k_B T)q_z$, respectively, is given by

$$S_{xx}^g = -\frac{k_B^5}{8\pi^3\hbar^6} T^4 \frac{\Lambda}{v^6\rho'} \frac{m^*}{en_e} \iint \frac{\xi^3(\xi^2+\xi_z^2)\, V_{\text{eff}}^2}{\sqrt{(\hbar k_\Gamma^Q/m_Q^* v)^2\xi^2 - \left[\sqrt{\xi^2+\xi_z^2} - (k_B T/2m^* v^2)\,\xi^2\right]^2}} \times \frac{e^{\sqrt{\xi^2+\xi_z^2}}}{\left(e^{\sqrt{\xi^2+\xi_z^2}}-1\right)^2} d\xi\, d\xi_z, \quad (5.9)$$

where ρ' is the mass density of GaAs. In the original paper, only deformation potential scattering was assumed. Piezoelectric scattering can be considered in the same formalism resulting in the same T^4 temperature dependence as in Eq. (5.9) when screening is included. Therefore, we have written S^g in Eq. (5.9) with an effective scattering potential V_{eff} which has to be replaced by the correct expression for deformation and piezoelectric scattering, respectively [36, 37]. The simplified notation puts forward all qualitative dependencies and facilitates the understanding of the underlying physics. Further details of this model can be found in chapter 1.

The basic principle of phonon drag remains the same also in the presence of a magnetic field. Of course, there is the Hall angle between J_e and E and, in exactly the same way, between J_g and ∇T which gives $E \| \nabla T$ just like in zero magnetic field. Thus, neglecting quantum oscillations we expect S_{xx}^g is constant and $S_{yx}^g = 0$. For 2DEGs, also detailed semi-classical calculations show that the magnetic field dependence is negligible at low temperatures [37]. In the quantum Hall regime, S_{xx}^g reflects oscillations in the density of states and $S_{yx}^g = 0$ in the theory [24, 25]. Thus, the Nernst-Ettingshausen coefficient is expected to be purely due to diffusion.

5.3 Experimental Details

The samples used in this study are GaAs-$Ga_{1-x}Al_xAs$ heterostructures MBE-grown at the University of Nottingham. All three samples 1A, 1B, and 2 were taken from the same wafer. Electron density n_e and mobility μ could be varied in the range $n_e = 1.0 \ldots 1.9 \times 10^{15}$ m^{-2} and $\mu = 60 \ldots 100$ m^2/Vs, respectively, by illumination with an infrared light emitting diode using the persistent photoconductivity effect. For sample 1A measurements were done for different densities in this n_e-range. The comparison between all samples is done for $n_e = 1.75 \times 10^{15}$ m^{-2} near the saturation density. We will mainly concentrate on samples 1A and sample 2 for representative data, all three samples gave consistent results.

The samples differ from each other in a detail of the sample geometry to be able to study what can be called geometry effects in addition to general features of the phonon drag thermopower in the fractional quantum Hall regime. The influence of the width w_m

sample	Mesa Hall bar		substrate	orientation ($\nabla T \| l$)		
	l_m (mm)	w_m (mm)	$l \times w \times d$ (mm^3)	l, l_m	w, w_m	d
1A	4.0	0.300	$9.5 \times 4.0 \times 0.40$	$\langle 100 \rangle$	$\langle 010 \rangle$	$\langle 100 \rangle$
1B	4.0	0.036	$9.5 \times 4.0 \times 0.40$	$\langle 100 \rangle$	$\langle 010 \rangle$	$\langle 100 \rangle$
2	4.0	0.300	$9.5 \times 4.5 \times 0.40$	$\langle 110 \rangle$	$\langle 1\bar{1}0 \rangle$	$\langle 001 \rangle$

Table 5.1: Details of the geometry for the three samples studied. Columns 2 and 3 give the dimensions of the Hall bar defining the 2DEG. Column 4 contains the substrate dimensions and column 5 gives the crystallographic orientation of the sample axes. The temperature gradient ∇T is oriented along the length l of the substrate.

of the conducting channel of the 2DEG is studied by comparing sample 1A (wide Hall bar) and sample 1B (narrow Hall bar). This comparison is mainly done to demonstrate experimentally the important distances in thermopower measurements which differ from the ones in resistivity measurements.

The phonon drag origin of the thermopower is demonstrated by orienting the temperature gradient ∇T along different crystallographic axes, $\nabla T \| \langle 100 \rangle$ for sample 1A and $\nabla T \| \langle 110 \rangle$ for sample 2. Because of the elastic anisotropy of GaAs the phonon mean free path changes which influences the measured thermopower. The Hall bar orientation is $l_m \| l \| \nabla T$, where l_m and l are the length of the mesa and the substrate, respectively. The sample dimensions and orientations are listed in Table 5.1. Details of the experimental setup for thermopower measurements are given in chapter 2.

5.4 The Phonon Drag Origin of Thermoelectric Power

To distinguish between diffusion and phonon drag thermopower, its temperature dependence is a suitable criterion. Diffusion thermopower is linear in temperature whereas phonon drag varies with a stronger power of T depending on the electron-phonon scattering mechanism involved. At low temperatures, $S \propto T^4$ is predicted for phonon drag thermopower [36] as is expressed in Eq. (5.9).

The experimental thermopower in zero magnetic field, S_0, is shown in Fig. 5.1 for samples 1A and 2. It is strongly temperature dependent approaching $S_0 \propto T^4$ at low temperatures, thus consistent with pure phonon drag. The statistical uncertainty for the exponent is about ± 0.25 in absolute value. A systematic error, e.g. due to the temperature range fitted, is difficult to quantify but is estimated to be at maximum of the same order. At higher temperatures, a strong temperature dependence of S is generally observed and identified with phonon drag [24, 26, 28, 38]. However, the theoretically expected T^4-dependence at low temperatures has not been observed in experiments so clearly before.

In addition to the similarity in T-dependence, Fig. 5.1 also shows that the absolute values differ significantly for the two samples. Sample 1A has the temperature gradient ∇T

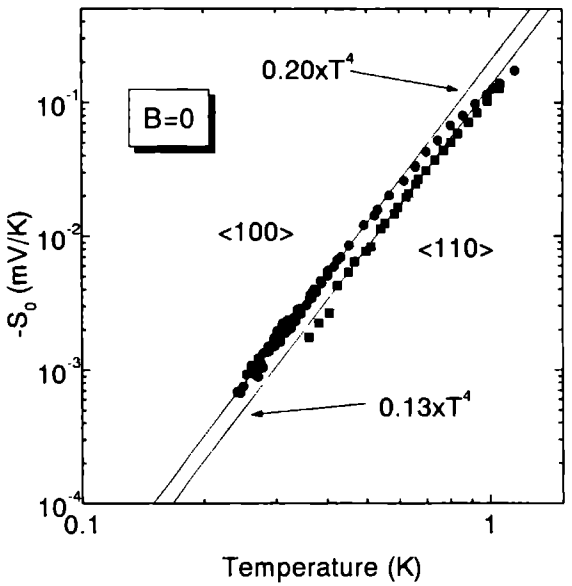

Figure 5.1: Temperature dependence of the zero field thermopower for sample 1A with $\nabla T \| \langle 100 \rangle$ and sample 2 with $\nabla T \| \langle 110 \rangle$. Lines are fits of a T^4-dependence at low temperature.

oriented along the $\langle 100 \rangle$ crystal axis, for sample 2 $\nabla T \| \langle 110 \rangle$. Since this is the only difference between the two samples we can assign the difference in thermopower to a different ∇T-orientation with respect to the crystal axes. We find $S(100)/S(110) = 1.54$ for the thermopower in zero field, with an uncertainty of about 20% including the systematic error.

The phenomenological models [Eqs. (5.7) and (5.8)] as well as the Boltzmann theory [Eq. (5.9)] show that phonon drag thermopower depends on the thermal conductivity λ or the phonon mean free path Λ, respectively. Fig. 5.2 presents the experimental thermal conductivity in the three samples. λ has a cubic temperature dependence $T \approx 1$ K. Note the good agreement between λ measured for the two different $\langle 100 \rangle$ samples, 1A and 1B, and the considerably lower λ for heat flow along $\langle 110 \rangle$ in sample 2. The experimental proportionality factors $\gamma = \lambda/T^3$ are $\gamma(100) = (9.42 \pm 0.66)$ W K^{-4}m^{-1} and $\gamma(110) = (4.87 \pm 0.57)$ W K^{-4}m^{-1}, with the statistical error of one standard deviation. Thus, we find experimentally the ratio $\lambda(100)/\lambda(110) = 1.93 \pm 0.39$, where an additional systematic uncertainty of about 15% originating from the finite size of the thermometers is included. This ratio is roughly similar to the ratio observed for thermopower.

The origin of the orientation dependence of λ is due to the elastic anisotropy of GaAs crystals. The thermal conductivity λ is in general given by [39]

$$\lambda = \frac{1}{3} C_V v \Lambda, \tag{5.10}$$

where C_V is the specific heat, Λ the effective mean free path, and v the effective phonon

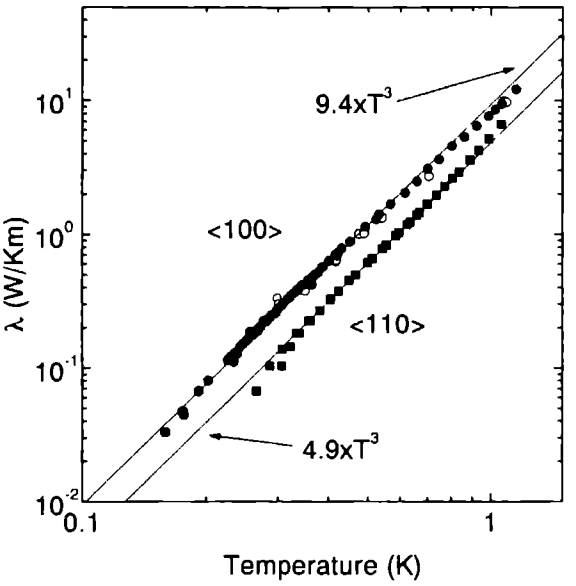

Figure 5.2: Thermal conductivity for heat flow along different crystallographic directions, i.e. ⟨110⟩ for sample 2 (■) and ⟨100⟩ for samples 1A (•) and 1B (○), respectively. Lines are fits of a cubic temperature dependence.

group velocity[1]. In GaAs-$Ga_{1-x}Al_xAs$ heterostructures, λ is completely dominated by long-wavelength acoustic phonons in the bulk of the GaAs substrate at the low temperatures as used in the experiments ($T \lesssim 1$ K). At these temperatures, defect, impurity and phonon-phonon scattering are negligible and Λ is limited by scattering at the sample boundaries as was first observed by H. B. G. Casimir [40]. The clean T^3-dependence observed in the experiments is characteristic for a constant Λ in the boundary scattering limit since $C_V \propto T^3$.

In elastically isotropic crystals, Λ is determined by the dimensions of the sample only. In elastically anisotropic crystals, however, phonon focusing has a considerable effect on the thermal conductivity. This influence has been studied theoretically by A. K. McCurdy [39] in great generality and we follow his treatment and notation in the analysis. Phonon focusing is a result of the phonon constant energy surface being non-spherical. The group velocity, and therefore the heat flow, is perpendicular to the the constant energy surface. Thus, group and phase velocity are not parallel and even an ideal, i. e. isotropic, heat source gives a heat flow focussed in certain directions. Consequently, the thermal conductivity in a real crystal depends on its geometry and crystallographic orientation and can be calculated given only the linear dimensions, density and elastic constants of the crystal [39].

[1]For details of the definition of ν and the effect of anisotropy on it we refer the reader to McCurdy's original paper [39].

The elastic constants of GaAs are [41] $C_{11} = 112.6$, $C_{12} = 57.1$, and $C_{44} = 60.0$ in units of $10^9\,\mathrm{N/m^2}$. These constants reduce to two important parameters needed in the calculation, the elastic ratio $C_{12}/C_{11} = 0.507$ and the anisotropy factor $A = 2C_{44}/(C_{11} - C_{12}) = 2.16$. The specific heat is [42] $C_V = 3.49 \times 10^{-6}\,\mathrm{J\,cm^{-1}\,K^{-4}} \times T^3$, the effective phonon velocity is computed as $v = 4.03 \times 10^5\,\mathrm{cm/s}$. Sample dimensions are listed in Table 5.1.

In the isotropic case, the (Casimir) mean free path Λ_C is given by [39]

$$\begin{aligned}\Lambda_C = (n^{1/2}D/4)\,\{&3n^{1/2}\ln\left[n^{-1} + (n^{-2}+1)^{1/2}\right]\\ &+3n^{-1/2}\ln\left[n + (n^2+1)^{1/2}\right]\\ &-(n+n^3)^{1/2} + n^3/2\\ &-(n^{-1}+n^{-3})^{1/2} + n^{-3/2}\},\end{aligned} \tag{5.11}$$

for rectangular samples of thickness D and width $w = nD$. In our case, $\Lambda_C = 1.06$ mm for sample 1A and $\Lambda_C = 1.09$ mm for sample 2. The elastic anisotropy in GaAs, however, leads to phonon focusing and thus enhanced thermal conductivity along ⟨100⟩ and slight defocusing along ⟨110⟩, especially for our samples with extreme width-to-thickness ratio and the shortest side face oriented in the ⟨100⟩ direction. Applying McCurdy's corrections to the case of GaAs, we obtain $\Lambda(100) = 1.39$ mm and $\Lambda(110) = 0.83$ mm for our samples. Therefore, the thermal conductivities for sample 1A and 2 should theoretically differ by a factor of 1.67 only because of their different crystallographic orientation. This is in reasonably good agreement with the experimental value of 1.93 ± 0.39.

In addition to this ratio the absolute values of Λ, obtained from the experimental λ using Eq. (5.10), can be compared with theory as well. We obtain $\Lambda(100) = 2.01$ mm and $\Lambda(110) = 1.04$ mm. Both values are about 40% higher than the theoretical ones. Such behaviour is expected since in the calculations totally diffusive scattering of the phonons at the sample boundaries is assumed. In realistic samples, however, part of the phonons are specularly reflected, especially at the top surface which is highly polished. For a fraction f of specular reflection, Λ is increased by a factor $F = (1+f)/(1-f)$ [43], thus a 40% increase corresponds to $f = 17\%$ specular reflection which seems a reasonable number.

For a comparison of the thermopower ratio with the corresponding ratio for λ it is important to note that the systematic error due to the finite size of the thermometers cancels since it enters identically into the calculation of λ and S, respectively, leaving an error of 13%. Therefore we obtain for the thermopower $S(100)/S(110) = 1.54 \pm 0.20$ and for the thermal conductivity $\lambda(100)/\lambda(110) = 1.93 \pm 0.26$ taking only statistical errors into account. Both ratios are quite close together showing that Λ affects both λ and S in a similar way[2]. Although the error ranges of the ratios for Λ and S slightly overlap the ratio for the thermopower is systematically a little smaller. Such a slight difference is not surprising because both S and λ measure averages over a variety of phonon modes. Moreover, two different scattering mechanisms, piezoelectric and deformation potential scattering, contribute to the thermopower and the scattering probabilities depend on phonon polarization and direction. Thus it is probable that S reflects not only a change in the average phonon mean free path but in addition a difference in phonon-electron scattering for different crystallographic orientations.

[2] At higher temperatures, the direct influence of the phonon mean free path on the thermopower has been observed by R. Fletcher *et al.* [38, 44] who changed Λ by a factor of 2 by polishing the back surface of the substrate and by this means altering the fraction of specular reflection of phonons at the sample boundaries.

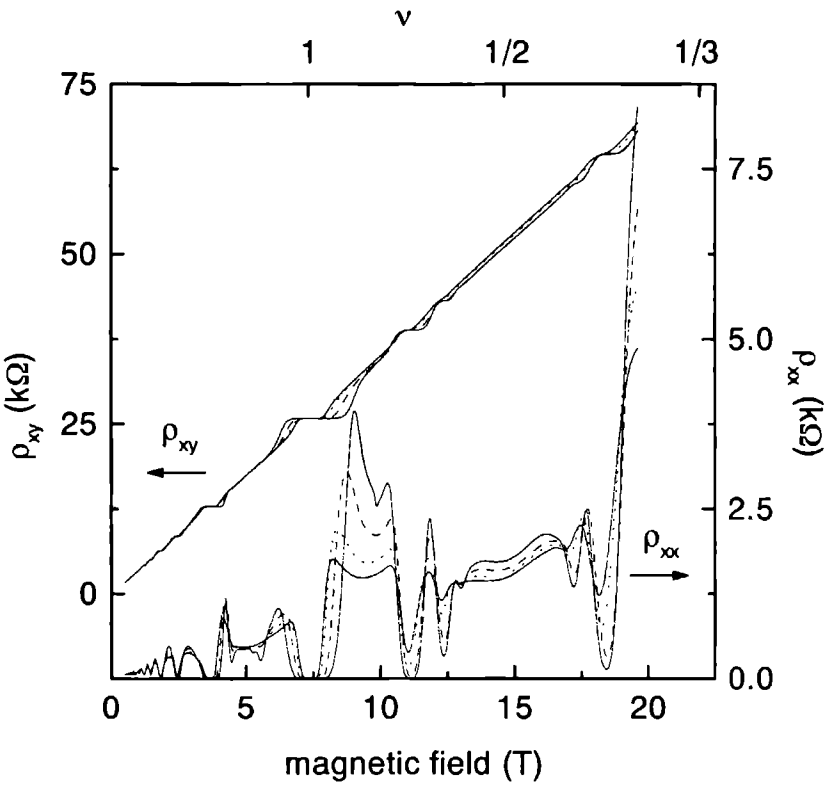

Figure 5.3: Longitudinal resistivity ρ_{xx} and Hall resistivity ρ_{xy} of sample 1A for $T = 206$ mK (continuous), 396 mK (dashed), 599 mK (dotted), and 785 mK (continuous), respectively.

In conclusion, both temperature and orientation dependence show the phonon drag origin of thermopower in our samples down to temperatures below $T = 200$ mK. In this section, we have only discussed the situation in zero magnetic field. However, the phonon system obviously is not affected by magnetic fields and the dependence of the thermopower on Λ, and therefore its phonon drag origin, remains valid in high magnetic fields as well (see Figs. 5.7 and 5.15).

5.5 General Magnetic Field Dependence

In this section we present an overview of the experimental results for the magnetic field dependence of the electrical and thermoelectric transport coefficients studied, i.e. the thermopower S_{xx}, Nernst-Ettingshausen coefficient S_{yx}, longitudinal resistivity ρ_{xx}, and Hall-resistivity ρ_{xy}. By means of this survey we highlight the central questions which are addressed in the detailed studies of section 5.6 and 5.7.

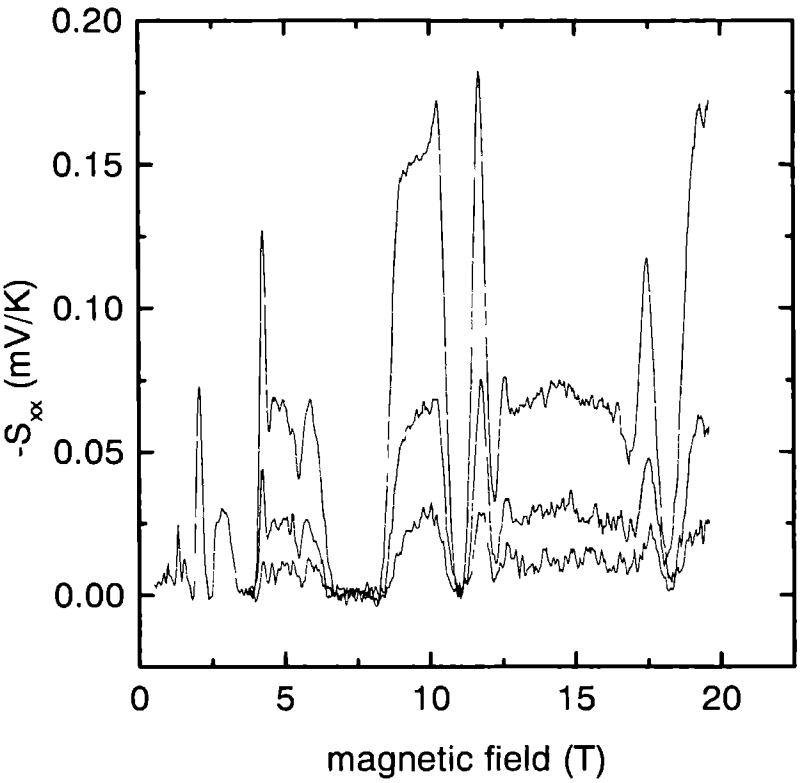

Figure 5.4: Thermopower of sample 2 at very low temperatures, $T =$ 298 mK, 240 mK, and 184 mK, respectively. Below $\nu = 2$ ($B = 3.6$ T), for clarity only the highest temperature curve is shown. The noise level increases, of course, at very low temperatures due to the rapidly decreasing signal size as is explained in chapter 2.

Fig. 5.3 gives a typical example for the well known quantum Hall effect. ρ_{xy} has plateaus at integer and fractional filling factors which become wider with decreasing temperature. In between the plateaus, ρ_{xy} shows a linear field dependence which is the most obvious around $\nu = \frac{1}{2}$ and $\frac{3}{2}$ as well as near $B = 0$. For the filling factors that ρ_{xy} is in a plateau, the longitudinal resistivity ρ_{xx} has minima going to zero at low temperatures; at higher T they are thermally activated.

The very low temperature behaviour of the longitudinal thermopower S_{xx} can be seen in Fig. 5.4 for sample 2. Figs. 5.5 and 5.6 show both coefficients of the thermoelectric power, S_{xx} and S_{yx}, for sample 1A and sample 2, respectively. S_{xx} has characteristic minima at integer and fractional filling factors which can be well understood within the hierarchical model. At these filling factors, the Fermi energy is in an energy gap. Because phonon energies are low compared to the cyclotron energy, states near the Fermi energy cannot be scattered into extended states in the center of a Landau level and the thermoelectric power

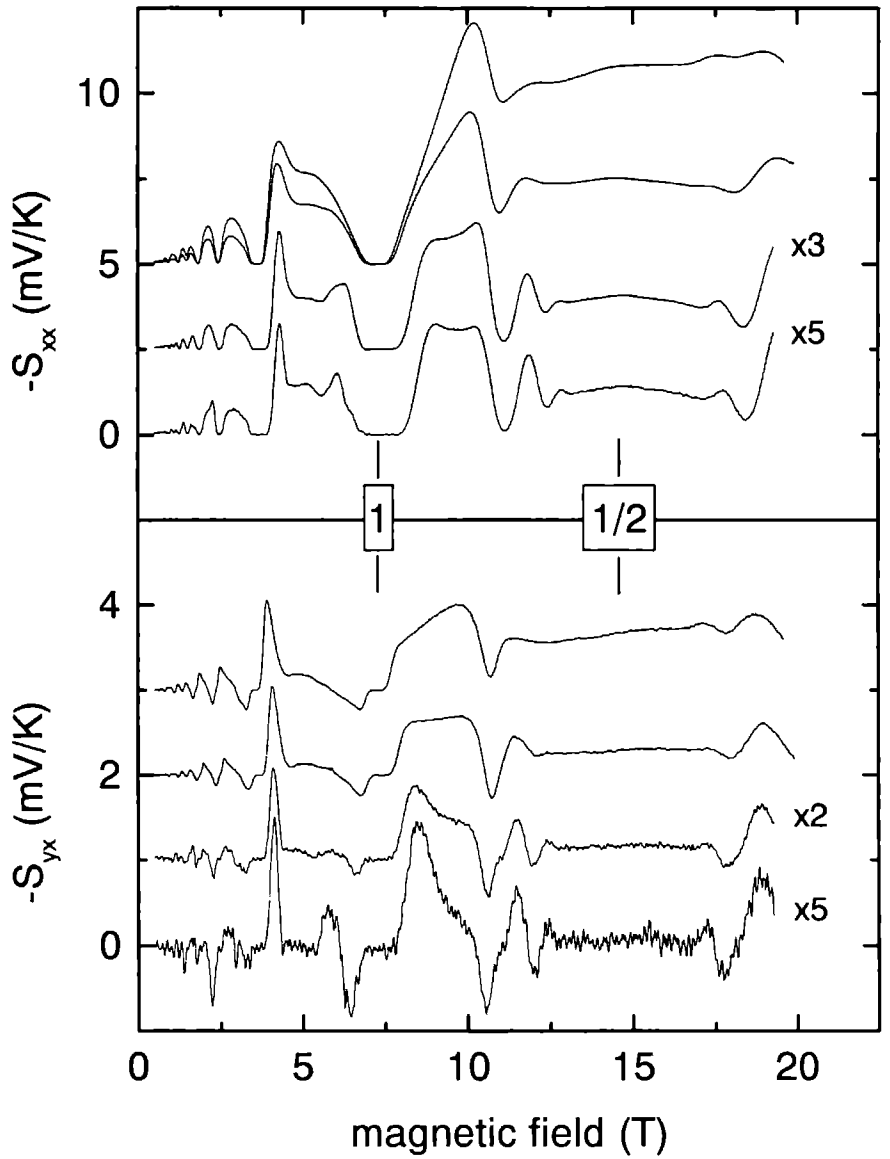

Figure 5.5: Magnetic field dependence of thermopower S_{xx} (top) and Nernst-Ettingshausen coefficient S_{yx} (bottom) of sample 1A for different temperatures (T = 985, 742, 474, and 373 mK, respectively). S_{xx} curves are offset by 5 mV/K (985 and 742 mK) and 2.5 mV/K (474 mK), respectively. S_{yx} curves are offset by 3, 2, and 1 mV/K for T = 985, 742, and 474 mK, respectively. Note the scaling factors for the two lowest T curves.

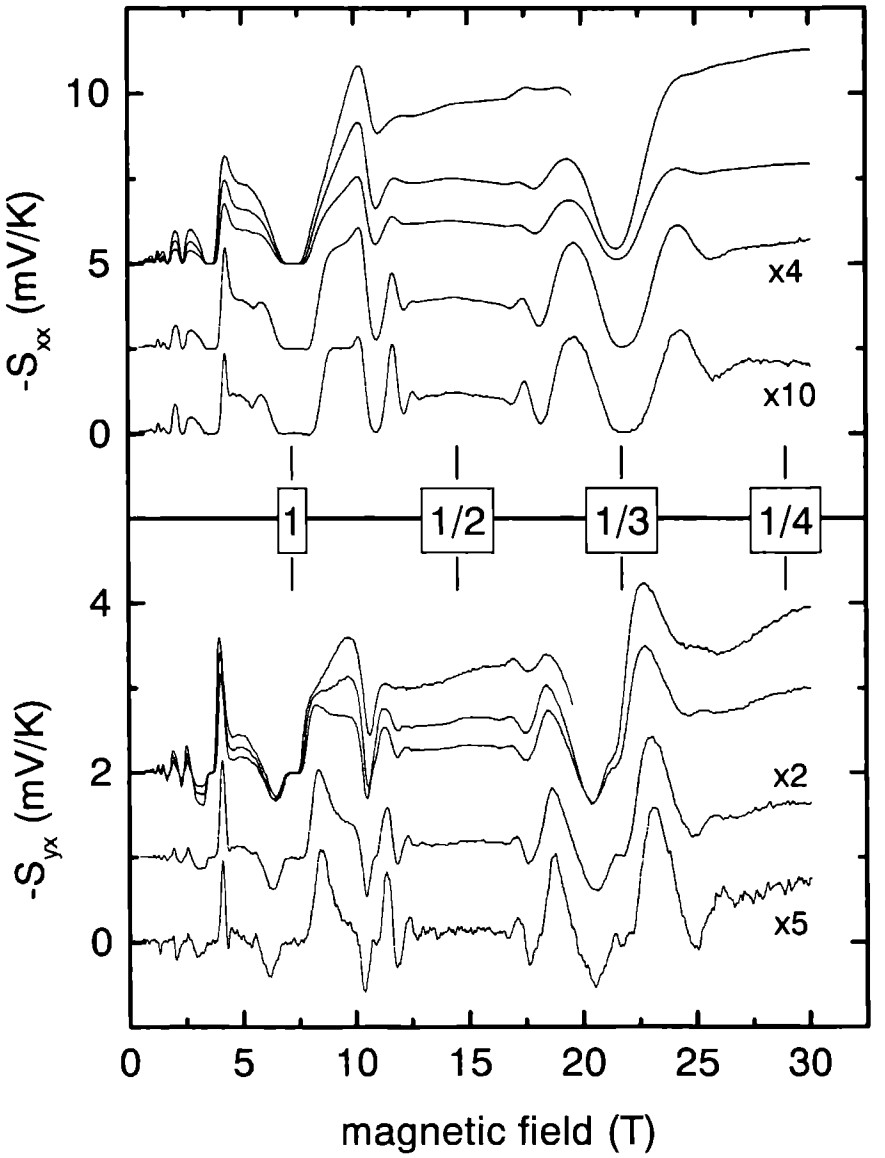

Figure 5.6: Magnetic field dependence of thermopower S_{xx} (top) and Nernst-Ettingshausen coefficient S_{yx} (bottom) of sample 2 for different temperatures ($T = 975, 829, 700, 504$, and 350 mK, respectively). Offsets are for S_{xx} (S_{yx}) 5 mV/K (2 mV/K) for the three highest T-curves and 2.5 mV/K (1mV/K) for the $T = 504$ mK curves. Note the scaling factors for the two lowest T curves. Important filling factors ν are indicated.

vanishes.

Whereas the minima at fractional filling factors are well understood in the hierarchical model, this theory fails in providing a convincing explanation for the regions in-between the minima in the thermopower. It was already remarked by Zeitler *et al* [26], who measured phonon drag thermopower in the ^{3}He-temperature range, that S_{xx} has another characteristic distinctly different from ρ_{xx} which was described as " ... the $\nu = \frac{1}{3}$ filling acts as a boundary between two different states. ... S_{xx} reveals two plateaus for $\frac{2}{3} > \nu > \frac{1}{3}$ and $\nu < \frac{1}{3}$ ... " [26]. This behaviour can be seen in the higher temperature curves in Fig. 5.6. Another observation not understood in the hierarchical model is the huge absolute magnitude of S_{xx} in the fractional quantum Hall regime as compared to zero magnetic field. In recent years, a theoretical model for the fractional quantum Hall effect was elaborated [1–3] which describes these states as new quasi-particles, the composite fermions. Section 5.6 is devoted to the manifestations of these fascinating quasi-particles in thermoelectric power.

S_{yx} has a characteristic which distinguishes it from the other transport coefficients. At filling factors where S_{xx} and ρ_{xx} have minima S_{yx} changes sign. Thus, qualitatively it has similarities with the derivative of the thermopower with respect to magnetic field, dS_{xx}/dB. This behaviour has been noted before in the integer [38] and fractional quantum Hall regime [26] but was so far not understood. Theory even predicts $S_{yx} = 0$ for phonon drag [24]. Section 5.7 solves this problem by relating S_{yx} to S_{xx} in a way similar to a known relation between ρ_{xx} and ρ_{xy}.

The magneto-thermopower of two samples with different ∇T orientation is shown in Fig. 5.7. The absolute value of S_{xx} for sample 1A differs for the entire magnetic field range by a constant factor compared to sample 2 whereas the curve shape is the identical. The scaling factor is the same as in zero magnetic field for S_0 (see Fig. 5.1). Thus, also in a magnetic field the scaling with the phonon mean free path remains valid for the thermopower. S_{yx} is very similar in the two samples in both absolute magnitude and curve shape [see Fig. 5.7(b)].

Fig. 5.8 compares TEP data of two samples, 1A and 1B, with largely different width of the conducting channel of the mesa, $w_m(1A) = 300\ \mu$m and $w_m(1B) = 36\ \mu$m, respectively, with otherwise identical properties (see Table 5.1). S_{xx} and S_{yx} are very similar in the two samples, especially in the quantum limit ($\nu < 1$). Note that although w_m differs by about an order of magnitude, S_{xx} and S_{yx} are obtained from the raw voltages using the same geometry factor just given by the distance between the contacts, i.e. the physical contacts between 2DEG and metallic pads. Thus, the geometry of the mesa between these contacts is of no importance as long as they are connected by a conducting path of the 2DEG. For comparison, the geometry factor to obtain resistivities in these samples differs, of course, by an order of magnitude.

The agreement of the measurements in these two samples can also be regarded as an indication for the accuracy of the absolute magnitudes obtained in the experiments. Except for this general agreement between samples 1A and 1B there is also a slight difference. S_{xx} in the narrow Hall bar of sample 1B has reduced amplitudes for the higher field peaks (spin up) of the spin-split Landau levels in the integer quantum Hall effect, e.g. $\nu = 2.5$. A similar behaviour is, even stronger, exhibited by ρ_{xx}. Also the higher field part near $\nu = \frac{3}{2}$ is reduced in amplitude which might be related to spin polarized states of composite fermions, the subject of section 5.6. Spin polarization can play an important role around $\nu = \frac{3}{2}$ [11, 45].

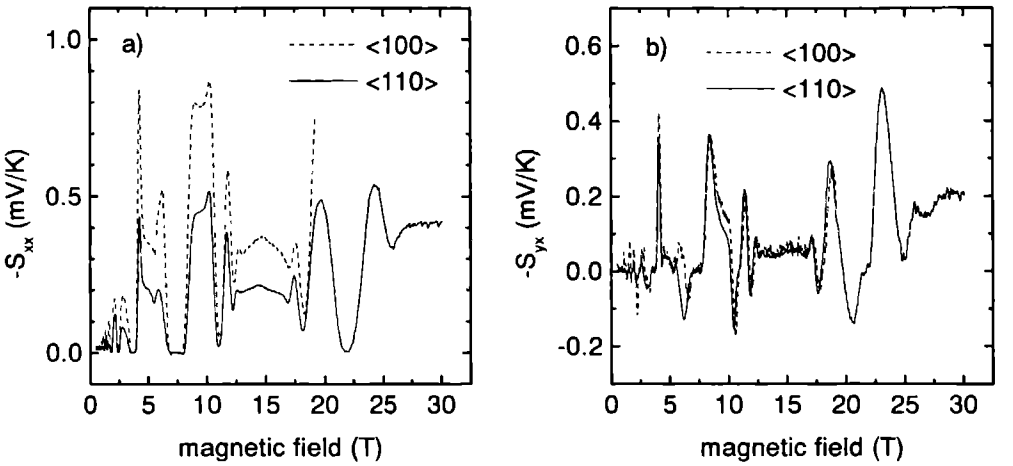

Figure 5.7: Comparison of S_{xx} (a) and S_{yx} (b) for temperature gradients ∇T oriented along different crystallographic directions. Sample 1A has $\nabla T \| \langle 100 \rangle$ (dotted curve, $T = 423$ mK), sample 2 has $\nabla T \| \langle 110 \rangle$ (continuous curve, $T = 424$ mK).

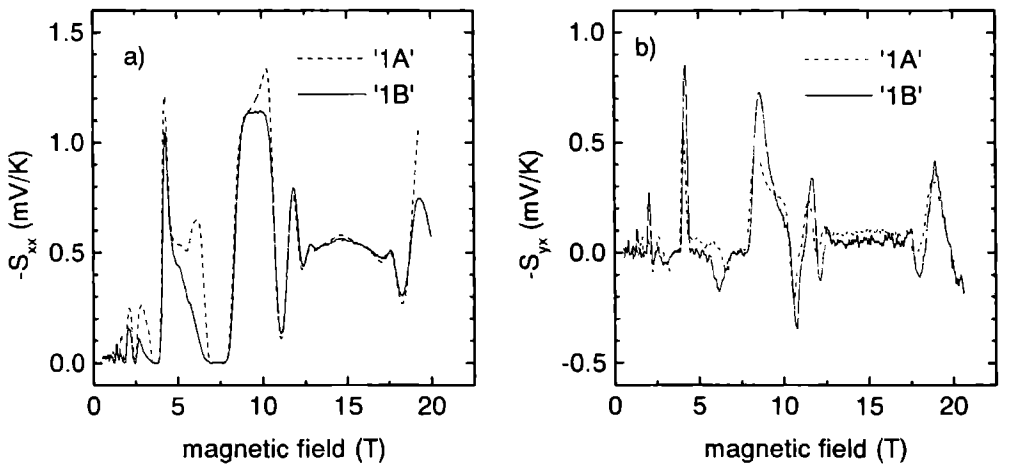

Figure 5.8: S_{xx} and S_{yx} for samples with different width w_m of the Hall bar at $T = 496$ mK. $w_m = 300$ μm and 36 μm for sample 1A (dotted curve) and 1B (continuous curve), respectively. The agreement between the two samples also demonstrates the level of accuracy for the absolute values.

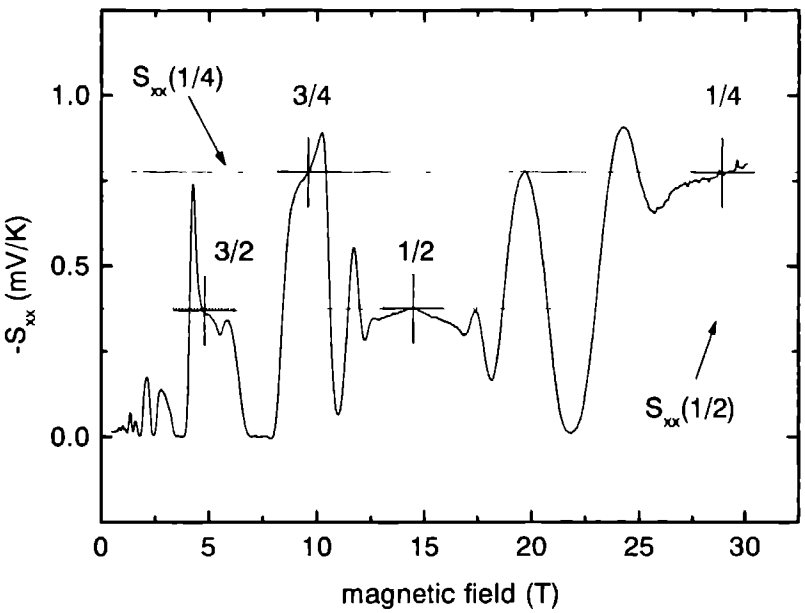

Figure 5.9: Example for S_{xx} in the fractional quantum Hall regime (sample 2, $T = 504$ mK). Even denominator filling factors which can be described as composite fermions are marked. Lines show that $S_{xx}(\frac{1}{2}) = S_{xx}(\frac{3}{2})$ and $S_{xx}(\frac{1}{4}) = S_{xx}(\frac{3}{4})$, respectively.

5.6 Thermopower in the Composite Fermion Picture

The composite fermion model identifies the minima at fractional filling factors as Landau levels of new quasi-particles. Therefore, the oscillatory structure in S_{xx} which was understood in the hierarchical model is, in a very intuitive way, automatically encountered with composite fermions as well (see section 1.1). The strong point of the composite fermion picture is that it provides an explanation for the experimental observations of the thermopower at even denominator filling factors which are not understood in the hierarchical model.

Fig. 5.9 presents a typical field sweep for S_{xx} at at low temperatures. Examining the even denominator filling factors which are of interest in the composite fermion-model, i.e. $\nu = \frac{1}{2}, \frac{3}{2}, \frac{1}{4}$, and $\frac{3}{4}$, one observes the striking result that S_{xx} is the same at $\nu = \frac{1}{2}$ and $\frac{3}{2}$. Also $S_{xx}(\frac{1}{4})$ and $S_{xx}(\frac{3}{4})$ have similar magnitudes and are roughly a factor of two higher than at $\nu = \frac{1}{2}$. Recalling that the number of flux quanta bound to an electron is $\Phi = 2$ for $\nu = \frac{1}{2}$ and $\frac{3}{2}$ and $\Phi = 4$ for $\nu = \frac{1}{4}$ and $\frac{3}{4}$ we conclude that the phonon drag thermopowers of composite fermions with the same Φ is identical.

Studying the temperature dependence of the ratio $\gamma(\nu_1, \nu_2) = S_{xx}(\nu_1)/S_{xx}(\nu_2)$ makes the relation between the even denominator filling factors even clearer. Fig. 5.10 (a) shows the ratios $\gamma(\frac{3}{2}, \frac{1}{2})$ and $\gamma(\frac{3}{4}, \frac{1}{4})$. In both cases, γ increases with decreasing temperature until

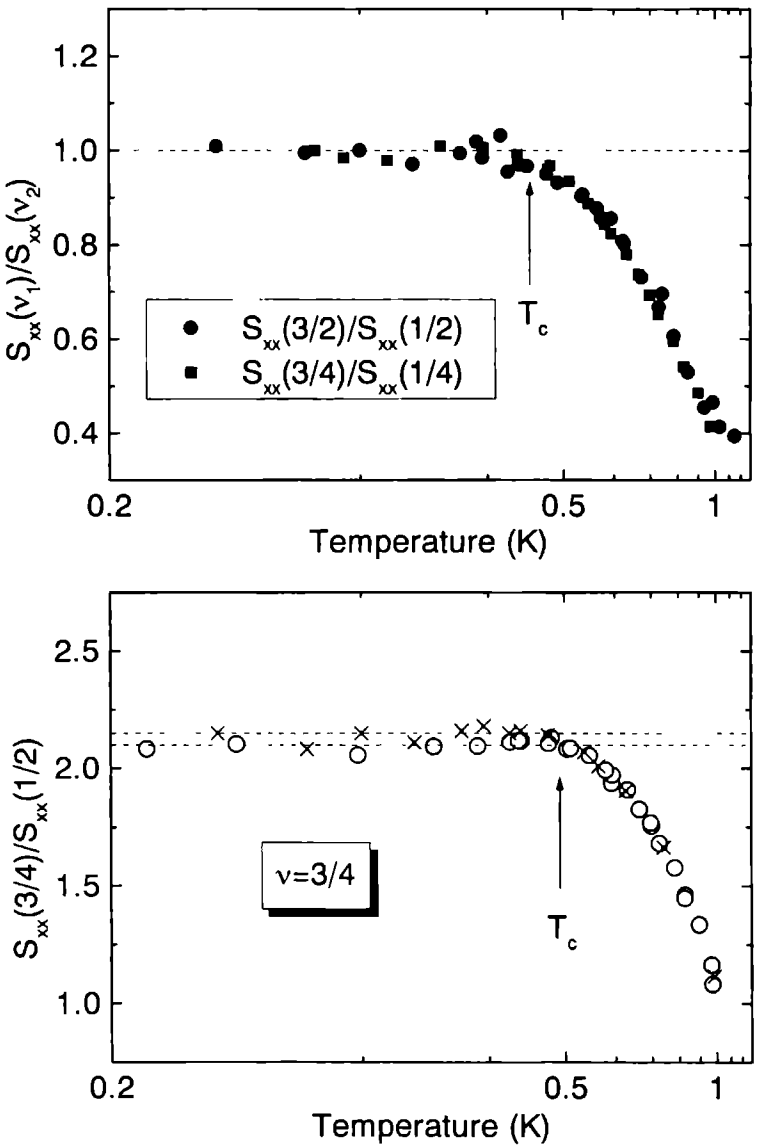

Figure 5.10: Ratios between different even denominator filling factors. a) $S_{xx}(\frac{3}{2})/S_{xx}(\frac{1}{2})$ and $S_{xx}(\frac{3}{4})/S_{xx}(\frac{1}{4})$ for composite fermions with the same number of flux quanta. Below $T_c \simeq 480$ mK, the ratios are unity (indicated by dashed line). b) Comparison between composite fermions with $\Phi = 2$ and 4 for sample 1A (×) and sample 2 (○). Below T_c, the ratio is constant. $S_{xx}(\frac{3}{4})/S_{xx}(\frac{1}{2}) = 2.15$ for sample 1A and 2.10 for sample 2, respectively.

ν	$\frac{1}{2}$	$\frac{1}{4}$	$\frac{3}{2}$	$\frac{3}{4}$
n_Q	n_e	n_e	$\frac{1}{3}n_e$	$\frac{1}{3}n_e$

Table 5.2: Quasi-particle density n_Q for the even denominator filling factors which are described as composite fermions.

a characteristic temperature T_c is reached. Below T_c, the ratios are constant and within experimental accuracy γ is unity. This is the more remarkable since the absolute value of S_{xx} is strongly temperature dependent varying by about two orders of magnitude over the temperature range where γ is constant. Fig. 5.10 (b) compares $S_{xx}(\frac{3}{4})$ to $S_{xx}(\frac{1}{2})$. A very similar behaviour is observed; only the constant value of γ is changed, $\gamma(\frac{3}{4}, \frac{1}{2}) = 2.15\,(2.10)$ for sample 1A (sample 2).

To understand the striking observation that composite fermion-states with the same number of flux quanta Φ have identical thermopower, we have adapted the Boltzmann model resulting in Eq. (5.9) for electrons in zero magnetic field to composite fermions in zero *effective* magnetic field. In the derivation, we have identified the scattering integral with the composite fermion-phonon scattering and used the fact that quasi-particle and total current density are related as [3] $J_{\text{tot}} = (n_e/n_Q)J_Q$ (for details of the derivation see chapter 1). Under these assumptions, we obtain in the limit of $q_d \ll 2k_f$, where $q_d \approx 4k_BT/\hbar v$ is the dominant phonon wave vector,

$$S_{xx}^{g,Q} = -A'T^4\frac{m^*}{n_e}\iint \frac{m_Q^* v}{\hbar k_f^Q}\xi^2(\xi^2+\xi_z^2)\,V_{\text{eff}}^2\,\frac{e^{\sqrt{\xi^2+\xi_z^2}}}{\left(e^{\sqrt{\xi^2+\xi_z^2}}-1\right)^2}\,d\xi\,d\xi_z, \tag{5.12}$$

with $A' = (k_B^5\Lambda/8\pi^3\hbar^6v^6\rho' e)$.

The difference between $\nu = \frac{3}{2}$, which is a $\nu = \frac{1}{2}$ composite fermion-state added to a filled Landau level, and $\nu = \frac{1}{2}$ is the difference in the density of quasi particles n_Q (see Table 5.2). Eq. (5.12) shows that the interaction with phonons depends, apart from n_Q independent quantities, on the ratio $m_Q^* v/\hbar k_F^Q$. Both m_Q^* and k_F^Q scale with $\sqrt{n_Q}$, hence their ratio is constant and we obtain $S_{xx}(\frac{3}{2}) = S_{xx}(\frac{1}{2})$ and in the same way $S_{xx}(\frac{3}{4}) = S_{xx}(\frac{1}{4})$. The experimental finding that indeed $S_{xx}(\frac{3}{2}) = S_{xx}(\frac{1}{2})$ can therefore be seen as a proof that the quasi-particle mass scales as $m_Q^* \propto \sqrt{n_Q}$ as predicted theoretically [3].

The above considerations are not only valid for the approximation Eq. (5.12) but also for the full expression Eq. (1.25) as can be seen in Fig. 1.5 (b) in chapter 1. Moreover, this figure shows another possible effect of changing n_Q, namely to shift the divergence at $q = 2k_F$ closer to q_d. However, for our experimental parameters, this effect is negligible.

There are two further remarks to make on our treatment of the state at $\nu = \frac{3}{2}$ which, as was stressed many times, only consisted in adjusting the quasi-particle density as $n_Q \to n_Q/3$. It has been shown by Wu and Jain [46] that the wave function of the composite fermions at $\nu = \frac{3}{2}$ is identical with the one at $\nu = \frac{1}{2}$. Therefore, the fact that S_{xx} is independent of n_Q will always hold also for more accurate theoretical models (compared to the effective scattering potential V_{eff} in this work) for the composite fermion-phonon scattering which might involve details of the wave function.

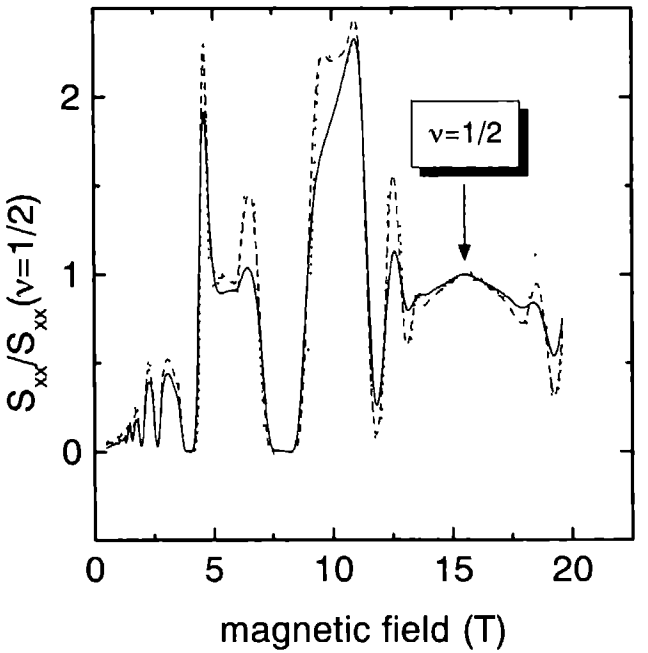

Figure 5.11: Normalizing thermopower sweeps to $S_{xx}(\frac{1}{2})$ provides a natural scaling for the entire field range. Data are from sample 1A with $n_e = 1.89 \times 10^{15}$ m^{-2} for $T = 343$, 436, and 584 mK, respectively. This representation also stresses the constant ratio to $S_{xx}(\frac{1}{2})$ for $\nu = \frac{3}{2}$ and $\frac{3}{4}$, whereas the relative thermopower at other filling factors is clearly temperature dependent.

Secondly, our description implicitly assumed that the composite fermions at $\nu = \frac{3}{2}$ are completely spin polarized[3]. However, it has been shown by Du *et al* [11] that the composite fermions at $\nu = \frac{3}{2}$ are only partially spin polarized. Therefore, the Fermi wave vector is not any more simply given by $k_F^Q = \sqrt{4\pi n_Q}$ but is smaller. Replacing n_Q by the density of quasi-particles with the majority spin direction solves this problem. Hence, the correct conclusion from the experimental observation $S_{xx}(\frac{3}{2}) = S_{xx}(\frac{1}{2})$ has to be that m_Q^* and k_F^Q depend in the same way on the quasi-particle density *and* the spin polarization of the state which is another manifestation of the origin of m_Q^* from electron-electron interaction.

The state at $\nu = \frac{1}{4}$ is described in the composite fermion picture in the same way as $\nu = \frac{1}{2}$ but with $\Phi = 4$ flux quanta attached to an electron. The resemblance of the two states with characteristic plateaus in the thermopower at moderately low temperatures was already remarked in the past [26] and the similar temperature dependence assigned to their composite fermion nature [18, 47]. We measure $\gamma(\frac{1}{4}, \frac{1}{2}) = 2 \ldots 2.5$, the value being slightly T-dependent at higher temperatures. However, this T-dependence is not dramatic. More-

[3]For $\nu = \frac{3}{4}$ this remains a valid assumption

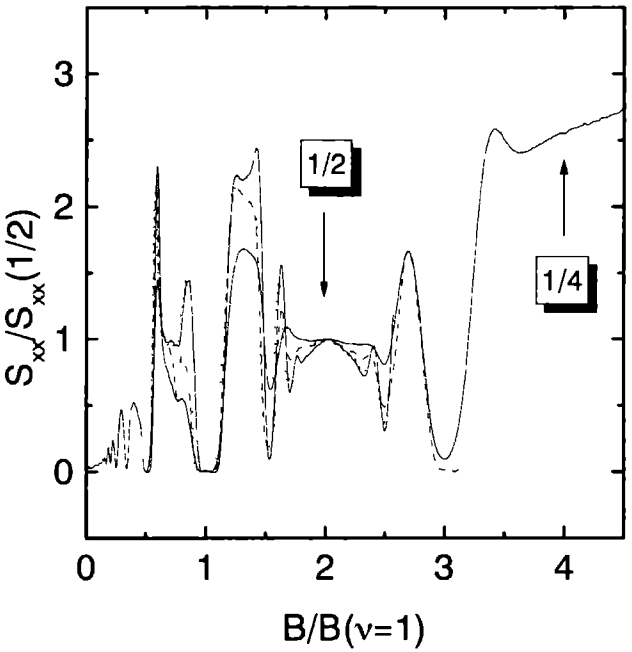

Figure 5.12: Normalized S_{xx} at $T = 436$ mK for four different densities n_e (in units of 10^{15} m^{-2}): 1.89 (continuous curve), 1.76 (dotted), 1.56 (dashed), and 1.04 (continuous), respectively.

over, it is remarkable how well behaved the the thermopower is around $\nu = \frac{1}{4}$ compared to ρ_{xx} which is strongly temperature dependent in this range and, at even lower temperatures, develops into an insulating phase. The increased thermopower at $\nu = \frac{1}{4}$ can again be related to a difference in m_Q^* and/or $V_{\rm eff}^Q$. There are indications from calculations in finite size systems that $m_Q^*(\frac{1}{4}) \approx 2m_Q^*(\frac{1}{2})$ [48]. Unfortunately, experimental data on $m_Q^*(\frac{1}{4})$ are scarce and not as accurate as for $\nu = \frac{1}{2}$ but show a mass enhancement of about this size [7].

We now return to the temperature T_c below which $\gamma(\nu_1, \nu_2)$ is constant. The composite fermion picture is valid for the quasi-particle states as long as it is valid for the incompressible states [2], i.e. the minima in the fractional quantum Hall effect. The minima in S_{xx} and ρ_{xx} at $\nu = \frac{4}{3}$ and $\frac{5}{3}$ which are related to composite fermions at $\nu = \frac{3}{2}$ become observable at about the same temperature as T_c. Thus, T_c can be identified with the formation temperature of composite fermions at $\nu = \frac{3}{2}$ and $\nu = \frac{3}{4}$, respectively. The fact that $T_c \simeq 480$ mK is the same in both cases is consistent with both quasi-particle states having the same (reduced) density $n_Q = n_e/3$ since their formation is due to electron-electron interactions.

The value of $S_{xx}(\frac{1}{2})$ is not only a meaningful quantity to compare with the thermopower at other even denominator filling factors, it also provides a natural reference point for the entire magnetic field dependence in the fractional quantum Hall regime (see Fig. 5.11). Scaling the thermopower with $S_{xx}(\frac{1}{2})$ makes the plot look like a typical ρ_{xx}-plot

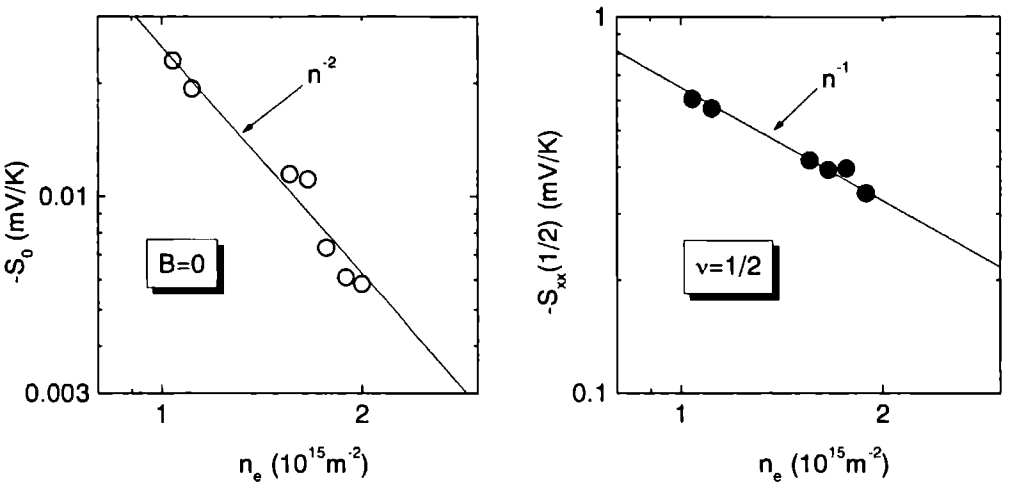

Figure 5.13: Density dependence of the thermopower in sample 1A for a) $B = 0$ and b) $\nu = \frac{1}{2}$ at $T = 440$ mK. Scales are double-logarithmic to show approximate power law dependences.

by taking out the strong T-dependence of the phonon drag leaving only the T-dependence of the electronic structure. Note that scaling by the value of S_{xx} at another filling factor would not give this satisfactory results underlining once again the particularity of $\nu = \frac{1}{2}$.

Apart from comparing even denominator filling factors with different n_Q one can also vary n_e directly. The total electron density was changed in successive steps in the range $n_e = 1.0 \ldots 1.9 \times 10^{15}$ m^{-2} by illumination with an infrared diode using the persistent photoconductivity of the 2DEG. Fig. 5.12 shows field dependencies for different n_e scaled to $S_{xx}(\frac{1}{2})$ as a function of $B/B(\nu = 1)$ for better comparison. The curves are similar to each other with the oscillatory structure being more pronounced for higher densities or magnetic fields. The relations between the composite fermion-states remain for $n_e > 1.5 \times 10^{15}$ m^{-2} as described above, for lower n_e there are deviations for $\nu = \frac{3}{2}$ and $\nu = \frac{3}{4}$. Since also the minima at $\nu = \frac{4}{3}$ and $\frac{5}{3}$ have disappeared we can assign this observation to composite fermion-states not being formed yet because T_c is too low for low electron densities.

Fig. 5.13 presents S_{xx} as a function of n_e at $\nu = \frac{1}{2}$ and at $B = 0$, respectively. $S_{xx}(\frac{1}{2})$ exhibits a clear $1/n_e$ behaviour; for $B = 0$ the dependence is stronger and approximately given by $S_0 \propto n^{-(1.5\ldots2)}$ depending a little on temperature. Eq. (5.12) has an explicit $1/n_e$ dependence in the prefactor and 'hidden' dependencies inside the scattering integral. As discussed above for the (absence of a) n_Q-dependence, the 'hidden' contributions cancel for composite fermions because $m^*_Q \propto \sqrt{n_e}$ and we obtain $S_{xx} \propto 1/n_e$ in agreement with experiment. For electrons, however, m^* is constant and there is an extra factor of $1/k_F \propto 1/\sqrt{n_e}$ which gives $S_0 \propto n_e^{-1.5}$. Moreover, there is an additional effect due to the divergence of $f(\xi, \xi_z)$ at $q = 2k_F$ coming closer to q_d at low n_e and which is stronger for electrons than for composite fermions because $k_F = k_F^Q/\sqrt{2}$. This contribution leads for electrons to a density dependence slightly stronger than $S_0 \propto n_e^{-1.5}$ as seen in the experiment as well.

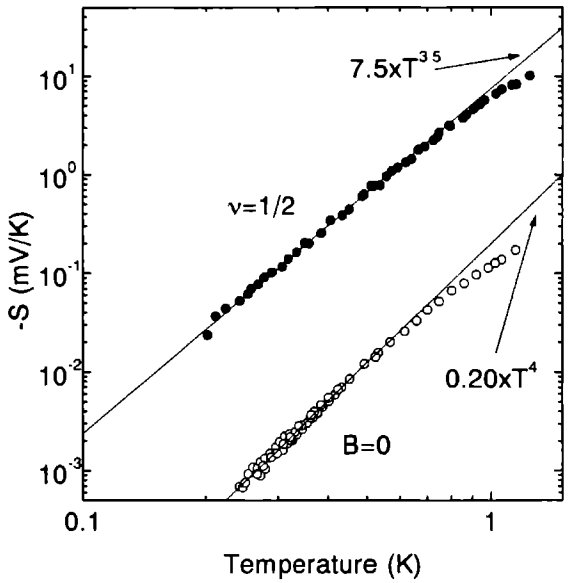

Figure 5.14: Temperature dependence of S_{xx} of sample 1A for electrons at $B = 0$ (○) and composite fermions at $\nu = \frac{1}{2}$ (●). Approximate power laws at low temperatures are indicated.

Fig. 5.14 compares the temperature dependences of S_{xx} for $\nu = \frac{1}{2}$ and for zero magnetic field. For $\nu = \frac{1}{2}$, we find $S_{xx}(\frac{1}{2}) \propto T^{3.5}$ very similar to the zero field case. We estimate the experimental error in the determination of the exponent of the power law to about ± 0.5. Thus, the temperature dependence of $S_{xx}(\frac{1}{2})$ agrees with S_0 for electrons in zero field and also with the theoretical prediction Eq. (1.25) within experimental accuracy. However, possibly the estimate of the experimental error is too conservative since we measure for two independent samples the same exponents which slightly differ between composite fermions and electrons.

One has to bear in mind that in the theoretical description we have used the same effective scattering potential V_{eff} with phonons for both electrons and composite fermions which might be a too crude simplification. A different dependence on the phonon wave vector q of either V_{eff} or screening would alter the resulting T-dependence [36]. However, it should be stressed that the difference is only marginal and that the temperature dependence of the composite fermion-thermopower strikingly resembles the zero field thermopower.

Whereas the temperature dependence is similar, the absolute value of S_{xx} is strongly enhanced compared to S_0. For $n_e = 1.76 \times 10^{15}$ m $^{-2}$, we observe $S_{xx}(\frac{1}{2})/S_0 \simeq 50$ (see Fig. 5.14). Following Eq. (5.12) this ratio should scale as

$$\frac{S_{xx}(\frac{1}{2})}{S_0} = \frac{m_Q^*/k_F^Q}{m^*/k_F}, \tag{5.13}$$

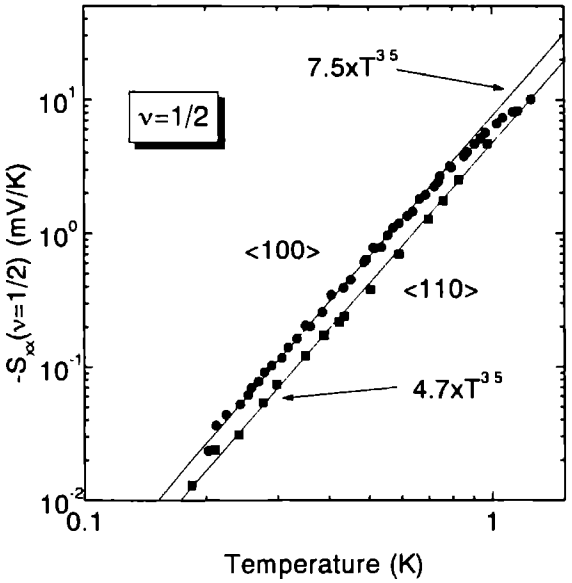

Figure 5.15: Temperature dependence of the thermopower of composite fermions, $S_{xx}(\frac{1}{2})$ for sample 1A with $\nabla T \| \langle 100 \rangle$ and sample 2 with $\nabla T \| \langle 110 \rangle$. Lines are power law fits at low temperature.

which in our case is $15/\sqrt{2} \approx 10$ using a typical value of $m_Q^* = m_e \simeq 15m^*$ from transport measurements in samples with comparable density [8]. Thus Eq. (5.13) accounts for an increase in absolute value by an order of magnitude but which is still a factor of 5 lower than is observed experimentally. Despite this shortcoming Eq. (5.13) correctly describes the general scaling between the thermopower of composite fermions and electrons. It is consistent with smaller ratios observed in lower density samples of typically $S_{xx}(\frac{1}{2})/S_0 \approx 20$ [18, 47]. Moreover, Eq. (5.13) explains the much smaller ratios found experimentally in the phonon drag thermopower of two-dimensional *hole* gases (2DHGs) of $S_{xx}(\frac{1}{2})/S_0 \approx 3$ [22, 23]. In 2DHGs the effective masses observed in transport for composite fermions at $\nu = \frac{1}{2}$ [9] are comparable to 2DEGs but are about an order of magnitude higher at $B = 0$.

To account for the missing factor of 5 there are two possibilities. One can assume an even more enhanced mass of $m_Q^* \sim 5m_e$. There have been masses reported in the range $m_Q^* = 2 \ldots 6m_e$ obtained by a different method [17]. However, the exact value was reported to be dependent on sample illumination. Therefore, we prefer to stick to the more commonly accepted values of $m_Q^* \approx m_e$ obtained from Shubnikov-de Haas analysis and rather put forward the possibility of an enhanced scattering potential for the composite fermion-phonon interaction which was so far assumed identical with V_{eff} for electrons.

Fig. 5.15 compares the thermopower at $\nu = \frac{1}{2}$ for samples 1A and 2 having different heat flow orientations, $\nabla T \| \langle 100 \rangle$ and $\nabla T \| \langle 110 \rangle$, respectively. As in zero magnetic field (see section 5.4), $S_{xx}(\frac{1}{2})$ differs by a constant factor at low temperatures between the two samples, the ratio is for composite fermions $S(100)/S(110) = 1.60 \pm 0.21$ compared to the zero

field value 1.54 ± 0.20. The particularly good agreement can be seen as an indication that composite fermions and electrons interact (on average) with the same phonons[4].

The phonon limited mobility μ_{ph} is another quantity depending on electron-phonon interaction. A phenomenological model for thermoelectric power, the Peltier approach, relates both quantities [see Eq. (5.7)]. In zero magnetic field, μ_{ph} is given by [24, 34]

$$\mu_{ph} = -\frac{v\Lambda}{ST}. \tag{5.14}$$

Eq. (5.14) is obtained under the assumption that phonon scattering is a negligible process for electrons (composite fermions), i.e.

$$1/\mu_{tot} = \mu_{imp} + \mu_{ph} \approx \mu_{imp}, \tag{5.15}$$

where indices 'tot', 'imp' and 'ph' denote total mobility and mobility limited by scattering with impurities and phonons only, respectively.

In their review of thermopower in two-dimensional electron systems [24], Gallagher and Butcher remarked on Eq. (5.7) and (5.14): "Thus these formulae are of little use unless μ_{ph} can be measured or independently calculated since the expected dependences upon T and n_e are obscured." In the meantime, μ_{ph} has indeed been measured independently by Kang *et al.* [17] for electrons at $B = 0$ and composite fermions at $\nu = \frac{1}{2}$. Thus, it certainly is interesting to compare μ_{ph} obtained from thermopower with these results. Since $\rho_{xx} = (ne\mu_{tot})^{-1}$ with the total mobility μ_{tot}, μ_{ph} can be obtained from resistivity using Eq. (5.15), i.e. $1/\mu_{ph}(\rho) = 1/\mu_{tot} - 1/\mu_{imp}$ where μ_{imp} is the mobility due to impurity scattering which has to be calculated. Therefore, it is only possible to determine μ_{ph} from the resistivity if it is *not* totally negligible for the scattering processes determining ρ. This validity limit is opposite to what is assumed to derive Eq. (5.14) for the thermopower. Obviously, there is an intermediate region where both descriptions should overlap. However, at low temperatures it becomes increasingly difficult to obtain μ_{ph} from ρ since e.g. for the data of Ref. [17] μ_{ph} contributes only 10^{-3} to the total resistivity at $T = 400$ mK and the result depends crucially on the calculation of the subtracted background of μ_{imp}.

Using the experimental data for thermopower and thermal conductivity ($v\Lambda = 3\lambda/C_V$) we calculate μ_{ph} with Eq. (5.14). Fig. 5.16 presents these results for $B = 0$ and $\nu = \frac{1}{2}$ together with the corresponding data of Kang *et al.* The temperature dependence observed for the phonon limited mobility is $\mu_{ph} \propto T^{-5}$ for electrons at $B = 0$ and $\mu_{ph} \propto T^{-4.5}$ for composite fermions at $\nu = \frac{1}{2}$. The conclusions from the comparison of the thermopower of these two states earlier in this section, i.e. the similarity for composite fermions compared to electrons in the coupling to phonons and the strong enhancement of its absolute value, applies in the same way to μ_{ph}. Note that the difference in thermopower for samples 1A and 2 due to the anisotropy of Λ is canceled for the mobility because $\mu_{ph} \propto \Lambda/S$. For comparison, Kang *et al* find $\mu_{ph} \propto T^{-5}$ for electrons at $B = 0$ and $\mu_{ph} \propto T^{-3}$ for composite fermions at $\nu = \frac{1}{2}$.

For electrons at $B = 0$, our data are in agreement in the overlapping temperature range with the results of Ref. [17] concerning the temperature dependence. The absolute value of $\mu_{ph}(\rho)$ obtained from resistivity is about a factor of 3 smaller than μ_{ph} obtained from

[4]Because different phonon modes have different group velocities and contribute differently to deformation potential and piezoelectric scattering, such a similarity in the ratios for composite fermions and electrons is not self-evident.

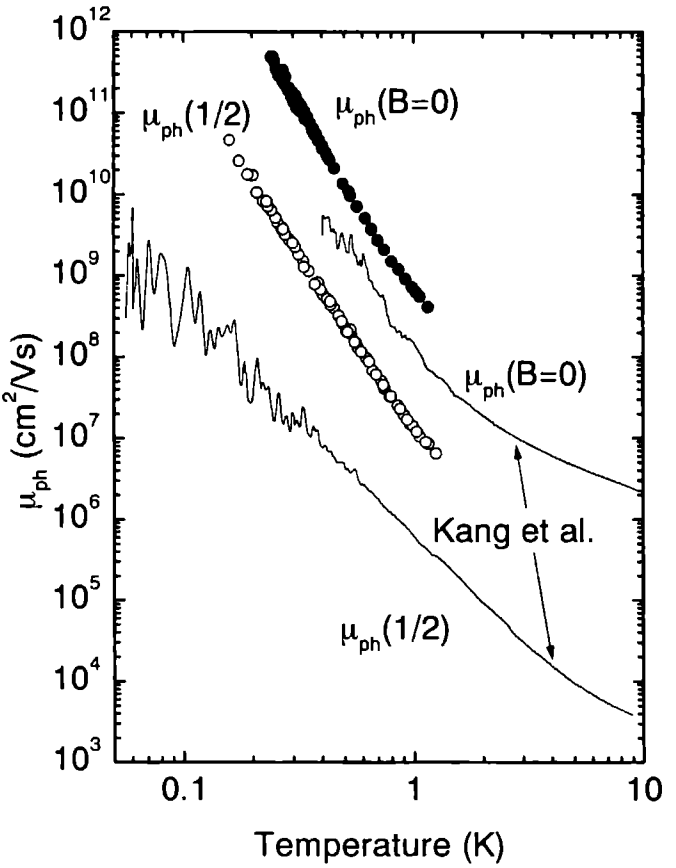

Figure 5.16: Phonon limited mobility $\mu_{\rm ph}$ of electrons at $B = 0$ (•) and composite fermions (○) at $\nu = \frac{1}{2}$, i.e. $B_{\rm eff} = 0$, obtained from the thermopower S_{xx} with Eq. (5.14) for sample 1A. Data of Kang *et al.* [17] extracted from the temperature dependence of ρ_{xx} are shown for comparison.

thermopower. For comparison, the impurity scattering dominated $\mu_{\rm tot}$ is about a factor of 6 lower for our samples than for the sample of Ref. [17]. In general, one would expect $\mu_{\rm ph}$ to be the same in different samples, in contrast to $\mu_{\rm tot}$, since the electron-phonon scattering in the nearly perfect GaAs crystals which are used for heterostructures should be identical[5]. However, the discrepancy in absolute value for $\mu_{\rm ph}$ should not be overestimated as it is rather convincing that two totally different methods give similar values and the same temperature dependence for $\mu_{\rm ph}$ on two totally different samples.

[5]Strictly speaking this is only true for samples with the same density n_e. Combining Eq. (5.14) with the result of the Boltzmann approach Eq. (1.20) we know that $\mu_{\rm ph}$ increases with n_e. The samples compared in this section have similar n_e.

In the case of composite fermions the results obtained from the two methods are distinctly different. Not only do the absolute values differ by more than an order of magnitude but also the temperature dependence clearly is not the same even allowing for rather big uncertainties because of the noise on the $\mu_{ph}(\rho)$ data. The reason for this discrepancy probably lies in the unknown impurity scattering background μ_{imp} which has to be subtracted. For electrons at $B = 0$, the temperature dependence of μ_{imp} is rather well known and an acceptable estimate of μ_{ph} can be made at not too low temperatures. For composite fermions this is not the case and additional assumptions on the impurity scattering have to be made [17]. Different models alter the final result for μ_{ph}. Thus, values of μ_{ph} for composite fermions calculated from ρ_{xx} are inconclusive until there is a well-established model for impurity scattering of composite fermions. In conclusion it can be stated that the most direct and hence reliable method to determine μ_{ph} at low temperatures is from thermopower measurements as well in zero magnetic field for electrons as in *effective* zero magnetic field for composite fermions.

Since the thermopower at even denominator filling factors is well described as a state with $B_{eff} = 0$ and the oscillations of the fractional quantum Hall effect are understood as the quantum oscillations due to Landau levels of composite fermions, it is straightforward to identify the region around $\nu = \frac{1}{2}$ as the low field thermopower of composite fermions. In this region, S_{xx} has a maximum at exactly half filling (see Fig. 5.17). Its amplitude increases with increasing density and decreasing temperature down to $T \approx 300$ mK, below this temperature there is a tendency to saturation although the increasing noise level prevents us from drawing further conclusions from it. The form of S_{xx} is strikingly symmetric around $\nu = \frac{1}{2}$, i.e. $S_{xx}(B_{eff}) = S_{xx}(-B_{eff})$, showing once again the significance of the effective magnetic field B_{eff} as the important parameter. The Nernst-Ettingshausen coefficient has a weak 'S-shape' structure in the same region of B_{eff}. The behaviour of the thermoelectric power is the more remarkable because in a semi-classical treatment the phonon drag contribution to S_{xx} is field independent to first approximation and $S_{xy} = 0$ [49]. In comparison, the Hall resistance ρ_{xy} is unaffected in this field range. For the longitudinal resistivity, a similar clear effect is absent in ρ_{xx} and only a minimum-like structure on a rising background is observed (see Fig. 5.3). This is probably due to an influence of the total magnetic field on τ_{imp} which, as was mentioned repeatedly, does not influence the thermopower.

As an origin for this effect, a diffusion contribution can be excluded because its amplitude is too small and the thermopower at and around $\nu = \frac{1}{2}$ has been shown to be due to phonon drag(see Figs. 5.7 and 5.15). There rather is a possible explanation related to a particularity of composite fermions. Eq. (5.12) shows that $S_{xx}(\frac{1}{2}) \propto m_Q^*$. Theory predicts weak divergences of the form of the quasi-particle effective mass as $m_Q^* \propto a' + b'/|B^*|^{0.5}$ or $m_Q^* \propto a + b \ln|B^*|$ for short range and Coulombic interactions, respectively, as $\nu \to \frac{1}{2}$ [3], and indications for a mass enhancement have been observed in Shubnikov-de Haas analyses of ρ_{xx} [8, 10] whereas in other similar experiments such an effect was not seen [7]. We have calculated the effect of a logarithmically diverging mass on S_{xx} using a simple distribution for the broadening of the effective field, $P(B_{eff}, B_0) = (1 - |B_{eff} - B_0|/\Delta B_{eff})/\Delta B_{eff}$, and assuming that B_{eff} affects only m_Q^*, thus, $S(B_0)/S(\frac{1}{2}) = \int P(B_{eff}, B_0)\, m_Q^*(B_{eff})\, dB_{eff} / m_Q^*(\frac{1}{2})$ for the normalized thermopower at B_0. Since the divergence is weak the integral $I(B_0) = \int P(B_{eff}, B_0) \ln|B_{eff}|\, dB_{eff}$ remains finite and can be solved analytically. The resulting function reproduces the smooth background in the vicinity of $\nu = \frac{1}{2}$ as can be seen in Fig. 5.17.

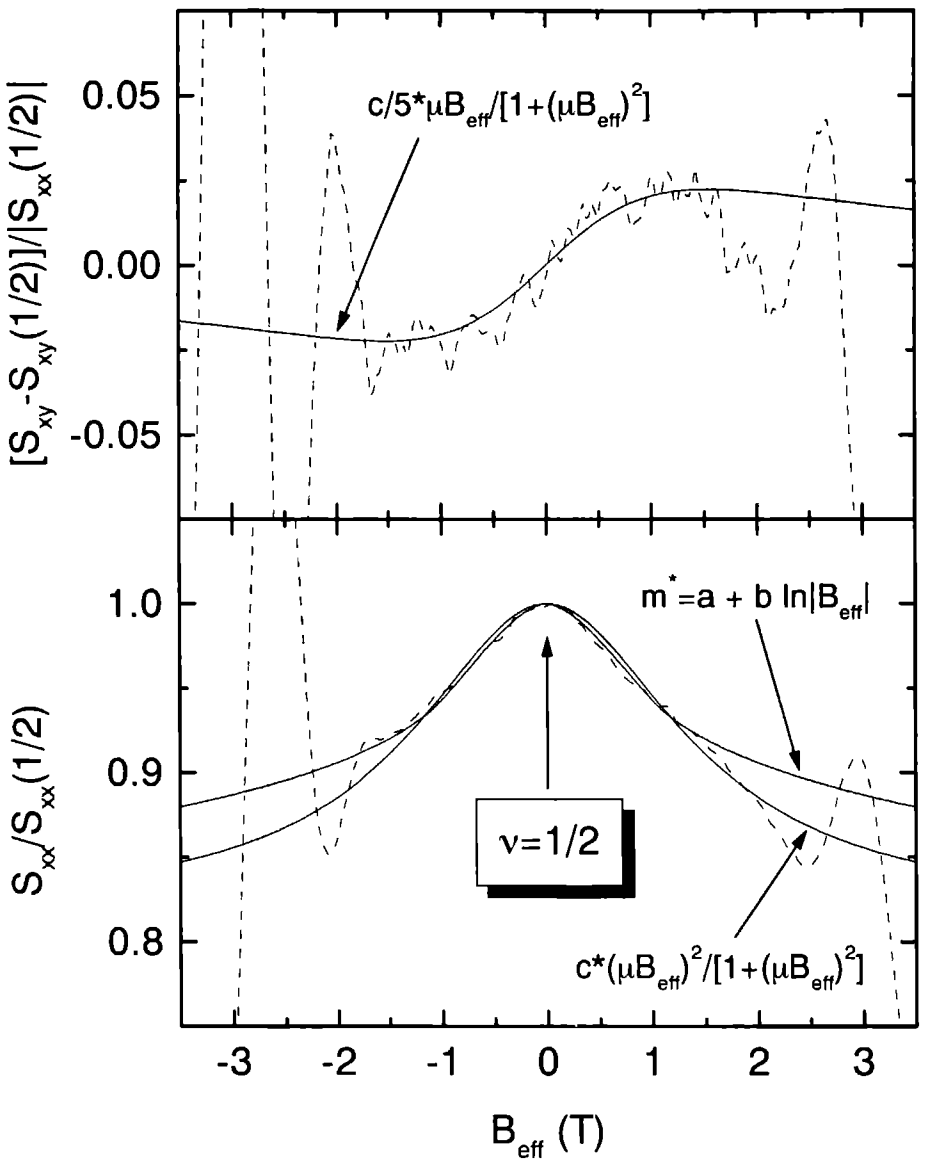

Figure 5.17: S_{yx} (top) and S_{xx} (bottom) in low effective magnetic field around $\nu = \frac{1}{2}$ at $T = 592$ mK. S_{xx} has a maximum which can be fitted either assuming a diverging effective mass or a semi-classical field dependence. The 'S'-shape observed in S_{yx} resembles a semi-classical field dependence. Details on the fits are given in the text.

The fit parameters for $T = 592$ mK and $n = 1.75 \times 10^{15}$ m^{-2} are $\Delta m/m_Q^*(\frac{1}{2}) = 0.15$, where $\Delta m = m_Q^*(\frac{1}{2}) - m_Q^*(\frac{1}{3})$, and $\Delta B_{\rm eff} = 0.076 \times B_{1/2}$. For higher temperatures, both fit parameters decrease in value. Such a behaviour is reasonable for $\Delta m/m_Q^*(\frac{1}{2})$ but seems rather odd if $\Delta B_{\rm eff}$ can indeed be interpreted as a smearing of $B_{\rm eff}$. Moreover, a diverging mass has no effect on S_{yx} and therefore fails to explain the 'S'-shape observed in experiments.

In another approach, the curve shapes can be related to a semi-classical field dependence around zero (effective) field. Such a field dependent contribution to phonon drag has, in contrast to more severe approximations [49], been obtained in a detailed extension to the zero field Boltzmann model of Ref. [30, 31] and which is given by [37]

$$\frac{S_{xx}^g(B) - S_0^g}{S_0^g} = -\frac{p\lambda^1}{1+p\lambda^1}\frac{(\mu B)^2}{1+(\mu B)^2}, \tag{5.16}$$

$$\frac{S_{xy}^g(B)}{S_0^g} = p\lambda^1\frac{\mu B}{1+(\mu B)^2}, \tag{5.17}$$

with $p = (E_F/\tau)(\partial\tau/\partial E)|_{E_t}$ is the energy dependence of the scattering at the Fermi energy E_F, and

$$\lambda^1 = \frac{k_B T}{2E_F}\sqrt{\xi^2+\xi_z^2}\left[1+\frac{2m_Q^* v^2}{k_B T}\frac{\sqrt{\xi^2+\xi_z^2}}{\xi^2}\right], \tag{5.18}$$

where again we have replaced electron by cf parameters. Note the sign in Eq. (5.16) which gives a maximum in S_{xx}/S_0 at $B = 0$ for $p > 0$. In our temperature range, this contribution is totally negligible around $B = 0$ for electrons [37] (for the same T and n_e as below for composite fermions we obtain $\lambda^1 = 0.017$). However, for composite fermions it may become observable since the parameters involved are different. The shape of the curve Eq. (5.16) reproduces the maximum in S_{xx} with a similar agreement as obtained with a diverging m_Q^* (see example in Fig. 5.17 at $T = 592$ mK). Parameters are $\lambda^1 = 0.22$ estimated from Eq. (5.18) with the experimental quantities involved and $\mu = 0.65\ \mathrm{T}^{-1}$ adjusted in the fit [$\mu(\frac{1}{2}) = 0.42\ \mathrm{T}^{-1}$ estimated from $\rho_{xx}(\frac{1}{2})$]. In addition, Eq. (5.17) gives roughly the shape of the experimental S_{yx} near $\nu = \frac{1}{2}$. However, the absolute magnitude has to be reduced by a factor of 5 if the fit parameters of the S_{xx}-maximum are taken. Such a decrease in amplitude is possibly related to a S_{yx}-contribution proportional to dS_{xx}/dB (see section 5.7) which gives a similar curve shape as Eq. (5.17) but with opposite sign (see Fig. 5.18) thus 'counteracting' a semi-classical field dependence. Thus, the field dependence seems to be in reasonable agreement with the experiments, but the predicted increase of λ^1 at higher temperatures in Eq. (5.18) is in contradiction to the decrease of the maximum observed in the experiments.

Therefore, the question, which one of the explanations (or a superposition of the two effects) is correct to describe the low-field magnetic field dependence of the thermopower of composite fermions, remains inconclusive for the moment. Both are able to reproduce the characteristic maximum, but fail to give a consistent picture for all temperatures and both coefficients S_{xx} and S_{yx} at the same time.

5.7 Nernst-Ettingshausen Coefficient in the Fractional Quantum Hall Regime

The Nernst-Ettingshausen coefficient S_{yx} is both intuitively and in detailed calculations expected to have no phonon drag contribution [24, 25], $S_{yx}^g = 0$, except for a semi-classical background which vanishes at low temperatures and at high fields [37]. Experimentally, however, S_{yx} is known to be phonon drag dominated in the integer and fractional quantum Hall regime [26, 38, 50]. Figs. 5.5 and 5.6 show the typical behaviour of S_{yx}. It is smaller than S_{xx}, but still of considerable size, and rich in oscillatory structure. It was already noticed in the past that the experimental S_{yx} resembles the derivative of the thermopower with respect to magnetic field, dS_{xx}/dB [26, 38, 50]. Such a behaviour would be understandable for diffusion thermoelectric power because of the Mott relation, but temperature dependence and absolute size of S_{yx} clearly show that this component is due to phonon drag, too.

To understand more about the origin of this phonon drag contribution to S_{yx}, it is illustrative to compare the observations for 2DEGs with the findings for 3D degenerate semiconductors where the thermoelectric power has many similarities with 2DEGs (see chapter 6). Here, too, the thermal conductivity is dominated by phonons, the longitudinal thermopower S_{xx} is governed by phonon drag at low temperatures, and the Landau level structure is visible in Shubnikov-de Haas oscillations. However, the Nernst-Ettingshausen coefficient has no phonon drag contribution and is completely due to diffusion. The only fundamental difference between these two systems is the dimension of the electron gas. Therefore, the explanation of the phonon-drag contribution to S_{yx} must be unique to low-dimensional systems and cannot be an extension to a model also applicable to 3D conductors.

In this section, we give an explanation for S_{yx} in 2DEGs which is specific to quantum Hall systems, i.e. for 2D. The Nernst-Ettingshausen coefficient S_{yx} can approximately be described by

$$S_{yx} = \alpha B \frac{dS_{xx}}{dB}, \tag{5.19}$$

where α is a dimensionless constant. Eq. (5.19) can be obtained in two different ways. Both approaches show the equivalence of Eq. (5.19) with a similar relation which holds for the two components of the resistivity in the quantum Hall effect,

$$\rho_{xx} = \alpha B \frac{d\rho_{xy}}{dB}, \tag{5.20}$$

and also for the electrical conductivity σ,

$$\sigma_{xx} = \alpha B \frac{d\sigma_{xy}}{dB}. \tag{5.21}$$

This relation, discovered by A. M. Chang and D. C. Tsui more than ten years ago [51], was found to describe the complex behaviour of the longitudinal resistivity ρ_{xx} remarkably well in a number of experimental studies [52–55]. It was only recently that Eq. (5.19) was given a theoretical explanation by S. H. Simon and B. I. Halperin [56].

Examining the general equations for electrical and thermoelectric transport, Eqs. (5.1) and (5.2), it can be noticed that ϵ and σ fulfill similar roles in Eqs. (5.1) and (5.2) because each relates a driving force (E or ∇T) to a current density (J or U). Therefore, we make the assumption that the two independent components of ϵ, ϵ_{xx} and ϵ_{xy}, are in the quantum Hall regime related in a way similar to Eq. (5.21), namely as $\epsilon_{xx} = \alpha_s B(d\epsilon_{xy}/dB)$, where α_s is not necessarily assumed to be identical to α. With the experimental condition $\nabla T_y = 0$, $S_{xx} = \rho_{xx}\epsilon_{xx} + \rho_{yx}\epsilon_{xy}$. Since the term $\rho_{xx}\epsilon_{xx}$ as well as its derivative are experimentally found to be negligible, it follows that

$$\begin{aligned} \alpha_s B\frac{dS_{xx}}{dB} &= \alpha_s B\frac{d\epsilon_{xy}}{dB}\rho_{yx} + \alpha_s B\frac{d\rho_{yx}}{dB}\epsilon_{xy} \\ &= \rho_{yx}\epsilon_{xx} + \rho_{xx}\epsilon_{yx} + \frac{\Delta\alpha}{\alpha_r}\rho_{xx}\epsilon_{yx}, \end{aligned} \tag{5.22}$$

where $\Delta\alpha = \alpha_s - \alpha$. In the experiments, we find $\alpha_s \simeq \alpha$ so that the last term is negligible. However, even if $\Delta\alpha \neq 0$, $\rho_{xx}\epsilon_{yx}$ is at most only 10% of the first two terms in Eq. (5.22). Thus Eq. (5.19) follows immediately from Eqs. (5.22) and (5.4). As might be expected, α_s relating the two components of S is the same factor as for the components of the thermoelectric tensor ϵ.

The second way to derive Eq. (5.19) has been proposed by S. H. Simon [57] and we will give his proof here. The idea is to rewrite the thermopower definitions in a way that they fulfill the fundamental equations necessary to derive the resistivity relation. These equations are

$$\nabla \cdot \boldsymbol{J} = 0 \tag{5.23}$$

$$\nabla \times \boldsymbol{E} = 0 \tag{5.24}$$

$$\boldsymbol{E} = \rho(\boldsymbol{r})\boldsymbol{J}. \tag{5.25}$$

The essential point is to assume that the resistivity is a function of position, i.e. to distinguish between microscopic $\rho(\boldsymbol{r})$ and macroscopic quantity ρ. Assuming several length scales of disorder in the electron density, which results in fluctuations $\delta\rho_{xy}(\boldsymbol{r})$ of the local Hall resistivity, and

$$\rho_{xx}(\boldsymbol{r}) \ll |\delta\rho_{xy}(\boldsymbol{r})|, \tag{5.26}$$

the resistivity relation Eq. (5.20) follows [56].

For the thermopower case, let $s = S(\boldsymbol{r})$ denote the microscopic and S the experimentally measured macroscopic quantity. In the case of $\boldsymbol{J} = 0$, we have

$$\boldsymbol{E} = s\nabla T. \tag{5.27}$$

Let us define a new vector $\boldsymbol{I} = \nabla \times (T\hat{z})) = \hat{z} \times \nabla T$, where $\hat{z}$ is the unit vector in z-direction, so $\boldsymbol{I}$ is just the vector ∇T turned by 90 degrees. With the definition of a new 2 by 2 matrix r, which is in some sense s rotated by 90 degrees, too,

$$r = \begin{pmatrix} s_{xy} & -s_{xx} \\ s_{xx} & s_{xy}, \end{pmatrix} \tag{5.28}$$

i.e. $r_{xx} = s_{xy}$ and $r_{xy} = -s_{xx}$, and the above definition of $\boldsymbol{I}$ we get $\boldsymbol{E} = r\boldsymbol{I}$. Thus, in terms of our new vector and matrix notation we have

$$\nabla \cdot \boldsymbol{I} = 0 \tag{5.29}$$

$$\nabla \times \boldsymbol{E} = 0 \tag{5.30}$$

$$\boldsymbol{E} = r\boldsymbol{I}, \tag{5.31}$$

which is exactly the same as the set of Eqs. (5.23-5.25). Since calculations give $S_{yx} = 0$ for the macroscopic[6] Nernst-Ettingshausen coefficient [24, 25], we assume this to hold approximately for the microscopic s_{yx} instead, i.e.

$$r_{xx} = s_{yx} \ll \delta s_{xx} = \delta r_{xy}. \tag{5.32}$$

Under the condition of Eq. (5.32), the calculations are exactly the same as for the resistivity [57] with the result that $R_{xx} = \alpha B(dR_{xy}/dB)$, where R denotes the macroscopic equivalent to r, or in terms of S,

$$S_{yx} = \alpha B \frac{S_{xx}}{dB}, \tag{5.33}$$

which is exactly Eq. (5.19).

A necessary condition for the above derivation is that fluctuations in the density translate to fluctuations in s_{xx} just as it is the case with ρ_{xy}. In section 5.6 we have shown that S_{xx} indeed depends on the density as well in $B = 0$ as in high magnetic fields. The exact dependence on n_e is of no importance to obtain the result, only α can slightly depend on the exact density dependence of s_{xx} [57]. For $s_{xx} \propto n_e^{-1}$ the same α is obtained as for the resistivity, in other cases α should at least be of the same order.

To verify the validity of Eq. (5.19) we numerically calculate this contribution, which we will denote S_{yx}^{calc}, from the experimental data for S_{xx} and compare it with the experimental S_{yx}. The scaling factor α was used as a fit parameter. An example is given in Fig. 5.18. The agreement between the calculated and the experimental curve is remarkable. The shape of the oscillations as well as the position of extrema and sign changes are well accounted for. Also the relative size of the oscillations between the integer and fractional quantum Hall regime is reproduced reasonably well. To quantify the impression of a resemblance between the curves we define a quality factor, $\Delta = \int (S_{yx} - S_{yx}^{\text{calc}})^2 dB / \int (S_{yx}^2 + (S_{yx}^{\text{calc}})^2) dB$, indicating the relative deviation, with $\Delta = 0$ for perfect agreement and $\Delta = 1$ for no correlation. Typically, we find $\Delta \lesssim 0.1$ for S_{yx}^{calc} when an additional background in the fractional quantum Hall regime, which is discussed on page 96, is accounted for (see page 96 for the discussion of this term). Anyway, the value of α does not depend on whether (and in what way) this background is accounted for or not.

There is a slight dependence of α on the range of magnetic fields investigated (see Fig. 5.19). In view of Simon's derivation of Eq. (5.19) this is not very surprising since α can depend on the functional dependence of S_{xx} on density and this changes between $B = 0$ and high magnetic fields as discussed in section 5.6. Furthermore, it is noteworthy that α does not depend on temperature (see Fig. 5.19) whereas its absolute value and the thermopower S_{xx} are strongly temperature dependent. In particular, the fixed relation

[6] In the theories, it is in fact the microscopic quantity s which is calculated and then identified with the macroscopic S.

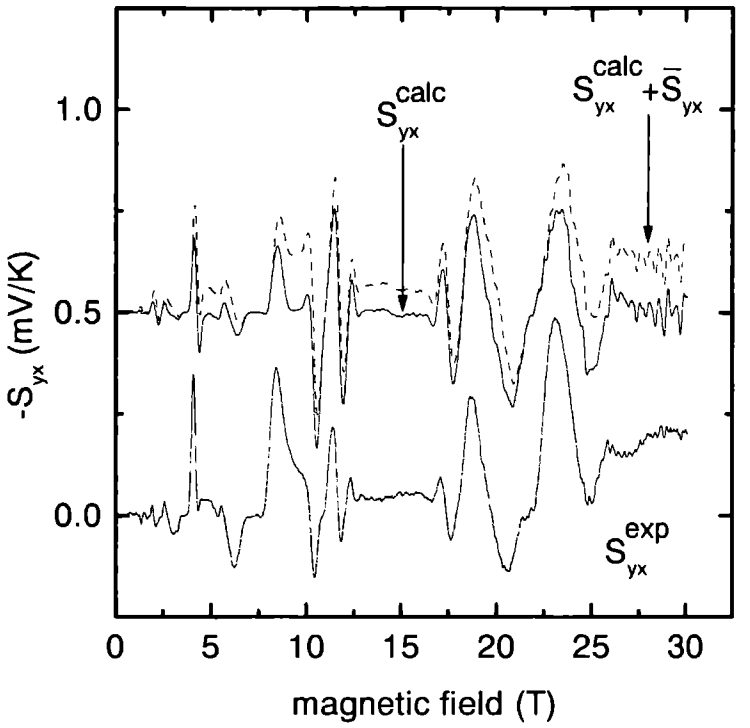

Figure 5.18: Experimental S_{yx} and calculated $S_{yx}^{\rm calc}$ (offset by 0.5 mV/K) for $T = 424$ mK in sample 2. $S_{yx}^{\rm calc}$ (continuous curve) obtained from Eq. (5.19) with $\alpha = 0.0269$, dashed curve has a contribution $+0.31 S_{xx}(B)$ added. Deviation compared with experimental S_{yx}: $\Delta = 12.7\%$.

between S_{yx} and S_{xx} via Eq. (5.19) with a constant scaling factor proves that S_{yx} is indeed given by phonon drag as well. This is an important detail because it definitely excludes diffusion, as an explanation for this component.

Examining the validity of the resistivity relation Eq. (5.20) in our samples, it is found to hold with a similar level of agreement ($\Delta \lesssim 0.1$) as for S_{yx} (see Fig. 5.20). The striking result of this analysis is that the values obtained for α are very similar in the two cases. In fitting, α is obtained with a standard deviation of $\sim 15\%$ for both S_{yx} and ρ_{xx}. Systematic uncertainties arise with the thermoelectric power (unlike the resistivity) from the dimensions of the contacts, and are reflected directly in α. These errors are sample-specific and are typically $\sim 20\%$. Thus, we conclude that the scaling parameters α are identical within experimental error for resistivity and thermoelectric power completely in line with the prediction from the theoretical proof of Eq. (5.19).

Concerning the exact value of α, the theory of Simon and Halperin gives an estimate for the order of magnitude by relating it to long range density fluctuations in the system [56], i.e. $\alpha \sim \delta n/n$. On the other hand, Coleridge *et al* [58] have obtained an explicit expression

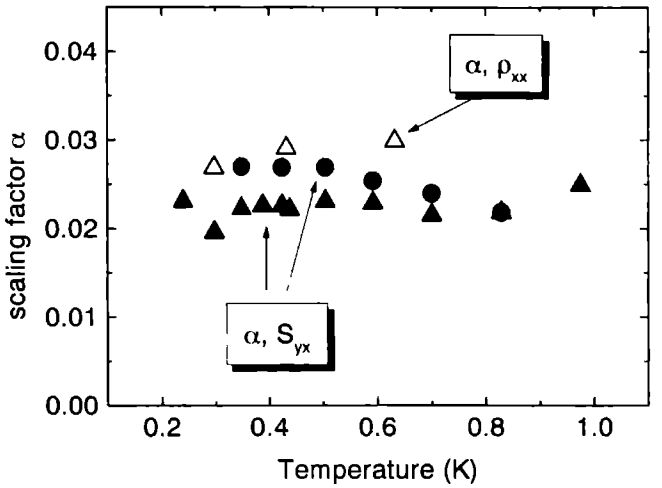

Figure 5.19: Scaling factor α obtained in the fits of Eq. (5.19) for S_{yx} (▲: fitting range $B \leq 20$ T; •: $B \leq 30$ T) and Eq. (5.20) for ρ_{xx} (△: $B \leq 20$ T).

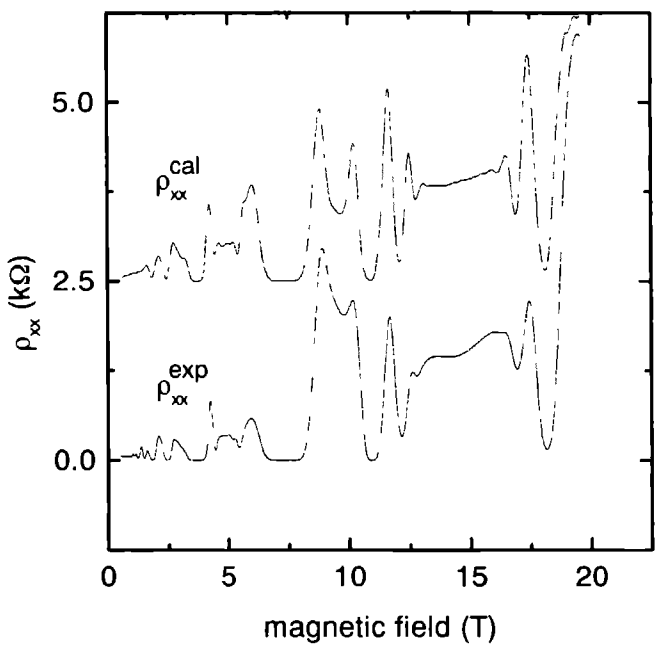

Figure 5.20: Experimental ρ_{xx} and calculated $\rho_{xx}^{\rm calc}$ (offset by 2.5 kΩ) at $T = 297$ mK for sample 2. Scaling factor $\alpha = 0.0269$ in Eq. (5.20), deviation $\Delta = 5.2\%$.

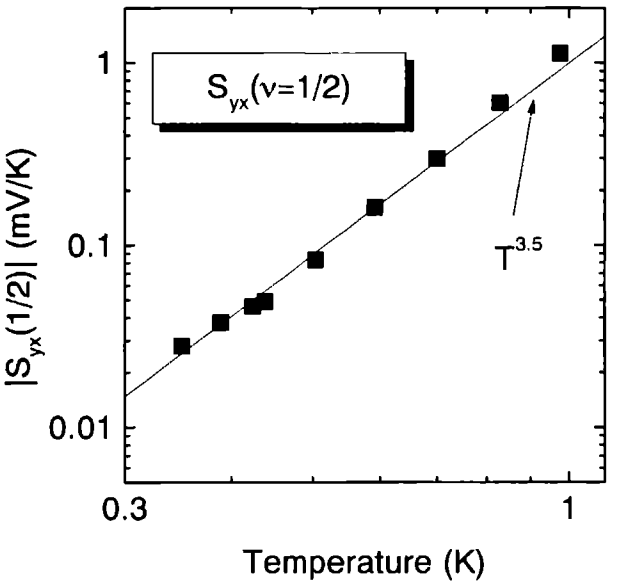

Figure 5.21: The temperature dependence of S_{yx} at $\nu = \frac{1}{2}$ in sample 2 is approximately $\propto T^{3.5}$ as for $S_{xx}(\frac{1}{2})$.

for α by comparing Eq. (5.20) at low fields to standard expressions for Shubnikov-de Haas oscillations, namely $\alpha = \tau_q/2\tau_t$, where τ_q and τ_t are the quantum and transport lifetime, respectively. In 2DEGs at low temperatures, both lifetimes are determined by impurity scattering. Therefore, we make the interesting observation that even in pure phonon drag thermoelectric power the Nernst-Ettingshausen coefficient still reflects details of the impurity scattering.

In addition to the contribution $S_{yx}^{\rm calc} = \alpha B(dS_{xx}/dB)$ we observe in the experiments another contribution to S_{yx} which modifies its background in the fractional quantum Hall regime. There is a constant 'offset' to S_{yx}, which we will denote by $\bar{S}_{yx}$, clearly visible around $\nu = \frac{1}{2}$ and $\nu = \frac{1}{4}$, but also at $\nu = \frac{3}{2}$ and $\nu = \frac{3}{4}$ (see Fig. 5.18). Eq. (5.19) cannot account for $\bar{S}_{yx}$ since $(dS_{xx}/dB) \simeq 0$ in these regions. At higher temperatures, where such a contribution was already observed [26, 28], the relative size of $\bar{S}_{yx}$ to S_{yx} increases because the weaker oscillatory structure in S_{xx} gives smaller amplitudes in the derivative. The temperature dependence of $\bar{S}_{yx}(\frac{1}{2})$ is similar to $S_{xx}(\frac{1}{2})$ (see Fig. 5.21), thus it is clearly due to phonon drag, too. Therefore, the ratio S_{yx}/S_{xx} is approximately constant around even denominator filling factors. In our samples, we measure typically $S_{yx}/S_{xx} \approx 20\%$; in other samples with lower density $S_{yx}/S_{xx} \approx 40\%$ is observed [26].

It is striking that the offsets in S_{yx} are only observed around filling factors which are related to composite fermion states. Thus, it is tempting to identify this contribution to an effect of composite fermions because the component S_{xx} is so well described in the composite fermion picture. This is also consistent with the fact that no such additional contribution to S_{yx} is observed in the integer quantum Hall effect for $\nu > 2$ where there are no

composite fermion related states.

At the moment, we have no explanation for this behaviour. Phenomenologically, the additional background is best described by a contribution proportional to S_{xx}, since the 'offsets' are only observed around even denominator filling factors and vanish for fractions like $\nu = \frac{1}{3}$, i.e. $S_{yx} = S_{yx}^{\rm calc} + CS_{xx}(B)$. The result of allowing for such an additional contribution to S_{yx} is given in Fig. 5.18 as well. Note that the effect is no experimental artifact of an unwanted admixture of S_{xx} measured in S_{yx} because $\bar{S}_{yx}$ changes sign under magnetic field reversal just like S_{yx}, whereas S_{xx} is an even function of field. A constant ratio C means in other words that there is a constant angle between the direction of the temperature gradient and the direction of the thermoelectric power at $\nu = \frac{1}{2}, \frac{3}{2}, \frac{1}{4}$, and $\frac{3}{4}$; $C = 0.2$ corresponds to $\vartheta = 11$ degrees.

5.8 Conclusions

We have measured the phonon drag thermoelectric power in the fractional quantum Hall effect. A zero field Boltzmann theory for phonon drag applied to composite fermions by carefully replacing the relevant parameters provides a consistent description for the thermopower S_{xx}. The main findings are a) composite fermions with the same number of flux quanta have identical thermopower, b) this condition can be used to determine the formation temperature of quasi-particles at $\nu = \frac{3}{2}$ and $\nu = \frac{3}{4}$, c) the temperature dependence of composite fermions $S_{xx}(\frac{1}{2}) \propto T^{3.5}$ is similar to $S_0 \propto T^4$ for electrons but d) enhanced in absolute value by nearly two orders of magnitude, e) the effective quasi-particle mass scales as the Fermi wave vector with density and polarization, i.e. $m_Q^* \propto \sqrt{n_Q}$, f) the dependence on the total electron density is $S_{xx}(\frac{1}{2}) \propto 1/n_e$, g) $S_{xx}(\frac{1}{2})$ and S_0 depend in the same way on the phonon mean free path, and h) the phonon limited mobility can be obtained from the thermopower giving results which are consistent for electrons but differ for composite fermions from data obtained by another method.

The Nernst-Ettingshausen coefficient S_{yx} is shown to be given by the relation $S_{yx} = \alpha B(dS_{xx}/dB)$ which is very similar to the known resistivity relation $\rho_{xx} = \alpha B(d\rho_{xy}/dB)$. Experimentally the scaling factor α is found to be identical for thermopower and resistivity. It is shown that both equations are in fact equivalent. In the fractional quantum Hall effect, a second contribution to S_{yx} is observed which gives constant 'offsets' in S_{yx} around filling factors $\nu = \frac{1}{2}, \frac{1}{4}, \frac{3}{2}$, and $\frac{3}{4}$ which are related to composite fermions. However, there is no convincing explanation for it yet.

5.9 References

[1] J. K. Jain, Phys. Rev. Lett. **63**, 199 (1989).

[2] J. K. Jain, Adv. in Phys. **41**, 105 (1992).

[3] B. I. Halperin, P. A. Lee, and N. Read, Phys. Rev. B **47**, 7312 (1993).

[4] *The Quantum Hall Effect*, edited by R. E. Prange and S. M. Girvin (Springer-Verlag, New York, 1987).

[5] *The Fractional Quantum Hall Effect*, edited by T. Chakraborty and P. Pietiläinen (Springer-Verlag, Berlin, 1988).

[6] R. R. Du, H. L. Stormer, D. C. Tsui, L. N. Pfeiffer, and K. W. West, Phys. Rev. Lett. **70**, 2944 (1993).

[7] D. R. Leadley, R. J. Nicholas, C. T. Foxon, and J. J. Harris, Phys. Rev. Lett. **72**, 1906 (1994).

[8] R. R. Du, H. L. Stormer, D. C. Tsui, A. S. Yeh, L. N. Pfeiffer, and K. W. West, Phys. Rev. Lett. **73**, 3274 (1994).

[9] H. C. Manoharan, M. Shayegan, and S. J. Klepper, Phys. Rev. Lett. **73**, 3270 (1994).

[10] P. T. Coleridge, Z. W. Wasilewski, P. Zawadzki, A. S. Sachrajda, and H. A. Carmona, Phys. Rev. B **52**, 11603 (1995).

[11] R. R. Du, A. S. Yeh, H. L. Stormer, D. C. Tsui, L. N. Pfeiffer, and K. W. West, Phys. Rev. Lett. **75**, 3926 (1995).

[12] L. P. Rokhinson, B. Su, and V. J. Goldman, Phys. Rev. B **52**, 11588 (1995).

[13] W. Kang, H. L. Stormer, L. N. Pfeiffer, W. Baldwin, and K. W. West, Phys. Rev. Lett. **71**, 3850 (1993).

[14] V. J. Goldman, B. Su, and J. K. Jain, Phys. Rev. Lett. **72**, 2065 (1994).

[15] J. H. Smet, D. Weiss, R. H. Blick, G. Lütjering, K. von Klitzing, R. Fleischmann, T. Geisel, and G. Weimann, Phys. Rev. Lett. **77**, 2272 (1996).

[16] R. L. Willett, R. R. Ruel, K. W. West, and L. N. Pfeiffer, Phys. Rev. Lett. **71**, 3846 (1993).

[17] W. Kang, Song He, H. L. Stormer, L. N. Pfeiffer, W. Baldwin, and K. W. West, Phys. Rev. Lett. **75**, 4106 (1995).

[18] U. Zeitler, B. Tieke, S. A. J. Wiegers, J. C. Maan, R. Fletcher, V. I. Fal'ko, C. T. Foxon, and J. J. Harris, in *High Magnetic Fields in the Physics of Semiconductors*, edited by D. Heiman (World Scientific, Singapore, 1995), pp. 38–45.

[19] V. Bayot, E. Grivei, H. C. Manoharan, X. Ying, and M. Shayegan, Phys. Rev. B **52**, 8621 (1995).

[20] B. Tieke, U. Zeitler, R. Fletcher, S. A. J. Wiegers, A. K. Geim, J. C. Maan, and M. Henini, Phys. Rev. Lett. **76**, 3630 (1996).

[21] B. Tieke, U. Zeitler, R. Fletcher, S. A. J. Wiegers, A. K. Geim, J. C. Maan, and M. Henini, Surf. Sci. **361–362**, 46 (1996).

[22] P. A. Crump, B. Tieke, R. J. Barraclough, B. L. Gallagher, R. Fletcher, J. C. Maan, T. M. Fromhold, and M. Henini, Surf. Sci. **361–362**, 50 (1996).

[23] P. A. Crump, *Classical and Quantum Electrical Transport in Two Dimensional Systems*, Ph.D. thesis, University of Nottingham, 1996.

[24] B. L. Gallagher and P. N. Butcher, in *Handbook on Semiconductors*, edited by P. T. Landsberg (Elsevier, Amsterdam, 1992), Vol. 1, pp. 721–816.

[25] T. M. Fromhold, P. N. Butcher, G. Qin, B. G. Mulimani, J. P. Oxley, and B. L. Gallagher, Phys. Rev. B **48**, 5326 (1993).

[26] U. Zeitler, J. C. Maan, P. Wyder, R. Fletcher, C. T. Foxon, and J. J. Harris, Phys. Rev. B **47**, 16008 (1993).

[27] U. Zeitler, R. Fletcher, J. C. Maan, C. T. Foxon, J. J. Harris, and P. Wyder, Surf. Sci. **305**, 91 (1994).

[28] U. Zeitler, *Electronic transport in three-dimensional and two-dimensional metallic semiconductors under extreme quantum conditions*, Vol. 441 of *Konstanzer Dissertationen* (Hartung-Gorre Verlag, Konstanz, 1994), Ph.D. thesis, Universität Konstanz.

[29] X. Ying, V. Bayot, M. B. Santos, and M. Shayegan, Phys. Rev. B **50**, 4969 (1994).

[30] D. G. Cantrell and P. N. Butcher, J. Phys. C: Solid State Phys. **20**, 1985 (1987).

[31] D. G. Cantrell and P. N. Butcher, J. Phys. C: Solid State Phys. **20**, 1993 (1987).

[32] N. W. Ashcroft and N. D. Mermin, *Solid State Physics* (Saunders College, Philadelphia, 1976).

[33] C. Herring, Phys. Rev. **96**, 1163 (1954).

[34] R. J. Nicholas, J. Phys. C: Solid State Phys. **18**, L695 (1985).

[35] M. J. Smith and P. N. Butcher, J. Phys.: Condens. Matter **2**, 2375 (1990).

[36] S. K. Lyo, Phys. Rev. B **38**, 6345 (1988).

[37] X. Zianni, P. N. Butcher, and M. J. Kearney, Phys. Rev. B **49**, 7520 (1994).

[38] R. Fletcher, M. D'Iorio, W. T. Moore, and R. Stoner, J. Phys. C: Solid State Phys. **21**, 2681 (1988).

[39] A. K. McCurdy, Phys. Rev. B **26**, 6971 (1982).

[40] H. B. G. Casimir, Physica **V**, 495 (1938).

[41] *Landolt-Börnstein, Numerical Data and Functional Relationships in Science and Technology*, Vol. III/22a of *New Series*, edited by O. Madelung (Springer-Verlag, Berlin, 1987), p. 87ff.

[42] J. S. Blakemore, J. Appl. Phys. **53**, R123 (1982).

[43] J. M. Ziman, *Electrons and phonons* (Clarendon Press, Oxford, 1960).

[44] R. Fletcher, M. D'Iorio, A. S. Sachrajda, R. Stoner, C. T. Foxon, and J. J. Harris, Phys. Rev. B **37**, 3137 (1988).

[45] D. R. Leadley, M. van der Burgt, R. J. Nicholas, P. J. Gee, J. Singleton, J. J. Harris, and C. T. Foxon, Surf. Sci. **361–362**, 22 (1996).

[46] X. G. Wu and J. K. Jain, Phys. Rev. B **53**, 1061 (1996).

[47] B. Tieke, R. Fletcher, S. A. J. Wiegers, U. Zeitler, J. C. Maan, C. T. Foxon, and J. J. Harris, Physica B **211**, 414 (1995).

[48] N. d'Ambrumenil and R. Morf, Surf. Sci. **361–362**, 92 (1996).

[49] R. T. Syme and M. J. Kearney, Phys. Rev. B **46**, 7662 (1992).

[50] R. Fletcher, J. C. Maan, K. Ploog, and G. Weimann, Phys. Rev. B **33**, 7122 (1986).

[51] A. M. Chang and D. C. Tsui, Sol. State Comm. **56**, 153 (1985).

[52] T. Rötger, G. J. C. L. Bruls, J. C. Maan, P. Wyder, K. Ploog, and G. Weimann, Phys. Rev. Lett. **62**, 90 (1989).

[53] N. G. Morawicz, K. W. J. Barnham, C. Zammit, J. J. Harris, C. T. Foxon, and P. Kujawinski, Phys. Rev. B **41**, 12687 (1990).

[54] H. L. Stormer, K. W. Baldwin, L. N. Pfeiffer, and K. W. West, Sol. State Comm. **84**, 95 (1992).

[55] A. A. Allerman, W. Xu, N. Hauser, and C. Jagadish, J. Appl. Phys. **77**, 2052 (1995).

[56] S. H. Simon and B. I. Halperin, Phys. Rev. Lett. **73**, 3278 (1994).

[57] S. H. Simon, private communication and to be published, 1997.

[58] P. T. Coleridge, P. Zawadzki, and A. S. Sachrajda, Phys. Rev. B **49**, 10798 (1994).

Chapter 6

Magneto-thermoelectric Properties of the Degenerate Semiconductor HgSe:Fe

Abstract

There are few previous data on the magneto-thermoelectric properties of degenerate semiconductors. Although magnetic quantum oscillations in the thermopower have been previously studied, quantitative, or even semi-quantitative agreement with theory was not achieved. We have developed a theoretical model allowing a quantitative description of both the oscillatory and non-oscillatory parts of the thermopower tensor S, and have studied its validity in an experimental system. For the experiments we have chosen a high mobility sample of HgSe:Fe ($n = 4.6 \times 10^{24}$ m^{-3}) and have measured both of the independent components of S in a transverse magnetic field B of ≤ 8 T at temperatures 1 K$< T <$60 K, together with the longitudinal and Hall resistivities and the thermal conductivity.

Our model predicts that the transverse component S_{yx} is not affected by phonon drag and all our data are in agreement with this. The absolute value of the non-oscillating part of S_{yx} depends linearly on T consistent with domination by diffusion. We observe large oscillations in S_{yx} which exhibit a phase shift of $\pi/2$ relative to the resistivity oscillations. By including elastic electron scattering into the diffusion theory we obtain excellent quantitative agreement for both the oscillations and the smooth background under all conditions of B and T, including the observed phase shift of $\pi/2$.

In contrast to S_{yx}, the longitudinal component S_{xx} shows a large contribution from phonon drag over most of the temperature range. S_{xx} exhibits quantum oscillations similar to S_{yx} but these are found to be in phase with those in the resistivity and are far too large to be explained by diffusion in any available model. Instead, they are well described by oscillations in electron-phonon scattering which modulates phonon drag in much the same way as is observed in

This work has in part been published in:
B. Tieke, R. Fletcher, J. C. Maan, W. Dobrowolski, A. Mycielski, and A. Wittlin, Physical Review B **54**, 10565–10574 (1996).

2-dimensional systems. Small oscillations are also observed in the lattice thermal conductivity and their magnitude is shown to be consistent with the same phonon-electron scattering being responsible.

Our analysis demonstrates that the study of the thermopower is a powerful tool in the understanding of both the elastic (through S_{yx}) as well as the inelastic (through S_{xx}) scattering of electrons in degenerate semiconductors.

6.1 Introduction

A full understanding of the magneto-thermopower of degenerate semiconductors has been slower to emerge than for the case of the resistivity. The lack of progress is partly because thermo-electricity is a more subtle phenomenon, but also because the experiments are more difficult to carry out. As far as we are aware, there is no comprehensive set of data available on either the oscillatory or non-oscillatory parts for both of the independent components of the thermopower of a degenerate semiconductor in a transverse magnetic field. This paper presents such a set using HgSe doped with Fe, chosen because it has a high mobility and is known to give large oscillations in the resistivity.

The early literature on thermomagnetic effects in degenerate semiconductors is summarized in reviews by Zyryanov and Guseva [1] and Puri and Geballe [2], the latter mainly dealing with very low carrier density systems which can be taken into the high field limit, i.e. only the last Landau level is occupied. The present work is concerned with the regime where many levels are occupied. A significant complication with thermopower is that it is much more sensitive to phonon drag than is resistivity, and it is often not clear what fraction of the experimental thermopower, especially in the case of oscillations, is to be ascribed to each of the two components, phonon drag and diffusion. As far as we are aware, all this early work assumed that the oscillatory phenomena were due only to diffusion and achieved limited quantitative success.

More recent work turned to normal metals and 2-dimensional electron gases (2DEGs). The latter are usually degenerate metals under the conditions of measurement for oscillatory phenomena (a recent review [3] gives many details) and have much in common with bulk degenerate semiconductors. The main difference is that, with a 2DEG, 3D phonons interact with 2D electrons, but in semiconductors both systems are inter-penetrating and 3D. In each case the phonon system is only weakly affected by electronic scattering. With 2DEGs it rapidly became clear that, under normal conditions, phonon drag was the dominant cause of the oscillations in the longitudinal thermopower (which we will refer to simply as the thermopower). Diffusion oscillations have never been reliably seen in the thermopower, though they have been observed in the transverse thermopower [4] (usually called the Nernst-Ettingshausen or NE coefficient).

Experiments on metals [5–7] showed that phonon drag plays little part in thermoelectric oscillations. Excellent agreement between theory and experiment was achieved for both the thermopower and NE coefficient by considering only diffusion effects. With suitable modifications, the work on metals provides the theoretical basis for some of the present analysis.

The fact that the oscillatory thermopower is dominated by phonon drag in 2DEGs but by diffusion in metals is easily understood. Phonon drag arises via electron-phonon cou-

pling and so is expected to oscillate with roughly the same relative magnitude as the electronic density of states at the Fermi level, at least to first order. In normal metals such oscillations are at the level of 1%, but in 2DEGs they vary up to 100%. Large density of states oscillations are also present in degenerate semiconductors, so one might expect these to be reflected in phonon drag oscillations in this case too.

The question then arises of how one makes a separation between phonon drag and diffusion oscillations with a degenerate semiconductor. The surprising answer is that the system itself makes such separation. Our model calculation shows that the NE coefficient is not influenced by phonon drag and we will demonstrate experimentally that this is indeed true within experimental error. This remarkable result enables us to examine the diffusion thermopower in some detail and we find that calculations based solely on diffusion reproduce the experimental data almost perfectly for both the oscillatory and non-oscillatory parts.

In contrast S_{yx} is dominated by phonon drag, including the oscillations, at least at relatively low temperatures. Previous work [8] on HgSe followed the accepted wisdom and analyzed these oscillations in terms of diffusion, but our data show that this approach is inappropriate. We are able to give a semi-quantitative explanation of the oscillatory part of S_{yy} at high fields and low temperatures in terms of phonon drag.

6.2 Theory

We will be interested in the components of the transport tensors σ, ϵ, Π and λ (for which the field is perpendicular to the current) as defined by the relations:

$$\boldsymbol{J} = \sigma \boldsymbol{E} - \epsilon \nabla T \tag{6.1}$$

$$\boldsymbol{U} = \Pi \boldsymbol{E} - \lambda \nabla T \tag{6.2}$$

where $\boldsymbol{J}$ and $\boldsymbol{U}$ are the electric and heat current densities due to an applied electric field $\boldsymbol{E}$ (more generally $\boldsymbol{E}$ is the negative of the gradient of the electrochemical potential) and temperature gradient ∇T. The thermopower tensor S is defined according to $\boldsymbol{E} = S\nabla T$ so that, from Eq. (6.1) with the boundary condition $\boldsymbol{J} = 0$, $S = \sigma^{-1}\epsilon = \rho\epsilon$ where ρ is the resistivity tensor. The magnetic field is taken to be along z, and it is assumed throughout that there is sufficient symmetry so that $\sigma_{xx} = \sigma_{yy}$, $\sigma_{yx} = -\sigma_{xy}$, etc. In the present case the heat conduction is primarily by phonons and we initially assume $\nabla T_y = 0$ (later we will make a correction for this not holding exactly). This is the same condition as for 2DEGs where the insulating substrate carries the heat. Therefore, the experiments measure the components of S_{ij} directly. Thus the thermopower is just S_{xx} and the NE coefficient is S_{yx} as follows:

$$S_{xx} = E_x/\nabla T_x = \rho_{xx}\epsilon_{xx} + \rho_{yx}\epsilon_{xy}, \tag{6.3}$$

$$S_{yx} = E_y/\nabla T_x = \rho_{xx}\epsilon_{yx} + \rho_{yx}\epsilon_{xx}. \tag{6.4}$$

In bulk metals the heat current is mainly carried by electrons which means that there is a transverse temperature gradient ∇T_y due to the Lorentz force and so the above equations are not valid in this simple form.

The thermoelectric tensor ϵ has two contributions, diffusion ϵ^d and phonon drag ϵ^g, which are linearly additive; this results in their contributions to S also being additive, i.e.

$S = S^d + S^s$. Throughout, oscillatory parts (i.e. the part resulting from the effects of magnetic quantization of the electrons) are denoted by a tilde, e.g. $\tilde{\epsilon}$, and non-oscillatory parts by a bar, e.g. $\bar{\epsilon}$.

The diffusion component is examined first under the assumption that elastic scattering is dominant in σ. Because the electron gas is degenerate, $\bar{\epsilon}^d$ can be calculated from the Mott relation [9], $\bar{\epsilon}^d = -L_o e T(\partial\bar{\sigma}/\partial\varepsilon)_{\varepsilon_F}$, and with spherical energy band results for the conductivity tensor $\bar{\sigma}$ one finds

$$\bar{\epsilon}^d_{xx} = \sigma_{xx}\frac{L_o e T}{\varepsilon_F}\left[\frac{3}{2} + p\frac{1-\beta^2}{1+\beta^2}\right] \tag{6.5}$$

$$\bar{\epsilon}^d_{yx} = \sigma_{yx}\frac{L_o e T}{\varepsilon_F}\left[1 + \frac{2p}{1+\beta^2}\right] \tag{6.6}$$

where $p = (\partial \ln\tau/\partial\ln\varepsilon)_{\varepsilon_F}$, e is the electron charge taken to be negative, i.e. $e = -|e|$, ε_F is the Fermi energy, $\beta = \omega_c\tau$ with τ is the transport lifetime and ω_c the cyclotron frequency, L_o is the Lorenz number $\pi^2 k_B^2/3e^2$ and k_B the Boltzmann constant.

With Eqs. (6.3) and (6.4) one finds the following expressions for $\bar{S}^d_{xx}$ and $\bar{S}^d_{yx}$ as a function of magnetic field:

$$\bar{S}^d_{xx} = \frac{L_o e T}{\varepsilon_F}\left[\frac{3}{2} + \frac{p}{1+\beta^2}\right] \tag{6.7}$$

$$\bar{S}^d_{yx} = \frac{L_o e T}{\varepsilon_F}\left[\frac{p\beta}{1+\beta^2}\right] \tag{6.8}$$

These field dependencies are essentially the same as with a 2DEG [10], with the former tending to the entropy per unit charge and the latter to zero as $B \to \infty$. Equivalent equations have been given by Kuleev *et al.* [11]

The oscillating part $\tilde{\epsilon}^d$ will be obtained in terms of $\tilde{\sigma}$ using a semi-classical approach introduced by Young [5], valid for elastic scattering. The derivation is analogous to that of the Mott result for the non-oscillatory parts, and in fact reduces to this when $k_B T \ll \hbar\omega_c$. One finds

$$\tilde{\epsilon}^d = -i\frac{\pi k_B}{e}\frac{D'(X)}{D(X)}\tilde{\sigma} = \alpha\tilde{\sigma} \tag{6.9}$$

where $X = 2\pi^2 k_B^2 T/\hbar\omega_c$, $D(X) = X/\sinh X$ is the thermal damping factor for oscillations in σ, $D'(X) = dD(X)/dX$ is the thermal damping factor for oscillations in ϵ, and $i = \sqrt{-1}$ indicates a $\pi/2$ difference in the phase of the oscillations. This phase difference is due to the fact that ϵ is essentially the derivative of σ with respect to electronic energy, though thermal averaging must be included to make the relation precise. The calculation of the oscillating diffusion contribution $\tilde{S}^d$ is similar to the case of the 2DEG [4] and the components are found to be

$$\tilde{S}^d_{xx} \simeq \alpha(\tilde{\rho}_{xx}\bar{\sigma}_{xx} + \tilde{\rho}_{yx}\bar{\sigma}_{yx}) = \frac{\alpha}{1+\beta^2}\left(\frac{\tilde{\rho}_{xx}}{\bar{\rho}_{xx}} + \beta^2\frac{\tilde{\rho}_{yx}}{\bar{\rho}_{yx}}\right) \tag{6.10}$$

$$\tilde{S}^d_{yx} \simeq \alpha(\tilde{\rho}_{xx}\bar{\sigma}_{yx} + \tilde{\rho}_{yx}\bar{\sigma}_{xx}) = \frac{\alpha\beta}{1+\beta^2}\left(\frac{\tilde{\rho}_{xx}}{\bar{\rho}_{xx}} + \frac{\tilde{\rho}_{yx}}{\bar{\rho}_{yx}}\right) \tag{6.11}$$

where $\bar{\rho}$ and $\tilde{\rho}$ are the non-oscillatory and oscillatory resistivities and the last step again assumes spherical energy bands. If absolute results are required the expressions for $\tilde{\rho}_{xx}$ and $\tilde{\rho}_{yx}$ from standard theories [12] may be substituted. However, for our purposes the above form is the most convenient. The sums of Eqs. (6.7) and (6.10) and Eqs. (6.7) and (6.10) give the full results for the diffusion components S^d_{xx} and S^d_{yx}, respectively.

Previous experimental results on degenerate semiconductors have been interpreted in terms of a different result for $\tilde{S}^d_{xx}$ given by Obraztsov [13], and so we briefly describe this in the following. Obraztsov finds $S^d_{xx} = \mathcal{S}/ne$ where $\mathcal{S}$ is the entropy of the electron gas. When the oscillations are sinusoidal so that harmonics can be ignored, the ensuing result for $\tilde{S}^d_{xx}$ can be written in terms of the relative amplitude of the oscillations in the density of states at the Fermi level $\tilde{\nu}/\bar{\nu}$ (which we obtain from Ref. [12]) as

$$\frac{\tilde{S}^d_{xx}}{\bar{S}^d_{xx}(\infty)} = -\frac{3}{X} D'(X) \frac{\tilde{\nu}}{\bar{\nu}} \tag{6.12}$$

where $\bar{S}^d_{xx}(\infty)$ is the high field limit of Eq. (6.7), i.e. $\bar{S}^d_{xx}(\infty) = \pi^2 k_B^2 T/2e\varepsilon_F$. No result is given for $\tilde{S}^d_{yx}$. Obraztsov made his calculation in the zero scattering limit and thus there was no impurity damping term. Schroder and Landwehr [8] added such a term since it appears to be essential from a physical point of view. By writing the result as above, the damping term is automatically included in $\tilde{\nu}/\bar{\nu}$. There is a very useful limit of this equation. As $X \to 0$, then $D'(X) \to -X/3$. In this case we obtain the simple result $\tilde{S}^d_{xx}/\bar{S}^d_{xx}(\infty) = \tilde{\nu}/\bar{\nu}$. This is a good approximation when $X < 1$. For larger X the ratio $\tilde{S}^d_{xx}/\bar{S}^d_{xx}(\infty)$ is always smaller and for large X, $D'(X) \to -2X\exp(-X)$. We note that the predicted phase shift is always π compared to $\tilde{\rho}_{xx}$. One might assume that Eqs. (6.12) and (6.10) are complementary and are perhaps valid under different conditions, but as far as we are aware this is not the case (the Appendix has further details).

We do not have as detailed a theory for the phonon drag part S^g. However, Zaremba [14] has shown that it is possible to write the phonon drag components of the thermoelectric tensor ϵ^g in the form $\epsilon^g = \sigma C$ where C is a constant which contains all the details of the electron-phonon scattering and σ is the conductivity tensor exactly as used above. The theory includes the classical effect of the Lorentz force through σ, but does not take into account magnetic quantization so C is not a function of B. From this definition it follows that $C = S^g_o$, i.e. the constant is just the phonon drag thermopower at zero field. Because of magnetic quantization, we expect the phonon-electron scattering probability to oscillate and we assume this can be allowed for by writing $C = \bar{C} + \tilde{C}$. When $k_B T \ll \hbar\omega_c$ it is reasonable to assume that $\tilde{C}/\bar{C} = \gamma\tilde{\nu}/\bar{\nu}$ where γ is a constant of order unity. This is analogous to the case of elastic scattering where a similar result holds. At higher temperatures γ will contain a thermal damping term analogous to $D'(X)$, but it will presumably be a different function for phonon drag which is an inelastic interaction. Thus, using Eqs. (6.3) and (6.4) we find

$$S^g_{xx} = S^g_o(1 + \gamma\tilde{\nu}/\bar{\nu}) \tag{6.13}$$

$$S^g_{yx} = 0 \tag{6.14}$$

In the case of S^g_{yx} the two terms in Eq. (6.4) exactly cancel, independent of field. Thus S^g_{yx} is predicted to have no phonon drag contribution for either the background or the oscillatory part. The physical reason for this result is as follows. The fact that $\epsilon^g = \sigma C$ means that

the electric current produced by phonon drag in Eq. (6.1) is equivalent to that from a fictitious electric field parallel to ∇T (assuming electrons). Thermopower is measured with no resulting electric current so a real electric field is set up (E of Eq. (6.1)) to provide the compensating current. Clearly this measured field is equal and opposite to the fictitious one, i.e. antiparallel to ∇T which has a component only along x in the present case.

The results also apply to the case of a 2DEG and the non-oscillatory parts are essentially the same as those predicted by Zianni, Butcher and Kearney [15], but it is known experimentally [10] that $\tilde{S}^{s}_{yx} \neq 0$ in this case, though it is small compared to either of the terms in Eq. (6.4). In bulk metals $\nabla T_y \neq 0$ and so the measured NE coefficient is a mixture of S_{xx} and S_{yx} and the phonon drag part is not expected to be zero.

6.3 Experiments

Data were obtained on two samples, but we report on only the one where we have a reasonably complete set of results on all the relevant coefficients. The other sample gave consistent data for the coefficients measured. The HgSe:Fe crystals were grown by the Bridgeman method at the Polish Academy of Science. The sample was oriented using standard Laue techniques and cut with a wire-erosion machine into the shape of a rectangular parallelepiped, with dimensions $9.0 \times 2.7 \times 0.80$ mm^3. The electron density was found to be 4.6×10^{24} m^{-3} independent of temperature, and the mobility 4.0 m^2/Vs at 4 K, decreasing with increasing temperature to $\sim$ 3.2 m^2/Vs at 50 K. Using an effective mass [16, 17] of $m^* = 0.065m_e$ gives a Fermi energy $\varepsilon_F \sim 0.155$ eV or 1800 K, so the gas is highly degenerate at all temperatures in these experiments. The [100] direction was perpendicular to the large face, and this was also the direction of the magnetic field B. A brief immersion in a solution of 5% Br in methanol produced polished surfaces.

The sample was indium soldered into the cryostat and a small strain gauge was epoxied to the free end for use as a heater. Silver filled epoxy was used to make contacts to four 50 μ manganine wires for use as potential leads; two similar wires were soldered with indium to act as current leads for resistivity measurements. The temperature and temperature gradient were measured with two 22 kΩ Philips surface mount resistors epoxied to the sample. These are useful from about 1-100 K and have negligible magnetoresistance over the whole temperature and field range ($B \leq 8$ T). Calibrations were made using a commercial Germanium resistance thermometer. Temperature was controlled with a capacitance thermometer which is insensitive to magnetic field.

An EM DC nanovoltmeter was used to measure potential differences across the sample. In all measurements in a magnetic field, suitable averages were evaluated for data taken at $\pm B$ to eliminate unwanted components, though these components were typically small.

The thermal conductivity of the samples was field dependent over the whole range of temperatures. This was typically a 5-30% effect and led to changes of the temperature gradient and the average temperature of the sample during field sweeps. Complete data on both of these effects were obtained and the thermopower was corrected for the change in gradient (on a continuous basis as a function of B), but not for the change in absolute temperature. This latter is negligible above about 15 K, and peaks at a few tenths of a degree near 6 K.

The main uncertainties in the data are systematic and arise from the finite size of the potential and thermometer contacts. The latter contributes an uncertainty of ~10% in the temperature gradient. The former gives ~10% uncertainty in the longitudinal electric field, but perhaps only a very small error in the transverse field. Thus we expect uncertainties of ~10% in any transverse thermal quantity (but probably much less for the Hall resistivity), ~10% for the thermal conductivity and longitudinal resistivity, and ~15% for the thermopower. Errors due to thermometer calibrations should be small over most of the range, but might become serious at the highest temperatures because of the poor sensitivity of the Philips resistors and the calibrating thermometer. At the upper limit ~ 100 K this might lead to further errors of ~10% in the thermal quantities. All other errors are believed to be small in comparison.

6.4 Results and Discussion

Field sweep data for most of the transport coefficients were taken over the range 1-55 K, but thermopower and thermal conductivity were measured up to about 100 K in zero field. This paper is primarily concerned with thermoelectric effects, but other coefficients are also important to the analysis. We first briefly review these auxiliary measurements.

6.4.1 Auxiliary Measurements

Figure 6.1 gives some representative data on ρ_{xx} as a function of field at various temperatures. We are mainly interested in such data for comparison with $\tilde{S}$ later. The modulation in the amplitude of the oscillations is known to arise from the lack of inversion symmetry of the zinc-blende crystal structure (see Ref. [17] for recent data and analysis) but the details are not relevant to the present work. A useful quantity for later use is the relative modulation in the electronic density of states $\tilde{\nu}/\bar{\nu}$ at the Fermi level due to magnetic quantization. Using the results of Roth and Argyres [12] who find $\tilde{\rho}_{xx}/\bar{\rho}_{xx} = (5/2)D(X)\tilde{\nu}/\bar{\nu}$ and the data in Figure 6.1, we estimate the peak-peak value of $\tilde{\nu}/\bar{\nu}$ to be ~ 0.4 at 8 T.

The Hall resistivity $\bar{\rho}_{yx}$ is linear in B over the range 1-50 K and shows that any variation in carrier concentration with temperature is no more than 1%. Small oscillations were superposed on the smooth background. The oscillatory component $\tilde{\rho}_{yx}$ is expected to be very small when $\beta \gg 1$. At low temperatures our experiments give a peak-peak value of $\tilde{\rho}_{yx}/\bar{\rho}_{yx} \sim -5 \times 10^{-3}$ at 8 T.

Ignoring a negligible thermoelectric correction (arising from the fact that thermal conductivity is measured with $\boldsymbol{J} = 0$ rather than $\boldsymbol{E} = 0$) the measured thermal conductivity is just λ that appears in Eq. (6.2). We denote the zero field value of λ_{xx} as λ_o and Figure 6.2 shows this as a function of temperature. The data are very similar to those obtained by Whitsett *et al* [18] on HgSe samples which did not contain Fe. The conductivity is dominated by phonons, say λ_o^g, at low temperatures, but by about 20 K the electronic contribution λ_o^e becomes visible (see below). The solid line is a calculation of λ_o^g using the same model and phonon scattering mechanisms as Whitsett *et al*, which include boundaries, electrons, Rayleigh, resonant scattering by quasi-localized phonons, and N and U phonon-phonon processes. We list the fitting parameters, since they should be useful in any future calculation of the phonon drag thermopower of this sample, but we refer the reader to the

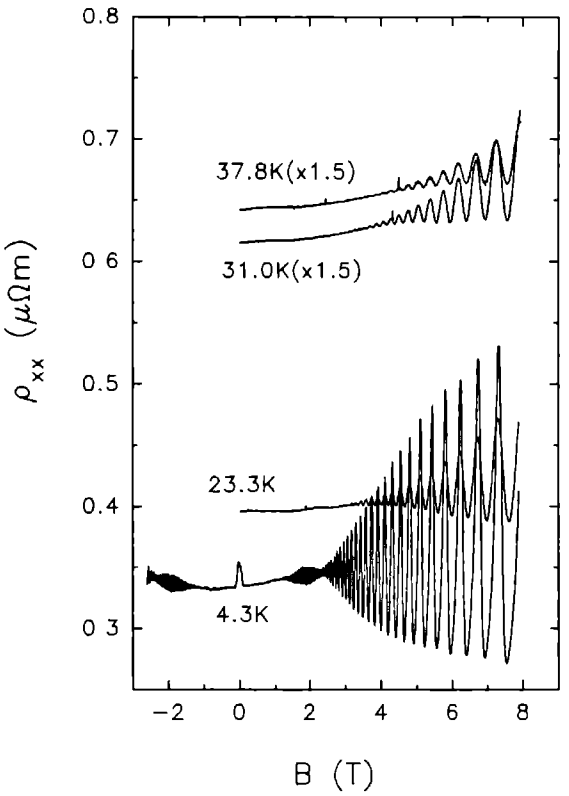

Figure 6.1: A selection of ρ_{xx} data at various temperatures. The upper two curves have been multiplied by 1.5 for clarity.

Whitsett *et al* paper for full details and definitions: boundaries $L = 1.50$ mm (after applying the correction of Wybourne *et al* [19]) and a specularity factor $F = 1.4$: Rayleigh $A = 2.9 \times 10^{-42}$ s^3: resonance $\omega_s = 5.1 \times 10^{12}$ s^{-1}, $\omega_\alpha = 3.3 \times 10^{12}$ s^{-1}, and $N = 7.5 \times 10^{27}$ m^{-3}: U-process $B_1' = 1.7 \times 10^{-17}$ s/K. Our N-process and electronic scattering are identical to those in Whitsett *et al*, with the latter restricted to the range of phonon wave vectors less than the diameter of the Fermi circle. Our values for boundary, Rayleigh and U-process scattering are all very similar, but the strength of the resonance scattering (N) is roughly a factor 2 higher. This last is responsible for the strong dip in λ_o near 15 K.

Figure 6.3 shows a selection of data on the thermal conductivity λ_{xx}, normalized to λ_o, as a function of field at various temperatures. The behaviour of the non-oscillatory background is seen to be significantly different at low and high temperatures. At high temperatures there is a rapid drop in λ_{xx} at low fields followed by an approximate saturation. This is due to the electronic contribution λ_{xx}^e. Taking the electronic thermal conductivity tensor $\lambda^e = LT\sigma$, where L is an effective Lorenz number, then with $\nabla T_y = 0$ (which is an approximation if λ_{xx}^e is finite) one has $\lambda_{xx} = \lambda^g + LT\sigma_o/(1+\beta^2)$. Thus, the electronic contri-

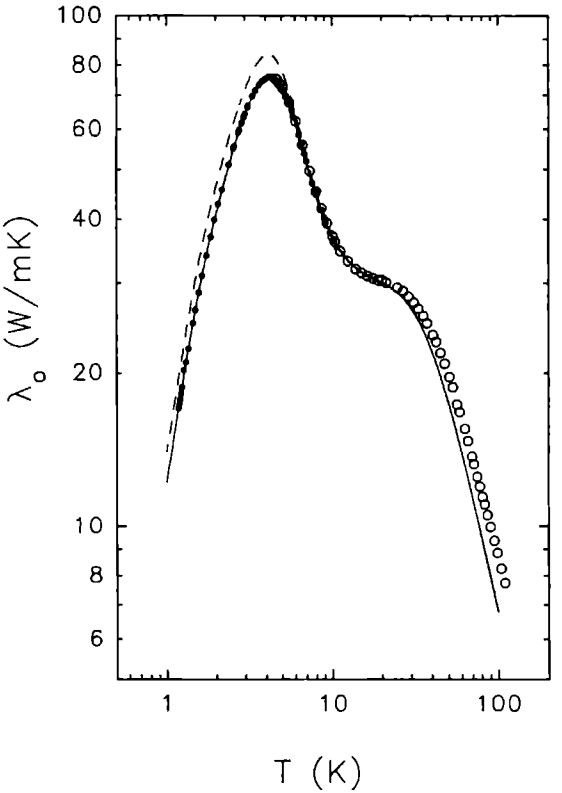

Figure 6.2: The measured zero-field thermal conductivity λ_o as a function of temperature. The two sets of symbols correspond to two different cooldowns. The solid line is fitted using the model of Whitsett *et al*, as described in the text, for the lattice thermal conductivity λ_o^g. The dashed line shows the effect of turning off the phonon-electron scattering in the calculation.

bution is suppressed by the Lorentz motion, which enables us to estimate its magnitude. It is visible only above $\sim$ 20 K and reaches about 10% of the total at $\sim$ 50 K. Whitsett *et al* [18] quote similar results obtained by a different method.

The difference in curve shapes in Figure 6.3 between 4-15 K implies that the decrease in λ_{xx} is due to a different mechanism. Above 20 K the saturation field is rather low and is governed by $\omega_c\tau = 1$; this field slowly increases with temperature due to the temperature dependence of μ. Below 20 K, where the electronic contribution becomes negligible, another mechanism appears with a higher saturation field. This behaviour may be related to the Fe impurities, though they do not seem to be connected with the dip in λ_o at about 15 K seen in Figure 6.2 since a similar dip is observed in undoped HgSe [18]. At even lower temperatures below 4.3 K the behaviour is again different with an abrupt drop in λ at very

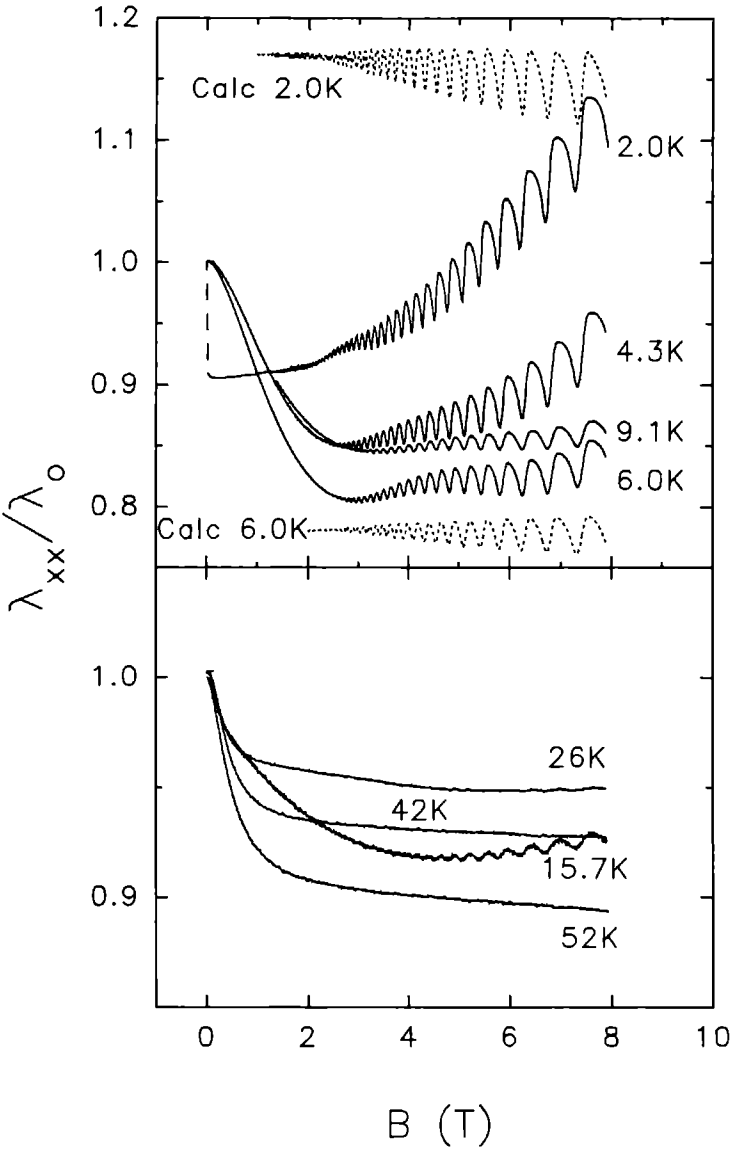

Figure 6.3: The thermal conductivity λ_{xx} as a function of field at various temperatures. The data are normalized to the zero-field values λ_o. In the upper panel the dotted curves are calculations of the oscillations at 2 K and 6 K assuming they are due to p-e scattering.

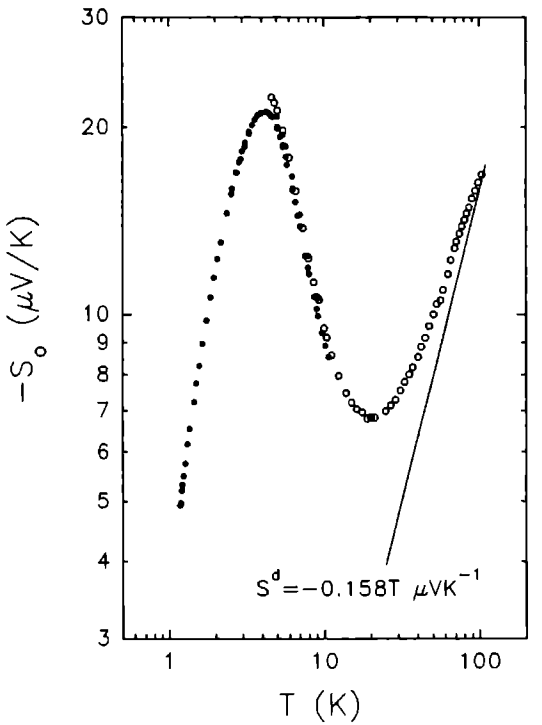

Figure 6.4: The thermopower at zero field S_o as a function of temperature. The two sets of symbols are the same two cooldowns as mentioned in Fig. 6.1. The straight line is the estimated diffusion component.

low fields ($\sim$ 0.1 T, as Figure 6.3 shows) which seems reminiscent of a phase change. The sharp decrease in λ_{xx} is mirrored by a similar drop in ρ_{xx} at the lowest temperatures.

The observed oscillations do not arise from oscillations in λ^e, which is negligible at low temperatures even before being turned off by the field, but are caused by the effect of magnetic quantization of the electrons on phonon-electron (p-e) scattering. They are clearly related to the quantity $\gamma\tilde{\nu}/\bar{\nu}$ that appears in Eq. (6.13) and in Section 6.4.2 we will give an analysis based on this idea.

6.4.2 Thermoelectric Coefficients

The thermopower S_{xx} at zero field, S_o, is shown in Figure 6.4. There is a small shift in the data between cooldowns which is not reflected in the thermal conductivity in Figure 6.2. The change might be intrinsic to the electronic properties, but might also be simply due to instabilities in the potential leads because of the use of Silver filled epoxy for the connections.

The straight line is the estimated diffusion part (explained below) and it is clear that phonon drag is completely dominant up to about 25 K. An interesting feature is that the

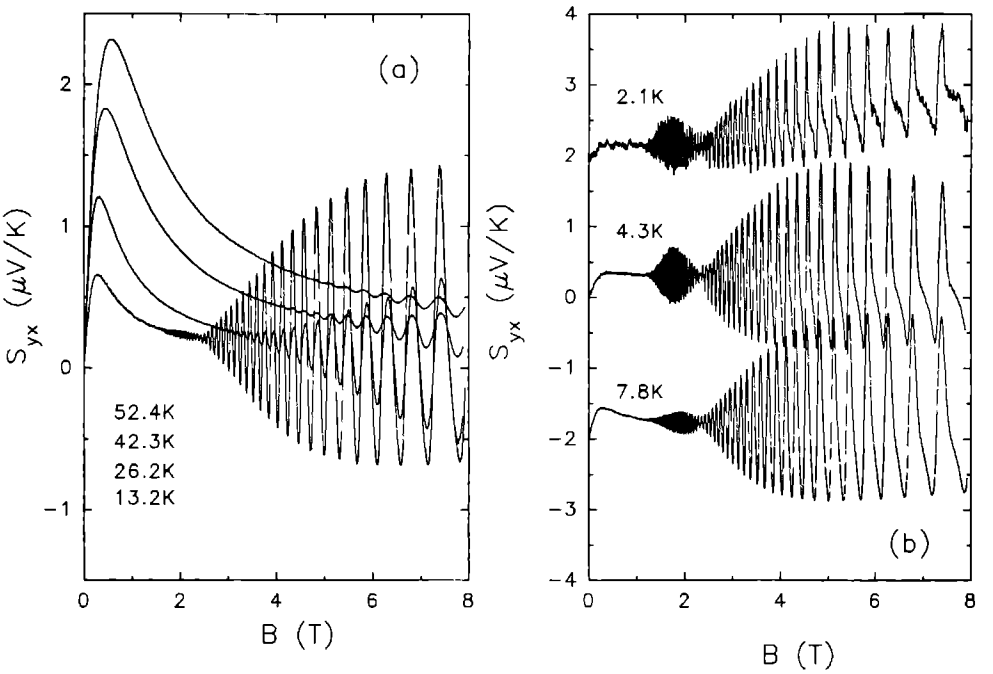

Figure 6.5: Examples of the Nernst-Ettingshausen coefficient S_{yx} as a function of magnetic field. Data in panel (a) are at higher temperatures, and those in panel (b) at lower temperatures. In panel (b) the curves at 2.1 K and 7.8 K have been offset by 2 μV/K.

ratio of S_o and λ is constant to a few percent over the range 1-6 K. This is unlikely to be coincidental and is probably a reflection of the fact that the same phonons are responsible for both S_o and λ_o in this temperature range. At higher temperatures most of the phonons can no longer interact with electrons. The cutoff phonon frequency for p-e scattering is related to the diameter of the Fermi sphere and corresponds to $\sim$ 15 K. The decrease in the ratio S_o/λ above $\sim$ 6 K is presumably related to this.

Figure 6.5 gives a selection of data on S_{yx} as a function of magnetic field at different temperatures. Kuleev *et al* [11] have recently published data on $\bar{S}_{yx}$ on a series of HgSe:Fe samples, but field dependencies were not given. According to Eq. (6.14) there should be no phonon drag in this coefficient, and the data do have the characteristics expected of the diffusion parts given in Eqs. (6.8) for $\bar{S}_{yx}$ and (6.11) for $\tilde{S}_{yx}$ as we will now show.

The non-oscillatory part of the experimental data have been fitted to Eq. (6.8) to find the amplitude $L_o eTp/\varepsilon_F$ and the mobility $\mu = \beta/B$ as a function of temperature. These fits to the smooth parts are essentially perfect, even when the oscillation amplitude is large. We find μ to be consistently lower than calculated from the Hall and longitudinal resistivity and ranges from $\sim$ 3.2 m^2/Vs at low temperature to $\sim$ 1.7 m^2/Vs by 50 K. The difference may be related to the distinction between the electronic relaxation times appropriate

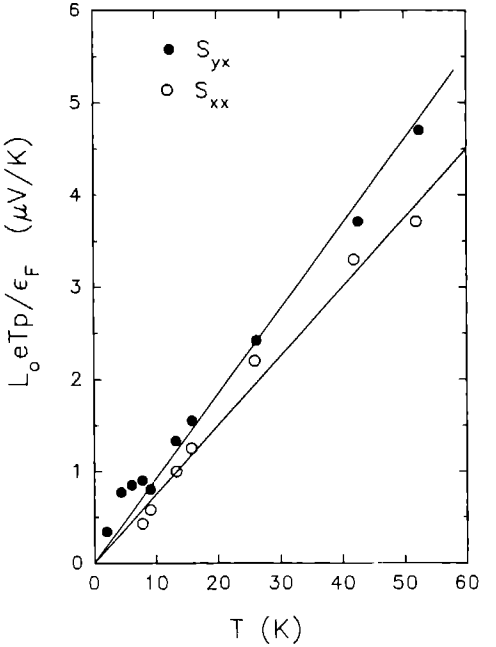

Figure 6.6: The quantity $L_o eTp/\varepsilon_F$ obtained from fits to the non-oscillatory parts of S_{yx} and S_{xx} respectively as a function of temperature.

to momentum and thermal transport, which our theory does not distinguish. Figure 6.6 gives $L_o eTp/\varepsilon_F$ as a function of T. The observed linear relationship shows that diffusion is dominant and p can be taken as constant. It should be noted that each term in the phonon drag part of Eq. (6.4) has a magnitude of $S_0^g \beta/(1+\beta^2)$ which is of the same form as the diffusion part given by Eqs. (6.8). At the peak of the phonon drag near 4 K, the ratio of former to the latter is about 60. If perfect cancelation of the two phonon drag terms did not occur, the residual would be easily recognizable since it would not be linear in T, as was found with a 2DEG [10]. There may indeed be a tiny peak near 4 K in Figure 6.6 possibly reflecting the peak in Figure 6.4, though the noise is similar in magnitude at these low temperatures. In any event the results imply that the two terms are matched to no worse than ~1%. With $\varepsilon_I = 0.155\, eV$ in Eq. (6.8), we find $p = -0.57$.

We have used Eq. (6.11) and the measured $\tilde{\rho}_{xx}$ (the contribution from $\tilde{\rho}_{yx}$ is completely negligible) to calculate the oscillatory contribution $\tilde{S}_{yx}$. The phase has been shifted by $\pi/2$ and we use the same mobility μ as required for the smooth background. At low temperatures the harmonics in $\tilde{\rho}_{xx}$ become very large and must be taken into account to obtain the observed waveform for $\tilde{S}^d_{yx}$. Thus we have extracted the fundamental and the first 2 harmonics using Fourier analysis, evaluated these contributions separately in the analysis and finally added them and the non-oscillatory parts to give the results shown in Figure 6.7. Notice there are no free parameters in this calculation. The correspondence be-

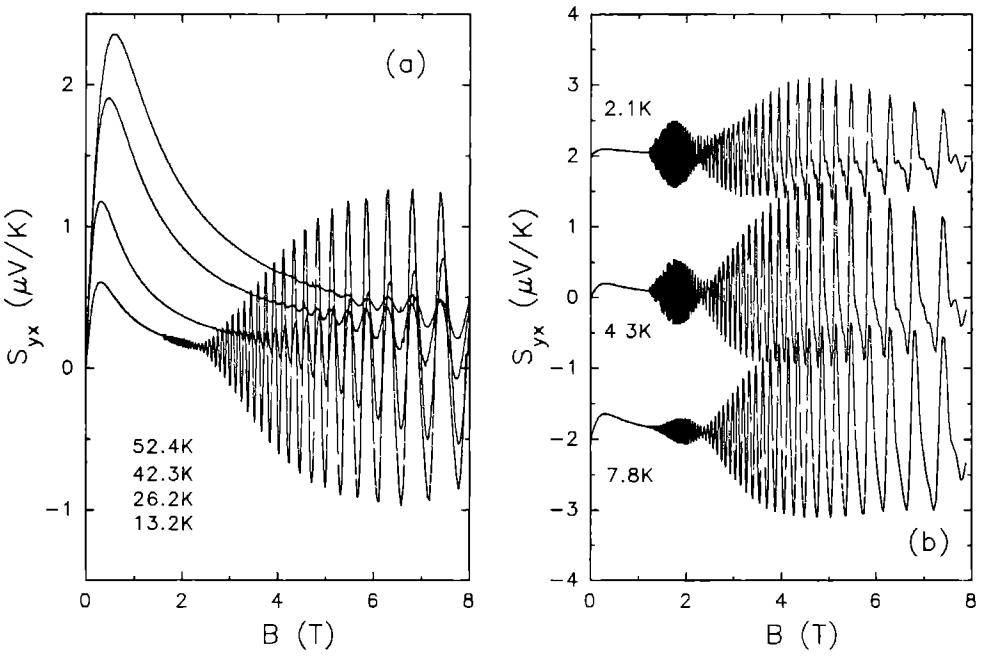

Figure 6.7: Calculated S_{yx} for the same temperatures as the experimental data in Figs. 6.5(a) and 6.5(b). In panel (b) the curves at 2.1 K and 7.8 K have been offset by 2 μV/K.

tween experiment and calculation is excellent at all temperatures and fields. We particularly draw attention to the triangular waveform at low temperatures which is well reproduced by the harmonic contributions. The sharp peaks of the calculated data superpose essentially perfectly onto the experimental data, both in magnitude and position.

The phases of $\tilde{\rho}_{xx}$ and $\tilde{S}_{yx}$ have also been compared directly from the experimental data using a method described previously [20]. In the range with the highest experimental accuracy ($B = 5 - 8$ T and $T > 15$ K) all the $\tilde{\rho}_{xx}$ data are found to have the same phase to an accuracy of $\leq \pm\pi/10$, and the same is true for $\tilde{S}_{yx}$. The two averages differ by almost exactly $\pi/2$ as predicted.

Figure 6.8 shows typical data for S_{xx} as a function of B at various temperatures. Above $\sim$ 9 K the non-oscillatory part shows a rapid rise followed by saturation. This is the effect of the second term containing p in Eq. (6.7) for $\tilde{S}^d_{xx}$ and, because p is negative, $\tilde{S}^d_{xx}$ increases with field. At lower temperatures this rise becomes swamped by the rapidly increasing phonon drag contribution which, according to Eq. (6.13), is independent of field. There is also a decrease with B at lower temperatures which is clearly related to the field dependence of λ_{xx} described in Section 6.4.1. A decrease in λ_{xx} implies more field dependent phonon scattering (other than p-e scattering) and consequently a decrease in phonon drag, but the origin of this feature is unknown.

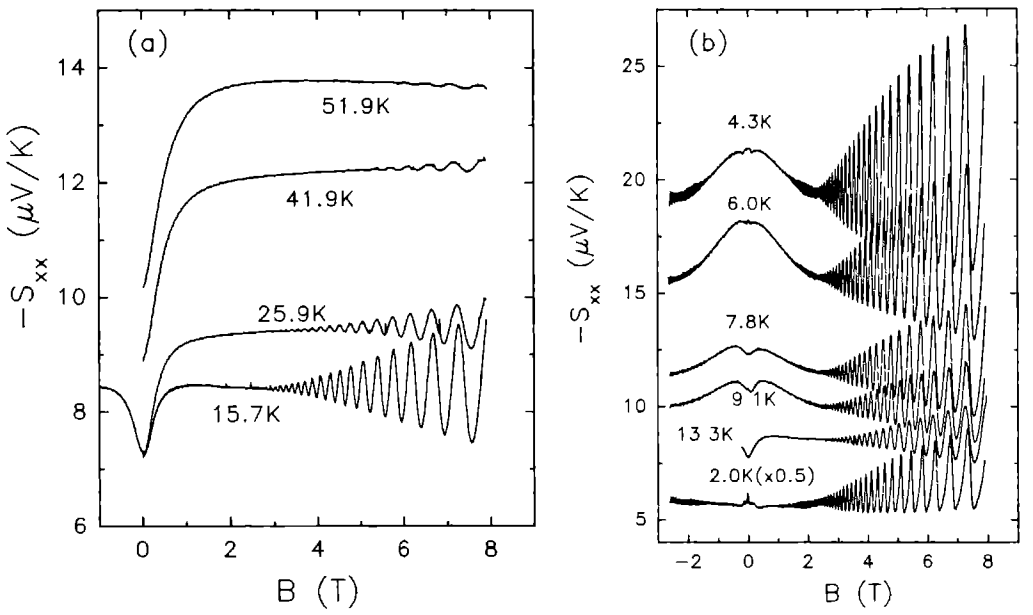

Figure 6.8: Examples of the thermopower S_{xx} as a function of field at various temperatures. Notice the scale change for the data at 2.0 K.

Above ~10 K the field dependence of the non-oscillatory background has been fitted to Eq. (6.7), with an additive constant to take phonon drag into account. The fits give μ consistent with those from $\bar{S}_{yx}$, and $L_o eTp/\varepsilon_F$ is shown on Figure 6.6. We find $p = -0.48$ compared to the value of -0.57 from $\bar{S}_{yx}$. The discrepancy is rather small and might simply reflect errors in sample dimensions, but it can also arise from the fact that the electronic thermal conductivity is not negligible above about 20 K. This means $\nabla T_y \neq 0$ which, in turn, implies that the thermopower and the NE coefficient are no longer precisely equal to S_{xx} and S_{yx} respectively. For example one finds that the NE coefficient is approximately given by $S_{yx} - S_{xx}(\lambda^e_{yx}/\lambda_{xx})$. At about 50 K this will appear to increase the magnitude of the NE coefficient by perhaps 20%, which leads to a value of p too high by the same factor. Although a similar relation holds for the thermopower, in these experiments this correction is negligible. The results for p are both consistent with the value of -0.5 expected from a constant electronic mean free path.

We have used $p = -0.50$ and Eq. (6.7) to calculate the diffusion component of the zero field thermopower S_o as a function of T, and this is the straight line shown in Figure 6.4. We also note that, at least above about 10 K, the consistency of the analysis in using $\bar{S}^d_{xx}$ to describe the field dependence of the measured thermopower means that the non-oscillatory part of the phonon drag is independent of field in agreement with Eq. (6.13).

The oscillatory part $\tilde{S}_{xx}$ is accurately π out of phase with $\tilde{\rho}_{xx}$ (S_{xx} is a negative quantity) over the whole temperature range which immediately shows that Eq. (6.10) cannot represent these data. The calculated amplitude is also too small at all temperatures. At

8 T and 4 K it predicts 0.07 μV/K compared with the observed 13 μV/K. The agreement improves at high temperature but is never good. At 50 K the measured amplitude at 8 T is ~ 0.08 μV/K compared with the calculated value of 0.03 μV/K.

The entropy result of Eq. (6.12) has the correct phase, but is also unsuccessful with the amplitude. For $T < 8$ K and $B = 8$ T, $X < 1$ so that $\tilde{S}^d_{xx}/\bar{S}^d_{xx}(\infty) = \tilde{\nu}/\bar{\nu}$ is a good approximation. Using $\tilde{\nu}/\bar{\nu} \sim 0.4$, Eq. (6.12) predicts $\tilde{S}^d_{xx} \sim 0.4\bar{S}^d_{xx}(\infty)$. Because $\bar{S}^d_{xx}(\infty) \sim (4/3)S^d_o$ and Figure 6.4 shows that S^d_o very small compared to S^g_o, then these oscillations are also negligible. At high temperatures the agreement improves as with Eq. (6.10). At 50 K and 8 T the calculated amplitude ~ 0.05 μV/K.

The poor agreement with either of the above diffusion results, especially at low temperatures, leads to the inevitable conclusion that the oscillations have their origin in phonon drag according to Eq. (6.13). In other words they reflect the changes induced in phonon-electron scattering due to magnetic quantization of the electrons. This identification does not appear to have been made before for degenerate semiconductors, but it is an obvious extension of the 2D case which is now well known [3]. At low temperatures the observed $\tilde{S}_{xx}/\bar{S}_{xx}$ is about 50% in accordance with $\gamma \sim 1$. When $k_BT \ll \hbar\omega_c$ we would expect the oscillation amplitude to scale with $\bar{S}_{xx}$. At 8 T this should be so for $T \sim 2 - 10$ K. Figure 6.8 does indeed show the expected scaling which is especially convincing given the strong variation of $\bar{S}_{xx}$ in this temperature range. For comparison we note that both Eqs. (6.12) and (6.10) predict a scaling as T under these conditions. Of course, at higher temperatures when $k_BT \ll \hbar\omega_c$ no longer holds, all contributions to the oscillations are thermally damped. For elastic scattering the damping term is $D'(X)$ in Eqs. (6.10) and (6.12), but the form of the damping term is not known for $\tilde{S}^g_{xx}$ and so we cannot estimate the relative contributions from diffusion and phonon drag to the high temperature oscillations.

Finally, we briefly return to the oscillations found in λ^g_{xx} mentioned in Section 6.4.1. An estimate of $\tilde{\lambda}^g_{xx}$ can be made as follows. Let the relaxation time for p-e scattering be τ_e and that for phonon scattering by all other mechanisms τ_a. Then $\lambda^g_{xx}/\lambda^g_o = (1/\tau_{eo} + 1/\tau_{ao})/(1/\tau_e + 1/\tau_a)$, where the extra subscript o specifies zero field. With some re-arrangement this gives $\lambda^g_{xx}/\lambda^g_o = (\tau_a/\tau_{ao})(1 + \eta_o)/(1 + \eta_o(\tau_{eo}/\tau_{ao})(\tau_a/\tau_e))$ where $\eta_o = \tau_{ao}/\tau_{eo}$ is the ratio of scattering of phonons by electrons to scattering by all other mechanisms at zero field. Elementary models [21] of phonon drag in 2D or 3D metals give the relation $S^g_o = \text{constant} \times C^g(\tau_{ao}/\tau_{eo})/(1 + \eta_o) \sim C^g(\tau_{ao}/\tau_{eo})$ where C^g is the lattice specific heat. Using this together with the similar relation $S^g_{xx} \sim C^g(\tau_a/\tau_e)$ we finally find

$$\frac{\lambda^g_{xx}}{\lambda^g_o} \simeq \frac{\tau_a}{\tau_{ao}} \frac{(1 + \eta_o)}{(1 + \eta_o(S^g_{xx}/S^g_o))}. \tag{6.15}$$

This should be appropriate when all the phonons participate in both λ^g and S^g, i.e. over the range 1-6 K approximately. The non-oscillatory variation $\bar{\lambda}^g_{xx}$ is caused by τ_a/τ_{ao} and the oscillatory part $\tilde{\lambda}^g_{xx}$ arises through the term S^g_{xx}. Using the experimental data for S_{xx} (which is essentially S^g_{xx}) as a function of B, we have calculated $\lambda^g_{xx}/\lambda^g_o$ at 2 K and 6 K using values of τ_a/τ_{ao} required to approximately match the background at high fields and $\eta_o = 0.09$, and the results are in good agreement with experiment as shown in Figure 6.2.

The required fraction of scattering by electrons is in keeping with our theoretical estimates in Section 6.4.1. Thus in Figure 6.2 the fitted curve for λ^g_o is given both with and without p-e scattering. The calculated ratio η_o varies from $\sim$0.15 at 1 K to 0.01 at 10 K. However,

by about 9 K the observed oscillations in λ^g_{xx} show that electronic scattering is larger than our calculation predicts, which probably implies that the calculation of p-e scattering is in error at higher temperatures.

6.5 Conclusions

Our model calculation of the thermopower tensor S for a degenerate semiconductor predicts that both components S_{xx} and S_{yx} have diffusion contributions, but that only the former will show phonon drag effects. Experimentally this is indeed found to be so for both the oscillatory and non-oscillatory parts. This remarkable difference between the components is clearly a very useful result which has not been previously recognized. One would expect 2DEGs to act in the same way, but a phonon drag component of S_{yx} has definitely been seen [10] in that case, though it is small. The reason for this discrepancy is not known and deserves close attention. These two cases are particularly simple experimentally because the absence of a transverse temperature gradient means that the NE coefficient gives S_{yx} directly, and similarly the thermopower gives S_{xx}.

The diffusion model we have used to describe both the oscillatory and non-oscillatory components of S_{yx} has been accurately confirmed. In particular, the oscillations in S_{yx} show excellent agreement with calculated amplitudes, and also the expected phase shift of $\pi/2$ compared to resistance oscillations. In contrast, the oscillations in S_{xx} are found to be due almost entirely to phonon drag, as is also true in 2DEGs. We have given a semi-quantitative argument for the amplitude of the phonon drag oscillations at low temperatures and high magnetic fields, but a full quantitative calculation is lacking. An analysis of the oscillations in the lattice thermal conductivity at low temperatures supports the identification of the oscillations in S_{xx} with phonon drag.

Previous experimental data on oscillations in the thermopower of degenerate semiconductors, particularly on HgSe [8], have been analyzed in terms of entropy oscillations, but we have shown these cannot be the cause, at least at low temperatures. It is unfortunate that we cannot see recognizable diffusion oscillations in S_{xx} because it means we are unable to distinguish which, if either, of the models for these oscillations is correct for this coefficient.

In bulk metals diffusion oscillations are dominant in both the thermopower and NE coefficient and conform to Eq. (6.9), but most investigations have involved magnetic breakdown so the situation is perhaps not completely clear-cut. Phonon drag oscillation have not been seen, which agrees with our contention that these are at the same relative level as the oscillations in the electronic density of states; these latter are typically at a level of 1% or less as a result of the high electronic density.

6.6 Acknowledgements

We are very grateful to ir. L. W. M. Scheurs for technical support in sample preparation and to Dr. Eugene Zaremba for illuminating discussions concerning phonon drag thermopower. This work was supported, in part, by a grant from the Natural Sciences and Engineering Research Council of Canada and is a part of a research program of the Stichting voor Fundamenteel Onderzoek der Materie (FOM) financially supported by NWO (Netherlands).

6.7 Appendix – Entropy Oscillations and Thermopower

Eq. (6.12) is from the high-field limit of Eq. (6.3), i.e. $S^d_{xx} = \rho_{yx}\epsilon^d_{xy}$, with ρ_{yx} taken to be B/ne and non-oscillatory. It is well known that, as $\beta \to \infty$, $\tilde{\epsilon}^d_{xy}$ is a direct measure of the non-oscillatory density of states at the Fermi level by virtue of the Mott relation applied to $\bar{\sigma}_{xy} = ne/B$. It therefore seems reasonable that the oscillatory density of states would appear in $\tilde{\epsilon}_{xy}$ and this is what Eq. (6.12) claims for the oscillatory part $\tilde{S}^d_{xx}$. However, other arguments suggest otherwise.

All calculations of σ_{xy} taking magnetic quantization into account are consistent with this coefficient having no oscillations as $\beta \to \infty$. Guseva and Zyryanov [22] and Horton [23] find that (ignoring the thermal damping term $D(X)$)

$$\sigma_{xy} = \frac{ne}{B}\left[1 + \frac{7}{2\beta^2}\left(\sqrt{\frac{\hbar\omega_c}{2\varepsilon_F}}\sum_r \frac{(-1)^r}{\sqrt{r}}\cos\left(\frac{2\pi\varepsilon_F r}{\hbar\omega_c} - \frac{\pi}{4}\right)\right)\right]. \tag{6.16}$$

The oscillatory corrections are a result of residual scattering effects whereby the electron scattering probability reflects the oscillations in the density of states, and go to zero as $\beta \to \infty$. The absence of oscillations as a function of B in the zero-scattering limit also implies there are no oscillations in the energy dependence of this coefficient. This can be seen directly from Eq. (6.16) where one can fix either ε_F or B and allow the other to vary. However, it is the zero-scattering limit that Obraztsov uses to calculate $\tilde{\epsilon}_{xy}$. The combination of these two results implies that $\tilde{\epsilon}^d_{xy}$ and $\tilde{\sigma}_{xy}$ are not related in this limit and cannot, for example, satisfy the Mott result which would be expected to hold when $k_B T \ll \hbar\omega_c$.

In contrast Eq. (6.9) is essentially the Mott result extended to the case of oscillations in the density of states with arbitrary $k_B T/\hbar\omega_c$, and cancels to the usual Mott relation given above in the high field limit $k_B T \ll \hbar\omega_c$. In the zero-scattering limit Eq. (6.16) predicts $\tilde{\sigma}_{xy} = 0$ and this means $\tilde{\epsilon}_{xy} = 0$ from Eq. (6.9). Lest it be assumed that this result has no basis other than Young's semi-classical arguments [5], they are supported by a quantum mechanical density matrix calculation by Horton [23] for free electrons. Horton gives results for $\tilde{\sigma}_{yx}$ (Eq. (6.16)) and $\tilde{\epsilon}_{xy}$ which are consistent with Eq. (6.9). Thus the two results Eq. (6.9) and Eq. (6.12) appear to be inconsistent. A resolution of this problem is clearly called for.

6.8 References

[1] P. S. Zyrayanov and G. I. Guseva, Soviet Physics Uspekhi **11**, 538 (1969) (Usp. Fiz. Nauk. **95**, 565 (1968)).

[2] S. M. Puri and T. H. Geballe, *Semiconductors and Semimetals*, edited by R. K. Willardson and A. C. Beer (Academic Press, NY, 1966) Vol. 1, p. 203.

[3] B. L. Gallagher and P. N. Butcher, in *Handbook on Semiconductors*, edited by P. T. Landsberg (Elsevier, Amsterdam, 1992) Vol. 1, p. 817.

[4] R. Fletcher, P. T. Coleridge and Y. Feng, Phys. Rev. B **52**, 2823 (1995).

[5] R. C. Young, J. Phys. (F) **3**, 721 (1973).

[6] R. Fletcher, J. Low Temp. Physics, **43**, 363 (1981).

[7] R. Fletcher, Phys. Rev. B **28**, 1721 (1983), Phys. Rev. B **28**, 6670 (1983).

[8] B. Schroder and G. Landwehr, Solid State Comm. **22**, 589 (1977).

[9] J. M. Ziman, *Electron and Phonons*, (Clarendon Press, Oxford, 1963) p. 500.

[10] R. Fletcher, J. J. Harris, C. T. Foxon, M. Tsaousidou and P. N. Butcher, Phys. Rev. B **50**, 14991 (1994).

[11] I. G. Kuleev, A. T. Lonchakov, I. I. Lyapilin and M. Tsidil'kovskii, Soviet Physics JETP, **76**, 707 (1993) (Zh. Eksp. Teor. Fiz. **103**, 1447 (1993)).

[12] L. M. Roth and P. N. Argyres, *Semiconductors and Semimetals*, edited by R. K. Willardson and A. C. Beer (Academic Press, N.Y., 1966) Vol. 1, p. 159.

[13] Yu. N. Obraztsov, Soviet Physics - Solid State **7**, 455 (1965) (Fiz. Tverd. Tela **7** 573 (1965)).

[14] Private communication and to be published.

[15] X. Zianni, P. N. Butcher, M. J. Kearney, Phys. Rev. B **49**, 7520 (1994).

[16] M. von Ortenberg, Sem. Sci. Tech. **8**, S16 (1993).

[17] M. Vaziri and R. Reifenberger, Phys. Rev. B **32**, 3921 (1985) and B**33**, 5585 (1986).

[18] C. W Whitsett, D. A. Nelson, J. G. Broerman and E. C. Paxhia, Phys. Rev. B **7**, 4625 (1973).

[19] M. N. Wybourne, C.G. Edison and M. J. Kelly, J. Phys. (C): Solid State Phys. **17**, L607 (1984).

[20] R. Fletcher, J. J. Harris and C. T. Foxon, J. Phys.: Condens. Matter **3**, 3479 (1991).

[21] For 2D see M. J. Smith and P. N. Butcher, J. Phys.: Condens. Matter **2**, 2375 (1990): For 3D see R. D. Bernard, *Thermoelectricity in Metals and Alloys*, (Taylor and Francis, London, 1972) p. 113.

[22] G. I. Guseva and P. S. Zyryanov, Phys. Stat. Sol. **25**, 775 (1968).

[23] Philip B. Horton, *Quantum Transport Theory of Free Electrons in a Strong Magnetic field*, PhD Thesis (1964), Louisiana State University, unpublished. Many of Horton's results are given in J. R. Long, C. G. Grenier and J. M Reynolds, Phys. Rev. **140**, A187 (1965).

Summary

This thesis describes the thermoelectric power (or simply thermopower) of a two-dimensional and a three-dimensional metallic semiconductor at low temperatures and in in high magnetic fields. The electrical conductivity of these systems is metal-like, i.e. finite at low temperatures. In metallic semiconductors the free electron concentration is orders of magnitude lower than it is in normal metals. Consequently, the electronic contribution to the thermal conductivity is negligible. Instead, it is governed by lattice vibrations, the phonons, and resembles that of an insulator/semiconductor.

An interesting aspect of the thermopower in these systems is that it is a measure for the interaction between electrons and phonons. An applied temperature gradient causes a phonon flow. Free electrons are dragged by this phonon flow from the hot to the cold side of the sample, a process denoted as *phonon drag*. The voltage due to the resulting charge build-up gives the thermopower, which in a magnetic field has a longitudinal component, S_{xx}, and a transverse component, S_{yx}, the Nernst-Ettingshausen coefficient.

A measurement of the thermoelectric power therefore provides information on the electronic structure of metallic semiconductors. In a 2-dimensional electron gas (2DEG), realized at the interface of a GaAs-$Ga_{1-x}Al_xAs$ heterojunction, the quantization of the electronic density-of-states in high magnetic fields into Landau levels leads to the observation of the integer quantum Hall effect. In the quantum limit, electron-electron interactions are the cause of a similar effect at fractional filling of a Landau level, the fractional quantum Hall effect.

The fractional quantum Hall effect has recently found an elegant explanation in the theory of composite fermions. Chapter 1 describes in detail this model which postulates the existence of new quasi-particles formed in high magnetic fields, the composite fermions. A composite fermion consists of an electron with an even number of magnetic flux quanta attached to it. After introducing the basic concepts of thermoelectric power, an existing thermopower theory based on a solution of the Boltzmann equation is combined with this composite fermion-picture to provide a description of the experimental results presented in chapters 3 and 5.

The experimental conditions to fulfill in the thermopower measurements are rather demanding and therefore the experimental techniques are described in chapter 2 in some detail. In order to observe quantum effects like the fractional quantum Hall effect, one has to reach very low temperatures and at the same time apply a considerable amount of heat to the sample to produce the necessary temperature gradient. The experiments have been set up in a plastic $^3He/^4He$-dilution refrigerator which avoids eddy-current heating in high field Bitter magnet. The lowest temperatures on the sample were 100 mK, the highest magnetic field used was 30 T.

Chapter 3 describes measurements of the phonon drag thermopower in the fractional

quantum Hall regime of different composite fermion-states. The thermopowers of different composite fermions are identical if the same number of flux quanta is bound in the quasi-particle, a behaviour which is understood in the theoretical description developed in chapter 1. Furthermore, the similarity observed in the experiment between the composite fermion-thermopower and the thermopower in zero magnetic field is a confirmation of the concept of a vanishing effective magnetic field for the quasi-particles in the composite fermion-theory.

A phenomenon in quantum Hall systems which has not been understood in the past is the existence of a phonon drag dominated transverse component S_{yx} of the thermoelectric power. The analysis of experimental data for a great variety of 2DEG-samples in chapter 4 shows that this component is related to the longitudinal thermopower S_{xx} as $S_{yx} = \alpha B(dS_{xx}/dB)$. The dimensionless scaling factor α is found to be the same as the one obtained from a similar relation between the two resistivity components. The equivalence of the thermopower and the resistivity relation is shown making certain assumptions.

A comprehensive study of the thermoelectric power on a set of three similar 2DEG samples, which differ only in a detail of the geometry, in high magnetic fields and for temperatures below 1 K is presented in chapter 5. The implications of the thermopower on the composite fermion-model and the fundamental relation between S_{xx} and S_{yx} are studied in greater detail than discussed in chapter 3 and 4, respectively. The thermopower depends on the orientation of the temperature gradient with respect to the crystallographic axes and it scales with the phonon mean free path. This behaviour demonstrates directly the phonon drag origin of the thermopower in these systems.

The magneto-thermoelectric properties of the three-dimensional metallic semiconductor HgSe doped with Fe is studied in chapter 6. Concerning the thermopower, this system is conceptually very similar to the 2D-systems discussed in the earlier chapters. Phonon drag is dominant in the longitudinal component S_{xx} but absent in the transverse component S_{yx}. This behaviour is in line with theoretical expectations but stands in significant contrast to the 2D case which demonstrates the fact that the relation between S_{yx} and S_{xx} discussed in chapters 4 and 5 is a characteristic feature of 2D quantum Hall systems only. In the 3D case, the absence of phonon drag in S_{yx} results in a purely diffusion dominated S_{yx}. The diffusion origin is clear form the temperature dependence and a $\pi/2$ phase shift of the oscillations. Theoretical calculations are shown to be in perfect agreement with the experimental data. The strong electron-phonon coupling in HgSe:Fe is seen in quantum oscillations in the (lattice) thermal conductivity which are in phase with the Landau level structure of the electronic density-of-states.

Samenvatting

Dit proefschrift beschrijft de thermospanning van een twee-dimensionale en een drie-dimensionale metallische halfgeleider bij lage temperaturen en in hoge magneetvelden. De elektrische geleiding van deze systemen is metallisch, i.e. eindig bij lage temperaturen. De vrije electronen concentratie in metallische halfgeleiders is ordes van grootte lager dan die in gewone metalen. Daarom is de elektronische bijdrage aan de warmtegeleiding te verwaarlozen. In plaats daarvan wordt de warmtegeleiding bepaald door roostertrillingen, de fononen, en lijkt deze op die van een isolator/halfgeleider.

Een interessant aspect van de thermospanning in deze systemen is dat zij een maat is voor de interactie tussen elektronen en fononen. Een aangelegde temperatuurgradient veroorzaakt een stroom van fononen. Vrije elektronen worden door deze fononen-stroom van de warme naar de koude kant van het sample "meegesleept", een proces dat *phonon drag* wordt genoemd. Dit leidt tot een ladingsopbouw en de resulterende spanning (gedeeld door het temperatuurverschil) is de thermospanning. In een magneetveld heeft deze een longitudinale component, S_{xx}, en een transversale component, S_{yx}, de Nernst-Ettingshausen coëfficient.

Een thermospanningsmeting levert informatie op over de elektronische struktuur van metallische halfgeleiders. In een 2-dimensionaal electronengas (2DEG), dat gerealiseerd wordt aan het grensvlak van een GaAs-$Ga_{1-x}Al_xAs$ heterojunctie, leidt de quantisatie van de elektronische toestandsdichtheid in hoge magneetvelden in Landau niveaus tot het ontstaan van het *integer quantum Hall effect*. Elektron-elektron interacties zorgen in de quantum-limiet voor een soortgelijk effect bij een niet volledig gevuld Landau niveau, het zogenoemde *fractional quantum Hall effect*.

Voor het fractional quantum Hall effect is onlangs in de vorm van de theorie van de *composite fermions* een elegante verklaring gevonden. Hoofdstuk 1 beschrijft in detail dit model dat het bestaan van nieuwe quasi-deeltjes die in hoge magneetvelden gevormd worden, postuleert. Zo'n quasi-deeltje wordt een *composite fermion* genoemd en bestaat uit een elektron waaraan een even aantal magnetische flux quanta gebonden is. Na de introductie van de basisconcepten van de thermospanning wordt een bestaande theorie, die gebaseerd is op een oplossing van de Boltzmann-vergelijking, gecombineerd met het *composite fermion*-model met als doel de beschrijving van de experimentele resultaten die in hoofdstuk 3 en 5 gepresenteerd worden.

De voorwaarden waaraan de thermospanningsmetingen moeten voldoen, zijn vrij stringent. Daarom worden de experimentele technieken in hoofdstuk 2 gedetailleerd beschreven. Om quantum-effecten zoals het fractional quantum Hall effect te bestuderen moet een heel lage temperatuur gemaakt worden, terwijl tegelijkertijd een niet te verwaarlozen stookvermogen aangelegd wordt om de noodzakelijke temperatuurgradient te produceren. De experimenten zijn opgezet in een $^3He/^4He$-mengkoeler met plastic warmte-

wisselaars om Foucault-stromen in hoge velden van Bitter magneten vermijden. De laagste temperatuur op het sample was 100 mK, het hoogste gebruikte magneetveld was 30 T.

Hoofdstuk 3 beschrijft metingen van de *phonon drag*-thermospanning van verschillende *composite fermion*-toestanden in het fractional quantum Hall gebied. De thermospanningen van verschillende *composite fermions* zijn hetzelfde als het aantal flux quanta, dat in de quasi-deeltjes gebonden is, hetzelfde is. Dit gedrag wordt met behulp van de theoretische beschrijving, die in hoofdstuk 1 ontwikkeld werd, begrepen. De overeenkomst tussen de thermospanning van *composite fermions* en de thermospanning van elektronen zonder magneetveld, zoals waargenomen in het experiment, is een bevestiging van het concept van een verdwijnend effectief magneetveld voor de quasi-deeltjes in de *composite fermion*-theorie.

Een fenomeen in quantum Hall systemen dat in het verleden nog niet begrepen werd, is het bestaan van een *phonon drag* gedomineerde transversale component S_{yx} van de thermospanning. De analyse in hoofdstuk 4 van de experimentele data van een groot aantal 2DEG-samples laat zien dat S_{yx} als volgt gerelateerd is aan de longitudinale thermospanning: $S_{yx} = \alpha B(dS_{xx}/dB)$. De schaalfactor α heeft dezelfde waarde als een soortgelijke schaalfactor die in hetzelfde sample verkregen wordt uit een vergelijkbare relatie tussen de twee componenten van de elektrische weerstand. De equivalentie van de thermospannings- en de weerstands-relatie wordt aangetoond onder bepaalde voorwaarden.

Een uitgebreid onderzoek van de thermospanning in hoge magneetvelden en bij temperaturen beneden 1 K in een set van drie soortgelijke 2DEG-samples, die alleen verschilden in details van de geometrie, wordt in hoofdstuk 5 gepresenteerd. De implicaties van de thermospanning voor het composite fermion-model en de relatie tussen S_{xx} en S_{yx} worden gedetailleerder bestudeerd dan in hoofdstuk 3 en 4. De thermospanning blijkt af te hangen van de orientatie van de temperatuurgradient ten opzichte van de kristallografische assen van het sample en zij schaalt met de vrije weglengte van de fononen. Dit gedrag toont direkt de *phonon drag*-oorsprong van de thermospanning in deze systemen aan.

De magneto-thermische eigenschappen van de 3-dimensionale halfgeleider HgSe gedoteerd met Fe, worden in hoofdstuk 6 bestudeerd. Qua thermospanning lijkt dit systeem conceptueel sterk op de 2D-systemen die in de eerdere hoofdstukken behandeld zijn. *Phonon drag* domineert de longitudinale component S_{xx}, maar ontbreekt in de transversale component S_{yx}. Dit gedrag is in overeenstemming met de theoretische verwachtingen, maar staat in contrast tot het 2D geval. Dit bewijst dat de relatie tussen S_{yx} en S_{xx}, zoals besproken in hoofdstuk 4 en 5, een karakteristieke eigenschap is van 2D-quantum Hall systemen. In het 3D geval wordt door het ontbreken van *phonon drag* in S_{yx} deze component alleen door diffusie bepaald. De diffusie oorsprong van S_{yx} blijkt uit de temperatuurafhankelijkheid en uit een faseverschuiving van $\pi/2$ van de oscillaties. Theoretische berekeningen komen perfect overeen met de experimentele data. De sterke elektron-fonon wisselwerking in HgSe:Fe komt tot uitdrukking in quantum oscillaties van de warmtegeleiding (van het rooster) die in fase zijn met de Landau niveau structuur van de elektronische toestandsdichtheid.

List of Publications

1. Even Denominator Filling Factors in the Thermoelectric Power of a 2-Dimensional Electron Gas.
   B. Tieke, U. Zeitler, R. Fletcher, S. A. J. Wiegers, A. K. Geim, J. C. Maan, and M. Henini.
   Phys. Rev. Lett., **76**:3630–3633, 1996.

2. Universal Behaviour of the Thermoelectric Power of Composite Fermions.
   B. Tieke, U. Zeitler, R. Fletcher, S. A. J. Wiegers, A. K. Geim, J. C. Maan, and M. Henini.
   Surf. Sci., **361–362**:46–49, 1996.

3. Magneto-thermoelectric properties of the degenerate semiconductor HgSe:Fe.
   B. Tieke, R. Fletcher, J. C. Maan, W. Dobrowolski, A. Mycielski, and A. Wittlin.
   Phys. Rev. B, **54**:10565–10574, 1996.

4. Origin of Magneto-Thermopower of Degenerate Semiconductors.
   B. Tieke, J. C. Maan, R. Fletcher, W. Dobrowolski, A. Mycielski, and A. Wittlin.
   In M. Scheffler and R. Zimmermann, editors, *The Physics of Semiconductors*, pages 83–85, Singapore, 1996. World Scientific.

5. Even Denominator Filling Factors in the Thermoelectric Power of a 2-Dimensional Electron Gas.
   B. Tieke, U. Zeitler, R. Fletcher, S. A. J. Wiegers, A. K. Geim, J. C. Maan, and M. Henini.
   In Thierry Martin, Gilles Montambaux, and J. Tranh Tan Vanh, editors, *Correlated Fermions and Transport in Mesoscopic Systems*, Gif-sur-Yvette, France, 1996. Edition Frontiers.

6. J. C. Maan, B. Tieke, A. K. Geim, R. Fletcher, U. Zeitler, and M. Henini.
   The Coupling of Composite Fermions to Phonons Measured with Magnetothermoelectric Experiments.
   Proceedings of 12th International Conference on High Magnetic Fields in the Physics of Semiconductors (SEMIMAG-96), 1996.

7. Evidence For Composite Fermions From The Magneto-thermopower of 2D Holes.
   P. A. Crump, B. Tieke, R. J. Barraclough, B. L. Gallagher, R. Fletcher, J. C. Maan, T. M. Fromhold, and M. Henini.
   Surf. Sci., **361–362**:50–54, 1996.

8. Phonon drag thermopower: composite fermions in zero magnetic field.
   S. A. J. Wiegers, B. Tieke, U. Zeitler, R. Fletcher, A. K. Geim, J. C. Maan, and M. Henini.
   Czech. J. Phys., **46**:2461–2462, 1996.

9. Thermoelectric power in the quantum-Hall regime at very low temperatures.
B. Tieke, R. Fletcher, S. A. J. Wiegers, U. Zeitler, J. C. Maan, C. T. Foxon, and J. J. Harris.
Physica B, **211**:414–416, 1995.

10. Tunneling Between Two-Dimensional Electron Gases up to 25 Tesla.
K. M. Brown, J. T. Nicholls, B. Tieke, S. A. J. Wiegers, P. J. M. van Bentum, E. H. Linfield, M. Pepper, D. A. Ritchie, and G. A. C. Jones.
Physica B, **211**:430–432, 1995.

11. The quantum-limit thermopower in two-dimensional electron systems.
U. Zeitler, B. Tieke, S. A. J. Wiegers, J. C. Maan, R. Fletcher, V. I. Fal'ko, C. T. Foxon, and J. J. Harris.
In D. Heiman, editor, *High Magnetic Fields in the Physics of Semiconductors*, pages 38–45, Singapore, 1995. World Scientific.

12. Anomalous magnetoresistance of folded pure Al foils.
B. Tieke, A. G. M. Jansen, P. Scheuzger, and P. Wyder.
Physica B, **194–196**:1209–1210, 1994.

13. B. Tieke, R. Fletcher, U. Zeitler, A. K. Geim, M. Henini, and J. C. Maan.
Fundamental relation between electrical and thermoelectric transport coefficients in the quantum Hall regime.
submitted to Phys. Rev. Lett. 1997.

Benno Tieke was born 18 May 1967 in Münster, Germany. He obtained the *Abitur* in June 1986 at the Pascalgymnasium, Münster.
He studied physics as an undergraduate from 1986 to 1988 at the Westfälische Wilhelmsuniversität Münster where he received the *Vordiplom* in September 1988, and as a graduate from 1988 to 1992 at the Universität Hamburg where he received the *Hauptdiplom* in November 1992. For his *Diplomarbeit*, entitled "Magnetoresistance of Pure Aluminium — Extrinsic Effects and Intrinsic Properties", under the supervision of Prof. Dr. P. Wyder (MPI Grenoble) and Prof. Dr. J. Kötzler (U Hamburg) he did research from August 1991 to November 1992 at the High Magnetic Field Laboratory in Grenoble, France. After having been to the Netherlands before for a practical stay at the Technische Universiteit Delft in October and November 1990 he returned to the Netherlands in December 1992 for his PhD research which is reported in this thesis. He worked at the High Field Magnet Laboratory of the University of Nijmegen in the group *Experimentele Vaste Stoffysica 1* as an *assistent in opleiding* from December 1992 to November 1996 and as a *junior onderzoeker* in December 1996 and January 1997.
Since February 1997 he is working as a research scientist at the Philips Research Laboratories, Eindhoven, in the group Optics.

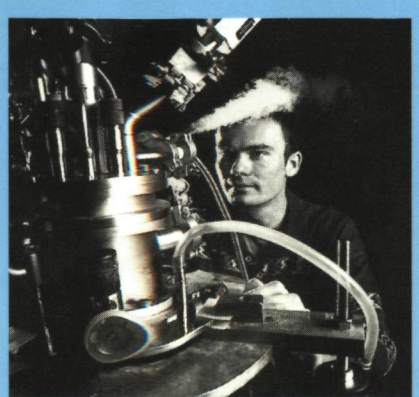

Photograph: Gerlo Beernink